Polymer-grafted Cellulose Nanocrystals and their Incorporation into Latex-based Pressure Sensitive Adhesives

Polymer-grafted Cellulose Nanocrystals and their Incorporation into Latex-based Pressure Sensitive Adhesives

By: Michael V. Kiriakou

McMaster University, kiriakmv@mcmaster.ca

A Thesis Submitted to the School of Graduate Studies in Partial Fulfillment of the Requirements of the Master of Applied Science Degree

Master of Applied Science (2020)

McMaster University (Chemical Engineering), Hamilton, Ontario

Title: Polymer-grafted Cellulose Nanocrystals and their Incorporation into Latex-based Pressure Sensitive Adhesives

Author: Michael V. Kiriakou, B.Eng & Scty (McMaster University, Hamilton, Ontario, Canada)

Supervisors: Dr. Emily D. Cranston & Dr. Todd Hoare

Number of Pages: xviii, 103

Lay Abstract

When the adhesives used in tapes, labels or sticky notes are produced using water-based reactions, they normally underperform compared to conventional adhesives produced using toxic solvents. To improve such water-based adhesives, adding nanocellulose (tiny particles derived from wood pulp) during synthesis has been shown to be an asset. Nanocellulose can be chemically modified to improve its compatibility with adhesive ingredients, and thus change the role of nanocellulose during adhesive manufacturing. In this thesis, modified nanocelluloses were added to water-based adhesives to evaluate their effect on performance (i.e., strength and stickiness). It was found that the reaction conditions during nanocellulose modification were crucial for obtaining highly modified particles that are compatible with adhesive ingredients. This work aims to provide insight for future production of less environmentally taxing adhesives made in water and expand the use of nanocellulose in new commercial products.

Abstract

This thesis investigates the effect of reaction media on the efficiency of grafting hydrophobic polymers *from* cellulose nanocrystals (CNCs) *via* surface-initiated atom transfer radical polymerization (SI-ATRP), with the goal of producing highly-modified CNCs for incorporation into latex-based pressure sensitive adhesives (PSAs). A latex is a dispersion of polymer particles in water made by emulsion polymerization; latexes are commonly used in paints, coatings, elastomers, inks/toners, household products, cosmetics, and adhesives. However, latex-based PSAs often underperform compared to their organic solvent-polymerized counterparts due to a lack of cohesive strength in the cast latex films. The environmental benefit of using latex-based PSAs synthesized in water is significant, but the development of strategies to improve their performance are required.

CNCs are hydrophilic rod-shaped nanoparticles with high mechanical strength. Adding CNCs to latex-based PSAs has been shown to improve both adhesive (i.e., tack and peel strength) and cohesive (i.e., shear strength) properties and offers a degree of sustainability because CNCs are derived from natural cellulose sources such as wood pulp. However, their hydrophilicity, particularly relative to the hydrophobic polymers used in PSAs, has constrained CNCs to the continuous (i.e., water) phase of the latex. To improve CNC compatibility with the dispersed (i.e., polymer) phase and improve their distribution in cast latex films, hydrophobic polymers can be grafted *from* CNCs. However, CNCs with a high polymer graft density are required to ensure their compatibility with monomers/polymers during latex synthesis.

To begin, grafting poly(butyl acrylate) (PBA) *from* CNCs using SI-ATRP in polar dimethylformamide (DMF) versus non-polar toluene was directly compared. The enhanced colloidal stability of initiator-modified CNCs in DMF led to improved accessibility to surface initiator groups during polymer grafting. As such, PBA-grafted CNCs produced in DMF had up to 30 times more grafted polymer chains than PBA-grafted CNCs produced in toluene. The PBA-grafted CNCs produced in DMF showed high contact angles when cast in a film and formed stable suspensions in toluene. This work highlights that optimizing CNC colloidal stability in a given solvent prior to polymer grafting is a more crucial consideration than solvent–polymer compatibility in the context of obtaining high graft densities and thus hydrophobic CNCs *via* SI-ATRP.

The improved polymer grafting method in DMF was then used to produce PBA and poly(methyl methacrylate) (PMMA)-grafted CNCs at two polymer chain lengths. Polymer grafted CNCs were incorporated *in situ* during a seeded semi-batch emulsion polymerization to produce PBA latex nanocomposite PSAs. Viscosity measurements revealed significant differences between latexes prepared with CNCs *versus* polymer-grafted CNCs, with the lower viscosities of the latter suggesting their incorporation inside the polymer particles. When CNCs with short polymer grafts were introduced into PSAs at 1 wt. % loading, they exhibited comparable tack and improved peel strength compared to unmodified CNCs (and all properties improved relative to the base latex without any CNCs). This is attributed to their improved distribution throughout the PSA, the enhanced wettability of the substrate with the CNC containing latex, and the increased polymer chain mobility achieved based on the low molecular weight of the grafts. CNCs with long polymer grafts aggregated in the latex and did not improve PSA properties. PMMA-grafted CNCs slightly outperformed PBA-grafted CNCs likely due to the higher glass transition temperature of PMMA. These results provide insight into future optimization of more sustainable latex-based PSA formulations as well as new commercial CNC-latex products, where the presence of low molecular weight grafts on CNC surfaces could improve polymer mobility and tack and peel strength.

Acknowledgments

I would like to give thanks to both of my supervisors Dr. Emily Cranston and Dr. Todd Hoare. Emily, your guidance and support over the last few years and the opportunities you have given me have been crucial for the work presented here and the work I will do in the future. Todd, I cannot thank you enough for your guidance on these projects and the in-lab home you have given me over the last two years. Both of your leadership and mentorship is truly appreciated.

I would like to thank all of my colleagues in both research groups. All of you made the time spent in lab fun, and the advice I have received over the years from all of you has made an impact on this work too.

From the Cranston group, thank you Stephanie Kedzior, Elli Niinivaara, Oriana Vanderfleet, Blair Morgan, Heera Marway, Mike Reid, Daniel Osorio and Taylor Stimpson. All of you made the lab environment a special and fun place to be. Special thanks to Stephanie, who without would have made this whole project a lot harder. Thank you for letting me bug you so much over the years, and thank you for being there even back when I was a summer researcher. Thank you to Elli for being the best VP operations I could have asked for over this time, and for keeping it as real as always. Your help with the work here is much appreciated. Thank you to Oriana for your valuable advice on TAing, courses, and watching over us in the office from the power desk on 4^{th} floor. Thank you to Heera for always being there for me time and time again for something as small as asking for a chemical or as big as running AFM for me. Blair “Chad” Morgan, it has been an absolute pleasure to work alongside you and to be there when we stopped that apocalypse.

From the Hoare Lab (and the era of chaos), there are so damn many of you. Jonathan Dorogin, Nate Dowdall, Taylor “Goose”trey, Matt Campea, Mitch Ross, Ali Affar, Yeetson Borne, Doren Singh, Eva Muller, Madeline Simpson, Ridhdhi Dave, Luis Portillo, Richie Ross, and Michael Majcher – Thank you all. Having your whole lab leave and having to graft *onto* a new group was definitely something that I was worried about, and it turned out to be some of the most fun I have ever had in my life. All of the memories of summer 2019 will never be forgotten.

Then, there are those outside of work who have been there from the early times: Peter Stuart, Christian Tropiano, Alex Doucette, Griffen Palmer, Mac Van dam, Alistair Boulby, Dawson Bonneville, Neil MacPhee, and Vlad Gritsichine. Some of you are high school, some of you university, but in the end of the day you guys have been there for me though this whole degree and I am forever grateful and blessed to have such a strong group of friends from such different times in my life.

Thank you to Linda, Michelle and Kristina in the Chemical Engineering office. The three of you are amazing and I am going to miss you all. Thank you to the following McMaster facilities: Biointerfaces Institute (BI), McMaster Analytical X-ray Diffraction Facility (MAX), and Health

Sciences Electron Microscopy Facility (EMF). Special thanks to Elna Luckham, Marta Princz and Zeynel Bayinder (BI), Jim Britten, Vicky Jarvis and Maureen Fitzpatrick (MAX), and Marcia Reid (EMF) for all your help with data collection and analysis. I would also like to thank Dr. Alex Adronov, Dr. Michael Thompson and Dr. Bob Pelton for all of the equipment use over the years with a special thanks to Dr. Pelton for being on my defence committee.

To all of my collaborators: Dr. Marc Dube, Vida Gabriel and Amir Pakdel – thank you so much for helping me with this work. Your guidance with polymer latex synthesis and my latex work over the years was so important for the story of this thesis. I also want to give a special thanks to Amir for all of the PSA testing you have done for me and to both Amir and Vida for always being so approachable and kind.

I would like to acknowledge the financial support provided in part by funding through the Natural Sciences and Engineering Research Council and the Ontario Graduate Scholarship. Also thank you to CelluForce and Richard Berry for providing us with our CNCs and being there to offer valuable insight into the context of our work and the impact it may have.

There are some of you were crucial for this thesis to be completed. Daniel-son Osorio, *i will never forget japan.* You have been so supportive through this degree, and some of the adventures we have had in the short time we have known each other (either in real life or hovering over a table/computer screen rolling dice) are legendary. Taylor “Tommy” Stimpson, you and I have grown from 2nd year babies to adults and I wouldn’t be where I was today without you. All your support over the years has meant so much to me – and to you and Dan, love you. Alex “Ethan” Sutherland, you are my D&D sugar daddy and I can’t express enough how grateful I am that you showed me this game. I have felt some of the realest emotion ever in your campaigns, and those moments will stay with me forever. I was sad when you had to go be an adult before Tommy and I, but you and Tommy are just a couple of blonde Chem Eng boys so… who wants to get in the juh? And finally, to my partner Nicole Amaral: I do not know what I would have done without you. You are so kind, so caring, and your support through all of this, and especially the last six months, has encouraged me to press on when I wanted to stop, or stop when I didn’t need to press on. Going through the same end-of-thesis experience (with their differences of course) at the same time was risky – what if we both had a meltdown at the same time. Then what happens?! Well somehow, it worked out didn’t it? Your emotional and physical support was the rock for me.

Finally, to my family: Mom & Dad you two have always supported me (unless I was being an idiot, and in that case you probably had to intervene) and I am so lucky to have such caring parents. Without you two I wouldn’t be the man I am today and I am forever grateful for having you two there for me. Dayna, you are the best little sister I could ask for and talking to you always brightens my day. Yongest lawn. And Cosmo you cutie, you are the weirdest dog ever but also such a good boy. Love you four so very much.

Table of Contents

Table of Figures

Table of Tables

List of Acronyms

AA	Acrylic acid
AFM	Atomic force microscopy
ANOVA	Analysis of variance
ATRP	Atom transfer radical polymerization
BA	Butyl acrylate
BiB	α-bromoisobutyryl bromide
BiB-CNC	Initiator-modified cellulose nanocrystal
BNC	Bacterial nanocellulose
CNC	Cellulose nanocrystal
CNF	Cellulose nanofibril
CrI	Crystallinity index
CRP	Controlled radical polymerization
CTA	Chain transfer agent
CuBr	Copper (I) bromide
Đ	Dispersity
DLS	Dynamic light scattering
DMA	Dynamic mechanical analysis
DMAP	4-(dimethylamine)pyridine
DMF	Dimethylformamide
DP	Degree of polymerization
D-PBA-*g*-CNCs	Poly(butyl acrylate) grafted cellulose nanocrystals produced in dimethylformamide
DSC	Differential scanning calorimetry
EBiB	Ethyl α-bromoisobutyrate

EDTA	Ethylenediaminetetraacetic acid
EHA	2-ethylhexyl acrylate
FTIR	Fourier-transfer infrared spectroscopy
g-CNCs	Polymer-grafted cellulose nanocrystals
GPC	Gel permeation chromatography
IBA	Isobornyl acrylate
KPS	Potassium persulfate
lsNMR	Liquid-state NMR
MC	Methyl cellulose
MMA	Methyl methacrylate
M_n	Number average molecular weight
NDM	1-dodecanethiol
NMP	Nitroxide-mediated polymerization
$-OSO_3^-$	Sulfate half-ester
PAH	Polyallylamine hydrochloride
PBA	Poly(butyl acrylate)
PBA-*g*-CNCs	Poly(butyl acrylate) grafted cellulose nanocrystals
PCL	poly(caprolactone)
PEI	polyethyleneimine
Phm	Parts per hundred parts monomer by mass
PMDETA	N,N,N’,N’’,N’’-pentamethyldiethylenetriamine
PMMA	Poly(methyl methacrylate)
PMMA-*g*-CNCs	Poly(methyl methacrylate) grafted cellulose nanocrystals
PNIPAM	Poly(N-isopropylacrylamide)
PSA	Pressure sensitive adhesive

PSTC	Pressure sensitive tape council
RAFT	reversible addition-fragmentation chain-transfer polymerization
ROP	Ring-opening polymerization
SDS	Sodium dodecyl sulfate
SI-ATRP	Surface-initiated atom transfer radical polymerization
ssNMR	Solid-state NMR
St	Styrene
TEA	Trimethylamine
TEM	Transmission electron microscopy
T_g	Glass transition temperature
TGA	Thermogravimetric analysis
T-PBA-*g*-CNCs	Poly(butyl acrylate) grafted cellulose nanocrystals produced in toluene
VAc	Vinyl acetate
XPS	x-ray photoelectron spectroscopy
XRD	x-ray diffraction

Declaration of Achievement

I declare that the research contribution which follows is original work, that I, Michael V. Kiriakou, have completed and written, with editorial assistance from supervisors Dr. Emily D. Cranston and Dr. Todd Hoare.

Chapter 3 experimentation, characterization, data analysis and manuscript drafting was performed by Michael Kiriakou unless stated otherwise. A list of technicians who assisted with data collection/ analysis can be found in the acknowledgment section at the end of chapter 3. Drs. Emily D. Cranston and Todd Hoare always directed research, assisted with interpretation of results and performed manuscript editing. Richard Berry (CelluForce Inc.) also assisted with manuscript editing.

Chapter 4 experimentation, characterization, data analysis and manuscript drafting was performed by Michael Kiriakou and assisted by Amir Pakdel (University of Ottawa) for PSA testing and data collection. A list of technicians who assisted with data collection/ analysis can be found in the acknowledgement section at the end of Chapter 4. Drs. Emily D. Cranston and Todd Hoare always directed research, assisted with interpretation of results and performed manuscript editing.

Chapter 1: Introduction and Objectives

1.1 Introduction

In recent years, there has been a push for sustainability across a wide range of industries, specifically to reduce the use of petroleum-derived chemicals. This drive towards sustainable practices, as well as safer chemistries, has led many industries to improve the efficiency of their processes, reduce the use of harmful chemicals, minimize waste, and implement as many non-toxic synthetic routes as possible without diminishing the quality of their services or products. Some of these goals have been, at least partially, achieved through the use of nanotechnologies, specifically those based on renewable resources. In particular, cellulose nanocrystals (CNCs) stand out based on their steadily increasing popularity in the academic[1,2] and patent literature,[3,4] and their growing use in industrial applications.[5–7]

While CNCs were discovered in the 1940s by Nickerson and Habrle,[8] their widespread popularity only occurred after a series of publications by Derek Gray and coworkers at McGill University in the 1990s.[9] CNCs are produced after natural cellulose containing materials, such as wood pulp or cotton, undergo an acid hydrolysis that degrades disordered cellulose regions into sugars, leaving behind crystalline cellulose nanorods.[1] Recently, this process has been scaled up to much success, with companies mass producing CNCs following a range of methods from a variety of starting materials. For example, CelluForce Inc. has achieved a ton-per-day output of CNCs produced by sulfuric acid hydrolysis, with various recycling and collection procedures which allow them to recover acid from the process for reuse and capture sugars to be used in other processes (e.g. fermentation to biofuels).

CNCs have been envisioned for a wide range of applications such as polymer and cement nanocomposites, oil & gas, food/cosmetics and biomedical materials.[10] However, their use often remains limited due to the abundance of surface hydroxy groups and their generally hydrophilic nature.[10] While problematic for compatibility and dispersion in non-polar organic solvents and hydrophobic polymers, the hydroxy groups enable CNCs to undergo a plethora of chemical modification pathways that can be used to improve these properties. A common covalent modification route for CNCs has been controlled polymer grafting, which allows for the growth of polymer chains from the CNC surface *via* the attachment of an initiating chemical group.[11] Specifically, surface-initiated atom transfer radical polymerization (SI-ATRP) has become the most popular form of controlled polymer grafting due to the wide range of monomers and solvents that can be used, allowing for the grafting of hydrophilic and hydrophobic polymers.[12] In the case of grafting hydrophobic polymers, a range of solvents with varying polarity has been demonstrated with success but without any direct comparison of how a given solvent may be more beneficial. The first objective of this thesis is thus to investigate the effect of reaction media on the grafting density achievable when CNCs undergo polymer grafting *via* SI-ATRP.

CNCs have been implemented as reinforcing agents, stabilizers, and rheological modifiers due to their unique properties such as high aspect ratio, large surface area, and high mechanical strength.[2] In polymer nanocomposites, defined as hybrid materials composed of a polymer matrix with a dispersed nanofiller, CNCs are often able to impart their high mechanical strength and stiffness even at low loadings.[13] However, the use of CNCs in CNC-polymer nanocomposites is generally limited due to the processing requirements in a variety of applications, such as the use of solvents or high temperatures which can aggregate or degrade the CNCs, respectively. Because of this, water-based CNC-polymer nanocomposites have become appealing for a variety of applications such as coatings, adhesives, and paints.[14] In many cases, the addition of CNCs into water-based polymer systems aims to produce materials that are comparable or even superior to their solvent-based counterparts, which in turn can help to improve the sustainability of the industries that have been using such solvent-based products to-date.

Pressure sensitive adhesives (PSAs) are a class of polymer-based adhesives that can be applied to a surface with gentle pressure and removed afterwards. Common examples of PSAs include masking tapes, sticky notes and labels. While conventional PSAs are produced through solvent-based polymerization, latex-based PSAs have become attractive as a means to improve the "greenness" of such products. Latex-based PSAs are produced *via* emulsion polymerization, a water-based heterogeneous polymerization process that produces polymer nanoparticles dispersed in the aqueous phase. However, latex-based PSAs are known to underperform compared to their solvent-based counterparts, leaving researchers to find ways to improve their overall performance while minimizing their environmental impact.[15]

CNCs can improve the performance of latex-based PSAs, leading to an increase in peel, tack and shear strength when blended into an existing polymer latex or added *in situ* during latex polymerization.[16] The *in situ* method produces better latex-based PSAs compared to blending due to a better dispersion of CNCs throughout the latex and more interactions between the polymer and the CNCs.[17] Notably, the addition of only 1 wt.% (based on monomer mass) of CNCs has been shown to greatly improve both the adhesive and cohesive properties of latex-based PSA, leading to better PSA film formation and enhanced reinforcement without requiring large amounts of (relatively high cost) CNCs.[16] While CNCs are often introduced into the water phase of these formulations, the use of hydrophobic CNCs in latex-based PSAs has not been fully realized. The second objective of this thesis is thus to use hydrophobic CNCs produced *via* polymer grafting in latex-based PSA formulations and asses their effect on the latex and adhesive properties. While the bulk latex is poly(butyl acrylate) and not a true PSA "recipe" that would normally contain both a low and high glass transition temperature polymer, this work acts as a precursor to answer questions about the advantages and disadvantages of covalently surface-modifying CNCs and incorporating such CNCs into latex-based PSAs.

In this thesis, CNCs were covalently modified with hydrophobic polymers (poly(butyl acrylate) and poly(methyl methacrylate) through a controlled grafting method, SI-ATRP, prior to their incorporation into latex nanocomposites. However, before producing the latex nanocomposites, the grafting of poly(butyl acrylate) *from* CNCs was maximized by using (polar) dimethylformamide as the reaction medium for SI-ATRP compared to (non-polar) toluene; hydrophobic CNCs were obtained. While previous work on CNCs and latex-based PSAs have used either unmodified or "slightly less hydrophilic" CNCs, this thesis presents the synthesis and application of a range of novel latexes and PSAs based on hydrophobic polymer grafted CNCs.

1.2 Thesis Objectives

CNCs have been shown to significantly improve the properties of latex-based PSAs, but a full understanding of how CNC surface chemistry (and thus the location of CNCs within a polymer latex) affects PSA performance has yet to be determined. While there are simpler and more "green" methods to modify the CNC surface with hydrophobic chemical groups or polymers, the control attainable when using SI-ATRP will enable us to elucidate what characteristics are most desirable when trying to compatibilize CNCs with monomers and polymers used in latex-based PSAs. The main objectives of this thesis are:

1. **To improve the grafting of hydrophobic polymer *from* CNCs** *via* SI-ATRP though an assessment of the grafting density as a function of the reaction media. Specifically, poly(butyl acrylate) was grafted *from* CNCs using SI-ATRP in both DMF and toluene, which are good solvents for CNC dispersion and the polymer respectively. This work provides insight into how the choice of solvent is important to obtain highly grafted CNCs when attaching hydrophobic polymers.

2. **To incorporate polymer-grafted CNCs into latex-based PSAs** and evaluate their effect on latex properties and adhesive performance. Polymer type, degree of polymerization, and the CNC loading into poly(butyl acrylate) latexes will be altered to understand what characteristics will maximize PSA properties and if these novel nanocomposites should be used in future PSA formulation or other latex applications (e.g. coatings, paints).

1.3 Thesis Outline

Chapter 1: *Introduction*

This chapter introduces the main themes, objectives, and outlines the work presented in this thesis.

Chapter 2: *Background and Literature Review*

This chapter presents an in-depth review of the current literature and critical concepts relevant to the research described in this thesis.

Chapter 3: *Effect of Reaction Media on Grafting Hydrophobic Polymers from Cellulose Nanocrystals via Surface-initiated Atom Transfer Radical Polymerization*

This chapter provides a side-by-side comparison of grafting hydrophobic poly(butyl acrylate) from CNC surfaces using either toluene (non-polar) or dimethylformamide (polar) as the reaction medium. Polymer grafting occurred regardless of the solvent used, but the graft density was 30 times larger when a polar organic solvent was used due to the enhanced colloidal stability of CNCs prior to grafting. Extensive characterization showed that highly hydrophobic CNCs could be produced while maintaining the CNC crystal structure and particle morphology, and the presence of more polymer chains on CNCs improved their overall thermal stability. This chapter has been submitted to *Biomacromolecules* for publication.

Chapter 4: *Incorporation of Polymer-grafted Cellulose Nanocrystals into Latex-based Pressure Sensitive Adhesives*

This chapter reports the synthesis of polymer latex nanocomposites containing poly(butyl acrylate)- and poly(methyl methacrylate)-grafted CNCs in a bulk poly(butyl acrylate) latex. The effect of polymer type, degree of polymerization, and CNC loading on latex and PSA properties was evaluated. Final latex particle size, viscosity, glass transition temperature, water contact angle, and transmission electron microscopy images determined that polymer-grafted CNCs with a low degree of polymerization were uniformly dispersed and/or located on the latex polymer particles. Polymer-grafted CNCs were found to improve both PSA tack and peel strength at higher loadings but did not improve shear strength. Additionally, CNCs grafted with low molecular weight polymers outperformed their higher molecular weight counterparts due to better incorporation and dispersion of the CNCs within the polymer matrix. This chapter is in preparation for publication.

Chapter 5: *Concluding Remarks*

This chapter summarizes the major contributions to knowledge resulting from this thesis work and presents suggestions for future work.

Chapter 2: Background and Literature Review

2.1 Cellulose

Cellulose is the most abundant type of renewable organic matter on earth, with an estimated 10^{11} tons produced globally every year.[18] There are an abundance of sources from which cellulose can be extracted, with plants, bacteria, fungi and even some animals (e.g. tunicates) being the most notable.[19] Cellulose is a high molecular weight homopolymer of β-1,4-linked anhydro-D-glucose units where every unit is corkscrewed 180° with respect to its neighbouring units.[1] Figure 2.1 shows the chemical structure of cellulose, where the repeated segment is comprised of glucose dimers known as cellobiose. Each cellulose chain has two distinct end-groups, the reducing and nonreducing ends that contain a hemiacetal and pendant hydroxy group respectively. The number of anhydroglucose units, or the degree of polymerization (DP) of cellulose, varies with the source of cellulose and the cellulose location in the organism, such as the plant primary cell wall.[1]

As a consequence of the chair conformation of glucose rings, hydroxy groups are positioned in the ring (equatorial) while hydrogen atoms are in the vertical (axial) position, resulting in a hydrophobic contribution to the chemical structure. While generally considered fairly hydrophilic, cellulose is probably more correctly labeled as amphiphilic[20], dictating for example its behavior at interfaces, reactivity, and solubility.[21] The chemical structure and ring conformation allow for chain aggregation *via* hydrophobic interactions, van der Waals forces and extensive inter- and intramolecular hydrogen bonding. The current understanding is that cellulose is biosynthesized as bundles of 10-36 cellulose chains (depending on the organism) known as elementary fibrils.[22,23] In plants, the elementary fibrils assemble further into microfibrils which pack into larger cellulose fibers. The packing of these cellulose structures and the relative composition of hemicelluloses, lignin and proteins are dictated during biosynthesis, which varies between cellulose sources.

Along an elementary fibril there exist highly ordered, or crystalline, regions and disordered, or amorphous, regions of cellulose. The crystalline regions, which are stabilized by the aforementioned inter- and intramolecular hydrogen bonded networks, can represent different amounts of the fibril depending on the cellulose source, method of extraction, or treatment. For example, the cellulose extracted from some plant species can represent 50% of the fibril structure while cellulose extracted from some algae can be almost 100% crystalline.[24] The disordered regions are less tightly bound, making them more prone to chemical, mechanical, or enzymatic degradation.[1]

2.2 Nanocellulose

The term nanocellulose defines cellulosic materials that have at least one dimension in the nanoscale. Nanocellulose is often organized into three categories: bacterial nanocellulose (BNC), cellulose nanofibrils (CNFs), and cellulose nanocrystals (CNCs). All nanocelluloses are high aspect ratio, ribbon-like or rod shaped nanoparticles with varying dimensions based on the method of extraction and the cellulose source. A summary of nanocelluloses is shown in Table 2.1, which provides an overview of typical sources, production methods and dimensions.

While chemically extracted CNCs are the focus of this work, BNC and CNFs have been used for a variety of similar research and applications. BNC is produced through the fermentation of sugars and plant carbohydrates *via* microorganisms. The cellulose in BNC has the identical structure to cellulose from plant sources, but is highly crystalline, has a higher DP, offers good mechanical properties, and consists of pure cellulose as opposed to being combined with other plant biopolymers.[2] This makes BNC ideal for medical and food applications, such as in vivo scaffolds and thickening agents respectively.[2,25] On the other hand, CNFs are isolated from plant cellulose *via* mechanical disintegration, tearing large cellulose fibers into fibrils with cross-sections in the nanometer range.[2] Because of their preparation, CNFs often contain both ordered and disordered cellulose and have a large size polydispersity, which coupled with their high aspect ratio allow for significant entanglement and gel formation at low concentrations. This makes CNFs excellent for use in hydrogel materials, flexible "plastic-like" applications, and the reinforcement of various polymer matrices.[2,25]

2.2.1 Cellulose Nanocrystals

The first reported case of CNCs produced *via* acid hydrolysis was in 1947 by Nickerson and Habrle,[8] followed by Ranby in 1949.[26] The conditions during the acid hydrolysis of cellulose produces the rod-shaped nanocrystals due to the chemically induced degradation of the disordered regions while the more acid resistant crystalline regions remain intact.[27,28] CNCs have gained academic and industrial interest due to their non-toxic and biodegradable nature as well as their amphiphilicity, high aspect ratio, and high mechanical strength.

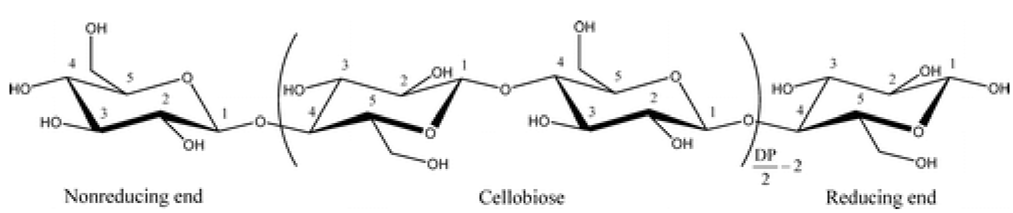

Figure 2.1. Chemical structure of cellulose. Figure reproduced from reference 1.

Table 2.1. Different types of nanocelluloses, their sizes, typical sources and production methods. Adapted from reference 25.

Type of nanocellulose	Synonyms	Typical sources	Production methods and average size
Bacterial nanocellulose (BNC)	Bacterial cellulose	Low molecular weight sugars and alcohols	Bacterial synthesis Width = 20-100 nm Different type of nanofiber networks
Cellulose nanofibrils (CNFs)	Microfibrillated cellulose (MFC) Nanofibrillated cellulose (NFC) Nanofibrils Microfibrils	Wood, sugar beet, hemp, flax	High pressure homogenization (often with chemical or enzymatic pre-treatment) Width = 5-60 nm Length = up to several μm
Cellulose nanocrystals (CNCs)	Nanocrystalline cellulose (NCC) Cellulose whiskers	Wood, cotton, hemp, flax, tunicate, algae, bacterial cellulose, wheat straw, ramie	Acid hydrolysis or oxidation Width = 5-70 nm Length = 100-250 nm (from plant sourced material), 100-several μm (from tunicate, algae, bacteria)

When produced by sulfuric acid hydrolysis, anionic sulfate half-ester ($-OSO_3^-$) groups are covalently attached *via* esterification of surface hydroxy groups (Figure 2.2), leading to colloidal stability of CNCs in water due to electrostatic repulsion between individual nanoparticles.[1] The grafting density of sulfate groups is typically in the range of 0.3-0.6 charges/nm^2 on the CNC surface.[29] Other acids may be used for acid hydrolysis, such as phosphoric or hydrochloric acid; both have a reduced colloidal stability as compared to sulfated CNCs. It has also been demonstrated that CNCs made by different routes have different thermal stabilities. Sulfated CNCs thermally degrade at lower temperatures than phosphoric or hydrochloric acid CNCs because of their higher surface charge density, whereas hydrochloric acid CNCs are uncharged and have the highest thermal stability.[30,31] Alternatively, CNCs can be produced though oxidative methods without the need for acids. Oxidative methods often provide CNC surfaces with carboxyl groups while still maintaining nanoscale particles that are highly crystalline.[32] The presence of carboxyl groups can open up CNCs to a variety of chemical modifications, whereas acid-based productions methods like the aforementioned sulfuric acid hydrolysis would require a post-synthesis modification step to obtain this functionality. Additionally, using peroxides can be highly-scalable and cost-effective since the reactive peroxides can be almost fully used up by the end of the reaction.

Due to the tightly packed cellulose chains in the crystalline regions, CNCs have a large elastic modulus when stress is applied perpendicular to their long axis. CNCs with a cellulose I structure (the native crystal structure of cellulose) have an average transverse elastic modulus of 137 GPa as determined by atomic force microscopy and x-ray diffraction, which is comparable to that of Kevlar (60-125 GPa) and almost as high as steel (200-220 GPa).[24] This mechanical performance and their inherent sustainability as a bio-based material make CNCs ideal candidates as natural reinforcing agents in polymer[1,13] and cement[10] nanocomposites.

The CNC aspect ratio (length/cross-section) is dependent on the cellulose source and has been shown to impact properties such as packing density,[33] rheological behaviour,[34] and mechanical reinforcement potential.[35] Average values span from 50-3000 nm in length and cross-sections of 3-20 nm[29,32] and are typically lower for cotton cellulose nanocrystals, with bacterial or tunicate crystals having the higher aspect ratios.[36]

Due to increasing interest in the development of commercial CNC-based products, CNC production has been scaled up over the last decade for high volume applications. *CelluForce Inc*, located in Windsor, Quebec currently operates the largest production facility producing one ton per day of sulfated CNCs using the typical sulfuric acid hydrolysis with bleached Kraft pulp and has recently started production of a variety of surface-modified CNCs as well. Other producers include Innotech Alberta (formerly Alberta Innovates Technology Futures), the *USDA Forest Products Laboratory*, Blue Goose Biorefineries, FPinnovations, Anomera, CelluloseLab and Melodea, who have the capacity to produce on the kg scale using wood and cotton cellulose sources.[29] It is important to note that while all of the aforementioned companies produce similar products, sufficient characterization of any CNC should be performed before its use since slight variation in CNC characteristics may affect their desired properties for a given application.

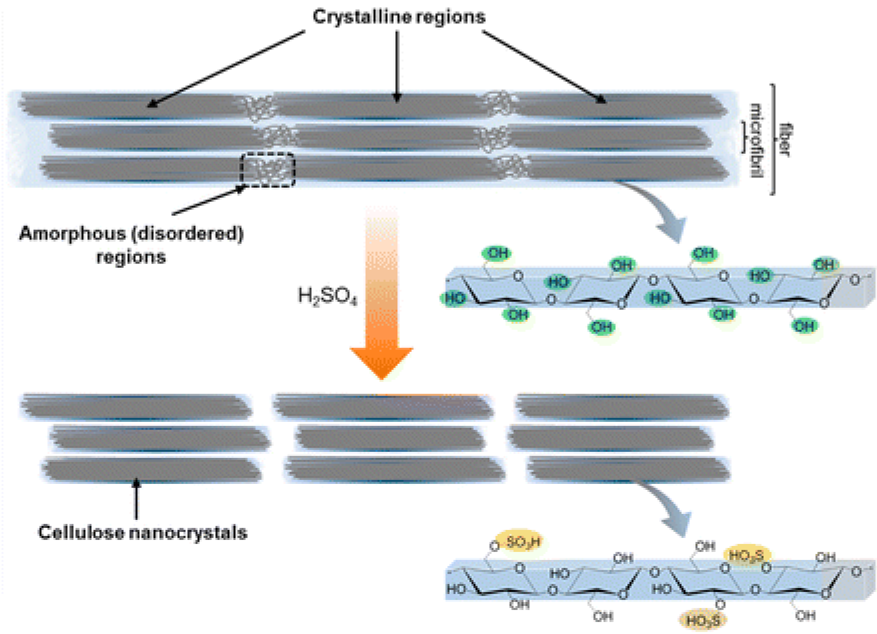

Figure 2.2. Schematic of sulfuric acid-based hydrolysis of cellulose fibers into cellulose nanocrystals with surface sulfate half-ester groups. Figure reproduced from reference 37. [37]

2.2.2 Surface Modification of Cellulose Nanocrystals

The surface of CNCs can be modified to impart new functionalities, tailor CNC compatibility with a given liquid/solid environment, or to improve dispersion/colloidal stability.[38] Methods of surface modifying CNCs include non-covalent modifications[38,39] (i.e., adsorption of polymers or surfactants), and covalent attachment of small molecules[39] or polymer chains.[11,12] The most common non-covalent route is the adsorption of auto-adsorbing polymers or cationic surfactants, which generally offers the simplest approach to CNC modification. Common small molecule covalent modifications include esterification, etherification, silylation, amidation and urethanization and are often employed to impart functionality for further modification.[2]

Polymer Grafting

CNCs can be surface modified with polymer chains through two main methods: polymer grafting *to*, in which pre-synthesized polymers are attached to the CNC surface, and polymer grafting *from*, in which polymerization is initiated from the surface and monomers are added one at a time (Figure 2.3).[12] While both methods lead to polymer grafting, each has benefits and setbacks, as outlined in the following sections.

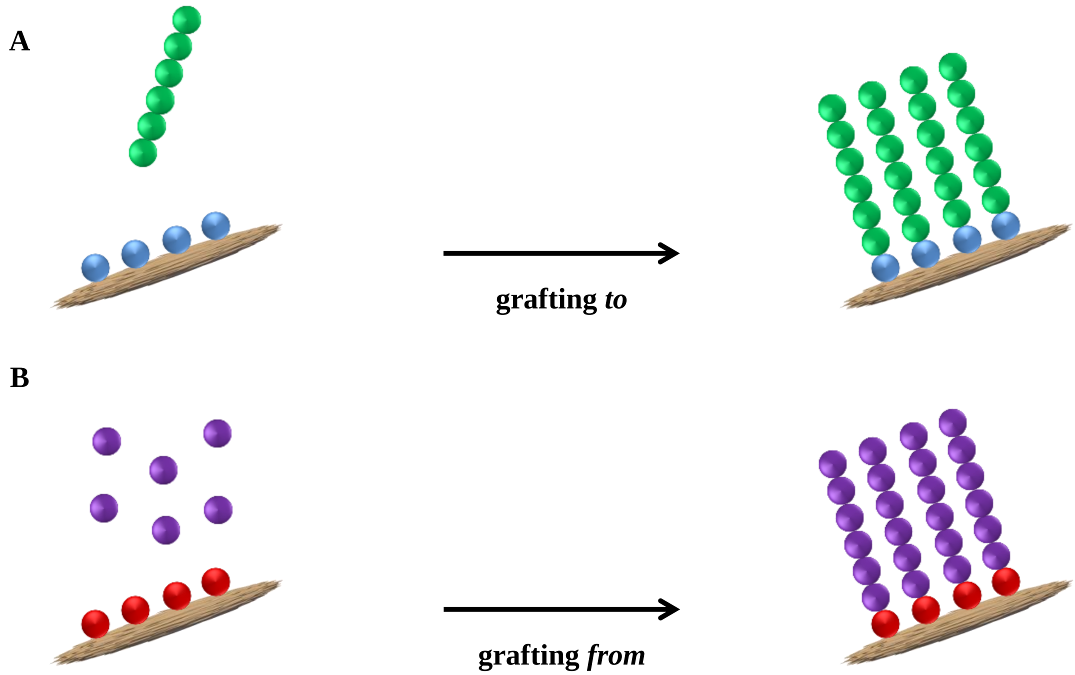

Figure 2.3. Schematic of A) grafting *to* CNCs with a given reactive group (blue) and a pre-formed polymer (green) and B) grafting *from* CNCs with attached initiator group (red) – the initiation site may be inherent to the CNC surface chemistry or added in a initiator attachment pre-polymerization step. Individual purple circles indicate monomeric units and chains of purple circles are polymers.

Grafting *to*

The grafting *to* method generally takes advantage of the abundance of hydroxy groups on the CNC surface and polymers with specific end-functionality. The main benefit of the grafting *to* method is the ability to characterize the polymers prior to their attachment to CNCs, obtaining information about their physical/chemical properties. However, the grafting density with grafting *to* is limited by steric hindrance, whereby long polymer chains entangle with one another or hinder the ability for polymer chain ends to find the CNC surface. For example, the work by Habibi et al.[40] grafted poly(caprolactone) (PCL) to the surface of CNCs using isocyanate-mediated coupling. In order to obtain a high density of polymer grafting, a reaction time of one week was required with continuous addition of coupling agent, which is less than ideal for high volume modification of CNCs.

Grafting *from*

The grafting *from* method can provide high grafting densities of hundreds of polymer chains per CNC. In contrast to grafting *to*, polymers that are grafted *from* are unable to be characterized fully without cleaving the polymers off the CNCs. To combat this, free polymer in solution is often produced (from "sacrificial imitator" in the liquid phase) and characterized, which has been shown to be comparable in DP to the grafted polymer.[41] Despite its characterization challenges, grafting *from* has become more popular than grafting *to* for CNCs, with most reports of CNC polymer grafting now using the grafting *from* approach.[12]

Grafting *from* is often divided into three groups: free radical polymerization, ring-opening polymerization (ROP), and controlled radical polymerization (CRP). Free radical is often carried out in aqueous conditions using a water soluble initiator. These reactions are favorable for CNCs since they are colloidally stable in water and will therefore be individually modified in their unaggregated state. Common water soluble initiators used for free radical polymerization including ceric ammonium nitrate,[42–48] potassium persulfate[49–57] and ammonium persulfate[58–61] have been used with a variety of water-soluble monomers. Free radical polymerization, while favourable due to its simplistic approach and use of water as a reaction solvent, lacks any control over the grafted polymer length and graft density, leading to a modification that is difficult to predict and characterize. Additionally, due to the use of water-soluble initiators, initiation occurs mostly in the aqueous phase rather than the particle surface, resulting in large amounts of free polymer in solution; This reduces the efficiency of polymer grafting and leads to a mixture that is difficult to purify.[12]

ROP is a method used to polymerize cyclic monomers from the CNC surface. ROP was first used by Habibi et al.[62] who grafted PCL from CNCs; the resulting CNCs were shown to maintain their morphology after grafting and were able to enhance the mechanical properties of solvent-casted PCL nanocomposites. Since then, ROP has been used to graft other cyclic monomers under different reaction conditions,[63,64,73–82,65,83–92,66,93–95,67–72] with ROP representing a method of polymerizing cyclic monomers from CNCs with good control of graft length and density.

Controlled radical polymerization has given rise to the majority of the polymer grafted CNCs to-date, with most processes designed based on atom transfer radical polymerization (ATRP), reversible addition-fragmentation chain-transfer polymerization (RAFT) and nitroxide-mediated polymerization (NMP) approaches.[96] In each case, the reactions are enabled by a combination of fast initiation and limited termination, with an equilibrium established between active radicals and dormant species. The fast exchange between the active and dormant species is what provides CRP with its excellent control over the dispersity and molecular weight of the grafted polymer.[12] Additionally, the requirement for initiator attachment to the CNC surface prior to polymerization allows for moderate control over graft density. ATRP has been the most explored method, not only out of CRP methods more generally but also among all grafting *from* methods reported for CNCs.[11,12,96] The popularity of ATRP comes from its tunability, the variety of monomers that can be polymerized, and wide range of solvents and other reactants that can be employed to optimize polymer grafting. There have not been many examples of using RAFT or NMP for grafting polymers *from* CNCs, mainly due to the complex nature of the chain-transfer agent attachment for the former and the limited monomer/reaction conditions that lead to effective polymerization for the latter. The main disadvantage of ATRP, unlike RAFT and NMP, is the requirement for extensive purification to remove the metal catalyst, which can lead to issues around product purity and process up-scaling.

ATRP was first reported by the Matyjaszewski group,[97] with the mechanism shown in Figure 2.4. Its adaptation as a general cellulose modification route was pioneered by the Malmstrom group, first with filter paper[98] as the substrate and later extended to nanocellulose.[99] There are now dozens of research groups worldwide that are skilled in surface-initiated ATRP (SI-ATRP) from CNCs, which has helped to move the field forward quickly.[11,12] In ATRP, an equilibrium between the propagating radicals and dormant species is achieved, allowing for control over the polymerization. The activation of growing polymer chains occurs when the dormant species and the transition metal complex in their lower activation state react to radicalize the particle surface; conversely, chains are deactivated when transition metal complexes in their higher oxidation state react with the propagating radicals. To control the reaction, the rate constants of the reaction, defined as k_{act} (activation), k_{deact} (deactivation) and k_p (propagation), can be altered by the choice of reaction solvent, temperature, monomer and transition metal complex.[100] In general, a high rate of initiation coupled with a fast deactivation step allows for the concurrent growth of polymer chains while still exhibiting proper control over chain length.

The first reported case of polymer-grafting from CNCs *via* SI-ATRP was in 2008 by Xu et al.,[101] who grafted poly(1,1,4,7,10,10-hexamethyltriethylenetetramine) from the CNC surface followed shortly thereafter with poly(styrene)[102] and poly(N,N-dimethylaminoethyl methacrylate)[103]. Important investigations into how SI-ATRP can be optimized followed next, with studies highlighting the tunability of surface-initiator immobilization,[104] grafting density limits,[105] and the use of sacrificial initiator and its role in estimating the molecular weight of the grafted polymer.[41] While initiator densities of up to 4.6 groups/nm^2 have been reported[106], most reports of SI-ATRP to date have achieved polymer chain densities of less than 1 chain/nm^2.[12] That being said, 1 chain/nm^2 is still considered to be a highly modified material, resulting in thousands of polymer chains grafted per CNC. With respect to polymer chain length, the highly tuneable nature of SI-ATRP has allowed for researchers to achieve chains as short as 10 monomer units[107,108] and as high as 1000 monomer repeat units[109]. In the last decade, most reports of using SI-ATRP for polymer-grafting from CNCs has focused on applying the method to hydrophilic polymers like poly(N-isopropylacrylamide)[105,110–114] and hydrophobic polymers like poly(butyl acrylate)[109,115] for the material's use in applications such as nanocomposites and emulsions.[11,12]

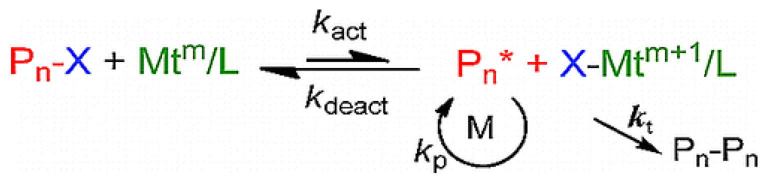

Figure 2.4. ATRP reaction mechanism. Figure reproduced from reference 97.

The complex nature of ATRP leads to a variety of factors that can affect the values of the rate constants k_{act} and k_{deact}, including the structure of the ligand, the monomer/dormant species, and the reaction conditions (i.e., solvent, temperature and pressure). In this thesis, the effect of solvent on the grafting of hydrophobic polymer from the CNC surface was evaluated. Specifically, the polar solvent dimethylformamide (DMF) and non-polar toluene were used as a reaction solvent to graft poly(butyl acrylate) from the CNC surface in order to assess the benefits of using a specific solvent for SI-ATRP of CNCs. We believe that the polymerization kinetics and the dispersibility of the CNCs in the chosen solvent both play a crucial role. While both DMF[107,108,124–127,116–123] and toluene[115,128] have been used to graft polymers from CNCs before, this study is the first direct comparison of solvents in which all other reaction conditions and components are kept constant. This work adds new insight into the choice of solvent when grafting hydrophobic polymers *via* SI-ATRP *from* CNCs while working toward the optimization of CNC polymer grafting.

Characterization of Surface-modified Cellulose Nanocrystals

The most common techniques for characterizing surface-modified CNCs are elemental analysis, Fourier-transform infrared spectroscopy (FTIR), x-ray photoelectron spectroscopy (XPS), x-ray diffraction (XRD), thermogravimetric analysis (TGA), differential scanning calorimetry (DSC), and solid-state or liquid-state NMR (ssNMR/lsNMR). Additionally, transmission electron microscopy (TEM) and atomic force microscopy (AFM) are used to visualize surface-modified CNCs and UV-visible spectroscopy (UV-vis) can be used to evaluate their colloidal stability in suspension. The following sub-section will summarize these characterization methods, which are outlined in detail in a review by Foster et al.[129]

Elemental analysis, FTIR and XPS are all used to learn about the chemical composition of modified CNCs. Elemental analysis is particularly useful when the modification contains an element different than carbon, oxygen or hydrogen, but can also be used to assess differences between C/H/O after modification. For example, when grafting bromine-bearing initiator groups for SI-ATRP, elemental analysis can be used to determine the bromine content in order to calculate the degree of substitution of the modification. Similarly, FTIR can be used to confirm the presence of chemical groups that are characteristic of a specific modification. For example, when grafting acrylate polymers from CNCs, the presence of a carbonyl peak implies that the polymer is present.[104] XPS can be used to confirm the presence of new elements and provide high resolution spectra for chemical bond information. A useful high resolution spectra is that of carbon and can be used to differentiate between four different types of carbon: C1 (C-C), C2 (C-O-C), C3 (O-C-O) and C4 (C=O); all have different binding energies. Unmodified CNCs only contain C2 and C3, while the presence of C4 or an increase in C1 is indicative of most acrylate-based polymers.[48] If using XPS, samples must be extremely pure since the presence of any carbon contamination will show up in the C1 peak.[130] Additionally, XPS is strictly a surface characterization technique, so the thickness of the modification on the CNC surface will affect the results.

XRD can be used to evaluate any changes in CNC crystallinity after modification. In particular, the maintenance of the characteristic peak for cellulose I can confirm that the modification did not disrupt the CNC crystal structure. In the case of grafting amorphous polymers, the maintenance of the cellulose I peak will confirm that any reduction in the calculated crystallinity % is only due to the presence of polymer.[127]

TGA is often used to examine changes in thermal stability after CNC modification. TGA measures the mass of a given sample as a function of temperature and can be used to determine the temperature at which a material thermally degrades. For example, the covalent attachment of polymers to CNCs will often yield a secondary degradation curve attributed to the polymer.[125] In some cases in which the grafted polymer has a higher thermal stability than the CNC, this can lead to an overall improvement in the thermal stability, as indicated by an increase in the temperature at which CNCs usually degrade (166°C for sulfated CNCs in acid form).[31] If the difference in temperature between cellulose and polymer degradation is large enough, TGA can be used to estimate the wt. % of polymer based on the mass loss attributed to each component.

DSC is used to determine the glass transition temperature (T_g) of the grafted polymer. T_g is a measure of polymer chain mobility and is the temperature at which a “glassy” polymer transitions into a soft rubbery state.[131] Covalently attaching a polymer to a hard surface such as a CNC will reduce chain mobility and thus increase T_g. Therefore, DSC can be used to confirm the covalent attachment of polymer chains.

The most common method of ssNMR for CNCs is ^{13}C- CP-MAS-NMR, which is a powerful tool to characterize phase transitions, crystallinity, physical transformation, and chemical modification.[129] For chemical modification, chemical shifts assigned to the newly formed bonds can be detected and used to quantify the extent of CNC modification. In the case of polymer-grafting, ssNMR can be used to determine the graft length of the grafted polymer chains. Additionally, lsNMR and ionic liquids have been used to quantify chain length and the degree of modification of the cellulose backbone, with the latter not being possible though ssNMR. For either ssNMR or lsNMR, the complexity of the methods and analysis make them tedious as compared to the previously mentioned techniques. Regardless, either method is a powerful tool for surface-modified CNC characterization and can be considered when the cleavage of a surface-grafted polymer for analysis cannot be completed.

When trying to visualize surface-modified CNCs, TEM or AFM can be used.[129] When using TEM or AFM, sample preparation is very important in order to reduce aggregation and drying artifacts. Films for TEM are cast on continuous carbon or copper grids, while hard substrates like silicon wafers are used for AFM. In the case of modified CNCs, the type of solvent needed to properly disperse CNCs may be vastly different than water. In that case, the compatibility between your substrate and the solvent should be considered. Additionally, the type of CNC modification should be compatible with the substrate so that CNC deposition is maximized.

In order to assess the colloidal stability of CNCs, UV-vis spectrophotometry can be used. Transmittance mode is typically used, in which the amount of light that penetrates the suspension is detected and can indicate the presence of well-dispersed nanoparticles.[129] If particles are well-dispersed, less light is scattered and thus a higher transmittance value is recorded. In water, a wavelength of 500 nm is often used to assess the colloidal stability of CNC suspensions. If the CNC modification makes it incompatible with water, solvents can be used but measurements must be conducted at a wavelength at which the solvent does not absorb light. CNC concentrations of 0.5-3 wt. % are often used for these experiments but should be optimized based on the material synthesized.[129]

2.3 Latex-based Pressure Sensitive Adhesives

Pressure sensitive adhesives (PSAs) are adhesives that instantaneously adhere to a surface upon light pressure and can be removed with a light pulling force. The most common products that utilize PSA technology are tapes, labels, and film applications. The polymerization methods that are commonly used to produce PSAs include emulsion, solution, hot-melt or radiation curing. The emerging emphasis on sustainable processes in the polymer industry has made emulsion polymerization (i.e., latex)-based PSAs attractive due to their use of water as a reaction solvent, which can reduce the possibility of runaway reactions and offer a better control over final product properties.[15]

Emulsion polymerization is classified as a heterogeneous free-radical polymerization. During an emulsion polymerization, monomer droplets are stabilized *via* surfactant and dispersed throughout water; when surfactant is added above the critical micelle concentration, a small fraction of monomer is located inside micelles. After the addition of a water-soluble initiator, free radicals polymerize dissolved monomer in the water phase. As these chains grow, their affinity for monomer-swollen micelles increases to a point where they enter and continue to propagate by reacting with the monomer present in the micelle. This particle nucleation step is completed once all monomer-swollen micelles that are not nucleated disband to supply growing particles with surfactant and monomer (i.e. phase 1). Next, monomer droplets act as reservoirs for the growing particles, supplying monomer and surfactant as polymerization continues to take place primarily in nucleated particles, thus growing the nucleated particles (i.e. phase 2). Once all monomer droplets are used up, only residual monomer remains inside latex particles and is consumed in the presence of remaining initiator radicals (i.e. phase 3). A not-to-scale schematic of this process is shown in Figure 2.5.

For PSA applications, latex particles are often 100-300 nm in diameter in order to optimize latex viscosity and particle packing during film formation.[132] In order to obtain consistent particle sizes, a seeded semi-batch technique can be used in which the seed latex (produced *via* an initial batch process) acts as a nucleation agent and the feed stage (*via* continuous process) grows the seed particles to their desired size. In most cases, monomers used for the production of latexes for PSA production have slight water solubility which facilitates monomer diffusion between larger monomer droplets and growing polymer particles.[133] These latexes can be used as-synthesized to produce PSAs or modified with additives either post-polymerization or *in situ*. Once latex synthesis is complete, PSAs are produced by casting a wet film against a backing material (known as a carrier) and drying the film though the evaporation of the solvent (i.e. water).

PSAs are often comprised of multiple polymers that vary in their glass transition temperature (T_g). Low T_g polymers (< 0°C) are used for their tackiness and fluid-like behavior at ambient temperatures. The most common low T_g monomers include 2-ethylhexyl acrylate (EHA), n-butyl acrylate (BA) and isobutyl acrylate (IBA). Additionally, high T_g polymers (> 0°C) like methyl methacrylate (MMA), vinyl acetate (VAc) and styrene (St) are used to improve the cohesive strength of PSAs, generally being incorporated at low concentrations such that the stickiness of the low T_g polymers is not lost.[15] The ideal formulation is usually comprised of 70-90% low and 10-30% high T_g polymers; however, the ratio between the two is often dependent on the PSA properties targeted. PSAs comprised of the previously mentioned monomers and other acrylic esters have become the most competitive PSA formulations in recent times due to the balance achieved between final PSA properties, reproducibility, and compatibility with other additives.

Aside from the type of polymer used, there are other factors that will affect the adhesive properties of a latex-based PSA. The polymer microstructure (i.e., molecular weight, crosslinking density, gel content) can affect the adhesive and cohesive properties of a PSA.[15] For example, low molecular weight polymers show a high level of flowability and wettability toward a surface, which will translate to good adhesive properties. However, lower molecular weight often leads to a reduced crosslink network and in turn a reduced cohesive strength. Conversely, a high molecular weight will show an improved cohesive strength at the expense of adhesive strength. In common formulations, either chain transfer agents (CTAs) or cross linkers are used to either reduce or increase the molecular weight of the polymer(s) respectively, often leading to latex-based PSAs that would suffer from either low adhesive or cohesive strength.[133]

While the production of latex-based PSAs is more sustainable than solvent-based methods, such latex-based formulations often suffer from performance issues. Specifically, the fast evaporation of solvents and reactions with atmospheric oxygen during film formation result in solvent-based PSAs forming a continuous gel network with high cohesive strength, something harder to achieve given the slower evaporation of water from latex-based PSAs.[134] In order to improve the adhesive properties of latex-based PSAs, researchers have employed the use of nanomaterials. The presence of nanoparticles in a PSA would produce a strong interphase layer between the nanoparticle and the polymer chains, thus regulating the load transfer between the two and improving the overall mechanical strength.[135] This improvement would be especially beneficial for latex-based PSAs, which usually suffer from low cohesive strength. To date different nanoparticles have been used to form PSA nanocomposites, including nano-SiO_2, nanoclays, carbon nanotubes, and CNCs.[16]

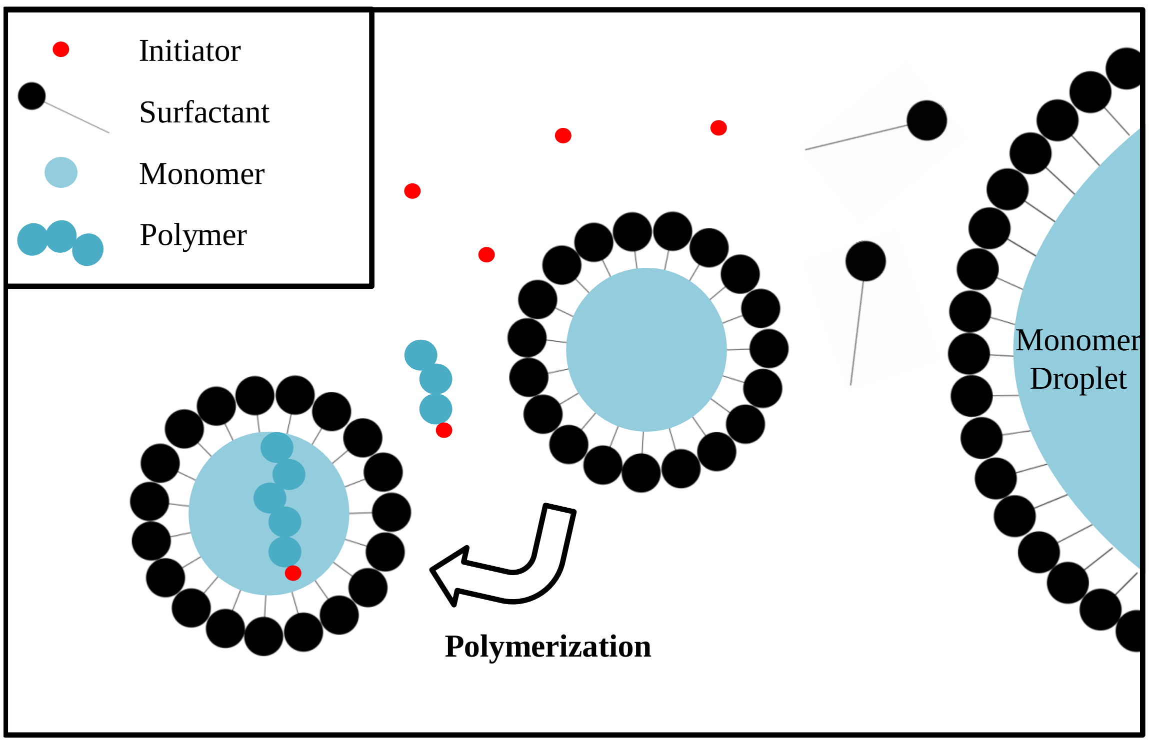

Figure 2.5. Emulsion polymerization schematic of polymer initiation in water phase, and then polymer chain growth in monomer-swollen micelles when the surfactant concentration is above the critical micelle concentration. Not drawn to scale.

2.3.1 Pressure Sensitive Adhesive Testing

PSAs are conventionally characterized by their peel adhesion, tack force, and shear strength. A summary of these tests is outlined in a review by Jovanović and Dubé[15] and described in the remainder of this section. Peel adhesion is the force required to peel a PSA film away from an adherend. These tests are often done with standard dimensions of a PSA film and on a standard surface with a pre-defined peel rate and angle (i.e. 90° or 180°). The mode of failure is also important when performing a peel test. While an adhesive failure is desired in which no residue remains after the adhesive is removed from the testing surface, cohesive failures (i.e., residues remain on substrate), unstable modes (i.e. the peeling force is unstable), or adhesive transfer (i.e., complete transfer of adhesive from support liner to test surface) may occur, all of which are undesired. Tack is defined as the ability of an adhesive to from a "quick" bond with another surface after brief contact with the adherend under light pressure. Tack depends not only on the interfacial and bulk properties of a PSA but also on the method used to measure tack. The three most common methods are 1) rolling ball, where a stainless steel ball is rolled down an inclined ramp of adhesive, 2) probe tack, where a probing material comes into contact with a PSA and pulled away, and 3) the loop method, where a loop of PSA comes into contact with a testing substrate and is pulled away at a 90° angle (Figure 2.6B). The differences between these testing methods and the metrics used to quantify them (i.e. displacement, force/probe area, force/unit area respectively) makes comparison between different test methods difficult. Lastly, shear strength is an indication of the adhesive's resistance to shearing forces and is related to the PSA's cohesive strength. The standard shear strength test is performed by applying a constant shear stress to an adhered sample and waiting until de-bonding occurs, similar to a creep test commonly used to assess the viscoelastic properties of polymers. As such, shear strength is measured in the number of hours it takes for an adhesive strip to fall after hanging a weight on it. A visual representation of these tests can be seen in Figure 2.6.

When testing PSAs, it is important that the environmental conditions, backing material, and adherend are kept constant. The choice of each of these factors is subject to change depending on the type of adhesive being produced and/or the standard chosen for use. The Pressure Sensitive Tape Council (PSTC) is a trade association responsible for PSA testing standards and has supplied a variety of testing methods for different PSAs for 60 years. For example, the standards chosen in chapter 4 of this thesis are PSTC16 (tack), PSTC101 (180° peel) and PSTC107A (shear), all which are done under room temperature and 50% relative humidity.[136]

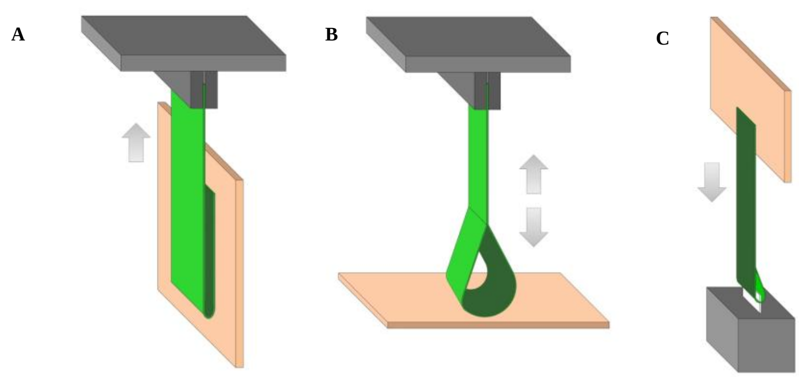

Figure 2.6. Graphical representation of A) peel strength, B) tack and C) shear strength PSA testing. Figure adapted from reference 148.

2.4 Polymer Latex Nanocomposites

Polymer nanocomposites have two phases: a polymer matrix and a dispersed phase containing a nanomaterial. The polymer matrix is the primary phase, making up most of the nanocomposite, while the dispersed phase is physically embedded into the polymer matrix. The addition of a nanomaterial to polymer latexes can improve both the latex (e.g. stability, viscosity) and casted film (e.g. mechanical, adhesive) properties, which can lead to product improvement or new applications all together.[14,16] In the context of a polymer *latex* nanocomposite, the primary phase would be latex polymer particles.

There are a variety of nanomaterials that have been employed as the dispersed phase for polymer latex nanocomposites, including spherical (e.g. nano-silicon dioxide, nano-titanium dioxide), fibrous (e.g. carbon nanotubes, nanofibers), layered (e.g. nanolayered silicate) and rod-shaped (e.g. cellulose nanocrystals) particles.[14,16] Nanomaterials are attractive due to their high specific surface area, surface chemistry and, in the case of fibrous or rod-shaped particles, high aspect ratio that can regulate a variety of chemical and physical interactions between the primary and dispersed phases. Additionally, a small amount of nanomaterial (0.5-5 wt. % total mass) is often enough to see substantial changes in desired properties like the ones previously mentioned.[14,16] This is attributed to high specific surface area of the nanomaterials and makes their use industrially feasible and cost-effective.

With the goal of producing more environmentally benign and sustainable polymer nanocomposites, the use of emulsion polymerization for the production of polymer latexes has become more popular. For coatings and adhesives, latex-based systems can eliminate the need for solvents during synthesis. Furthermore, the use of a sustainable nanomaterials (e.g. CNCs) can further reduce the environmental impact of a polymer latex nanocomposite. The following subsections investigate the use of CNCs in water-based polymer systems.

2.4.1 Cellulose Nanocrystals in Water-based Heterogeneous Polymer Systems

CNCs have been employed in dispersion, suspension, miniemulsion, and Pickering emulsion polymerization reactions, either as a particle stabilizer (Pickering stabilizer) or a co-stabilizer.[14] Additionally, CNCs have been used as an additive in miniemulsion and emulsion polymerization either though post-synthesis blending or *in situ* addition. We note here that the term “Pickering emulsion polymerization” defines any emulsion polymerization in which a traditional small-molecule surfactant was not used, regardless of the kinetic similarities to the traditional method that uses such a surfactant.

Both unmodified[137–145] and surface-modified CNCs[145–151] have been used as stabilizers for monomer droplets in water-based heterogeneous polymerization. The first series of reports on this topic was from Capron and co-workers, who were attempting to produce CNC-stabilized emulsions but polymerized their oil phases *via* suspension polymerization for imaging purposes.[33,152,153] Since then, other researchers have employed this method of CNC-based stabilization in suspension, miniemulsion, and Pickering emulsion polymerization intentionally. In a study by Limousin et al.,[139] CNCs were used to stabilize methyl methacrylate and butyl acrylate latexes in the presence of a cationic initiator. The use of said initiator promoted the adsorption of CNCs onto the monomer droplets, which resulted in the formation of highly coated polymer particles known as "armoured latex particles". The resulting latex had an improved Young's modulus but led to brittle films.[139]

A variety of surface modified CNCs has been used to stabilize monomer droplets, and the subsequent polymer particles, including carboxylated CNCs,[150] CNCs modified with alkyl compounds,[147,150] acetylated CNCs,[149] aldehyde CNCs,[151] and polymer-grafted CNCs.[145] In each case, the surface modification was employed as a way to improve droplet/particle stabilization as compared to using unmodified CNCs. Regardless of surface chemistry, using CNCs as stabilizers allows for the elimination of surfactants while still maintaining the potential to tune latex stability, particle size and viscosity.

When paired with electrostatically bound surfactants or auto-adsorbing polymers, CNCs can be used as a co-stabilizer. Work by Kedzior et al.[138] used CNCs with either anionic or cationic surface charge in conjunction with anionic or cationic surfactants to tune the polymer particle structure, showing that micrometer-sized particles could be achieved when using oppositely charged CNCs and surfactant. In addition, CNCs were combined with methyl cellulose (MC) to prepare PMMA particles with a double morphology.[148] In this example, PMMA nanoparticles were stabilized by excess MC via dispersion polymerization while MC-modified CNCs stabilized micrometer sized PMMA particles. While co-stabilized polymers do not achieve the same level of "greenness" as their CNC-only stabilized counterparts, these systems have shown to provide a high level of particle size tunability.

Recently, a study by Jiménez-Saelices et al.[143] used CNCs in suspension polymerization and investigated the effect of monomer water solubility on latex particle size. This worked showed that the monomer solubility in water was a key factor for tuning the particle size distribution. For example, the stabilization of styrene monomer resulted in both a nano- and micron-sized droplets (and later polymer particles) while the use of the more hydrophobic monomer lauryl methacrylate resulted in only micron-sized droplets/particles. Additionally, the use of both oil and water-soluble initiators yielded both micro- and nanoparticles from isobornyl acrylate despite there only being micron-sized droplets prior to polymerization, suggesting the importance of initiator on latex particle size. Building on this, Glasing et al.[145] produced CNC and polymer-grafted CNC stabilized latexes via microsuspension polymerization and investigated the effects of initiator solubility and surface charge on particle size. The results showed that the polymer-grafted CNCs could produce smaller (5-9 μm) styrene droplets than unmodified CNCs (18-20 μm); additionally, initiators with slight water solubility produced surfactant-free nanoparticles, which was a result of homogenous nucleation in the water phase.

Overall, these studies showed that not only CNC type and concentration but also monomer and initiator solubility characteristics will affect the particle size of CNC/polymer latexes.[143,145]

Cellulose Nanocrystals in Emulsion Polymerization

As an additive to emulsion polymers, CNCs have been either blended post synthesis or added *in situ* during latex polymererization.[14] The first ever CNC/polymer nanocomposite was reported by Favier et al.[154] in 1995, who blended CNCs and acrylic latex. While these methods are straightforward, CNC incorporation though blending is often done by first dispersing CNCs in water at low concentrations, which in turn dilutes the resulting CNC-loaded latex. Since most applications call for high concentration latex (> 30 wt.%) to be used, the post-blending method can be problematic. Adding dried CNC powders to latexes does not result in uniform CNC dispersion, and extensive mixing/sonication can damage the latex; as such, this is not a recommended route. Overall, blending CNCs into a range of latexes has been employed in the last 25 years and generally improves the mechanical properties of water-borne heterogeneous polymer systems.[14]

The alternative to blending is to incorporate the CNCs *in situ,* by which they are distributed in the water phase of the reaction before polymerization. In this case, no dilution of the latex is necessary since the water designated for the reaction can be used to disperse the CNCs. This method also eliminates the need for post-synthesis processing and can lead to more cost-effective one-pot nanocomposite production methods. The first case of incorporating CNCs *in situ* was reported by Mabrouk et al.[155] for a poly(styrene-co-hexylacrylate) latex produced *via* miniemulsion polymerization. The addition of 5 wt.% (based on monomer mass) of CNCs to a 20 wt.% (of polymer) latex enhanced the storage modulus of the latex by 500% when above the glass transition temperature of the polymer. In this case, the CNCs alone were not able to stabilize the latex, so reactive silane was added.

To ensure that CNCs stay un-aggregated during polymerization, the dispersion of CNCs in the suspension before adding them to the reaction mixture has been investigated. For example, Dastjerdi et al.,[17,156] Ouzas et al.,[157,158] Pakdel et al.,[159] and Gabriel et al.[160] demonstrated that for CNC-loaded emulsion polymerization reactions spray dried CNCs should be magnetically stirred for one hour before undergoing three 5 minute probe sonication cycles (in an ice bath with resting periods between each cycle to minimize heat build-up). Other considerations include the type of surfactant used (where oppositely charged surfactant to the surface charge of the CNCs may induce CNC-surfactant interactions which are undesired if CNCs need to remain dispersed though the water phase), pH, and system impurities, all of which affect latex stability, polymerization kinetics, CNC colloidal stability, and thus the properties of the final latex. Additional considerations are needed when working with hydrophobic CNCs, which must be dispersed into the oil phase to minimize aggregation in water.

Another challenge when adding CNCs *in situ* during polymerization is the limitation of loading CNCs without inducing polymer coagulation or low monomer conversion. To date, CNC suspensions have been loaded into the reactor using the available water for the reaction either with other reactants for a miniemulsion[155,161–163] or added in the seed[16,156–160] (i.e., batch) for semi-batch emulsions. CNC loadings are generally limited to maximum 2 wt.% (based on monomer mass) to reduce complications associated with increased viscosity and mixing issues that can jeopardize the stability of a given system.

Loading limitations are especially present when using hydrophobic CNCs, for which dispersing in water is not possible. From this, the oil phase must be used as a dispersing medium in order to obtain a proper dispersion of CNCs, which can further limit the concentration of hydrophobic CNCs added since the oil phase is often less than 50% of the total latex mass. This method of hydrophobic CNC dispersion in the oil phase has been employed in previous work[164] to disperse poly(butyl acrylate)-grafted CNCs (PBA-*g*-CNCs) into methyl methacrylate monomer before a miniemulsion polymerization. The goal was to incorporate PBA-*g*-CNCs inside the monomer droplets such that they would be incorporated into the latex particles after polymerization (Figure 2.7)[164]. We note that CNCs that remain in the monomer/polymer phase must be hydrophobic and unaggregated; intermediate wettability would favor CNCs as Pickering emulsifiers at the monomer-water interface, while aggregation would make the CNCs too large for incorporation into the polymer particles.[164] The same method of dispersing polymer-grafted CNCs into the monomer phase prior to polymerization was employed in the work described in Chapter 4 to maximize the efficiency of polymer-grafted CNC loading, herein using a semi-batch emulsion polymerization instead of a miniemulsion polymerization.

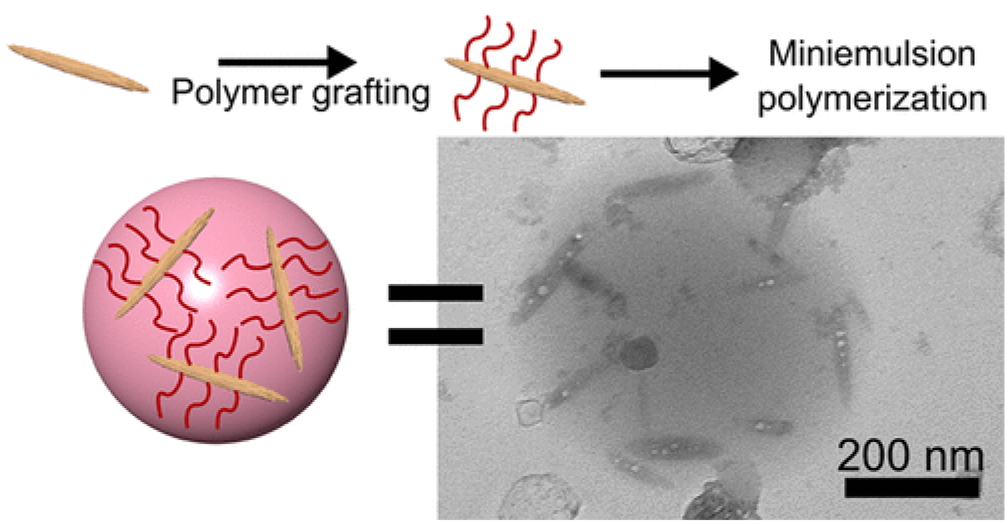

Figure 2.7. Schematic showing polymer-grafted cellulose nanocrystals incorporated into PMMA latex particles. Figure reproduced from reference 135.

Cellulose nanocrystals in Latex-based Pressure Sensitive Adhesives

As mentioned, CNCs have been incorporated into latex-based PSAs either though post-synthesis blending[17] or *in situ* addition.[17,156–160,165] Adding CNCs *in situ* has become the preferred way of making CNC-latex PSAs, leading to significant adhesive property enhancement compared to blending. For example, Dastjerdi et al.[17] showed that a CNC-poly(butyl acrylate-co-methyl methacrylate) latex to which CNCs were added *in situ* offered a 3.8× improvement in tack, a 6× improvement in peel, and a 20× improvement in shear strength; CNCs added though post-synthesis blending offered a 2.4× improvement in tack, a 1.5× improvement in peel, and a 6.4× improvement in shear strength. . Regardless of the CNC incorporation method, CNCs were able to improve all three PSA properties, which is very uncommon for PSAs containing nanoparticles for which normally the improvement in adhesive strength results in a decrease in cohesive strength (or vice versa).[17] The improvement of latex-adhesive performance with the addition of CNCs was attributed to the presence of well-dispersed CNCs throughout the water phase, leading to a good distribution of CNCs after film formation. Other effects include changes in wettability, an improved crosslinked network, and film forming abilities, all which were attributed to the addition of CNCs.

CNCs have been employed for a variety of co-polymer formulations, which are summarized in Table 2.2. While a variety of polymers has been used, their compatibility with CNCs can affect the ability for CNCs to improve PSA properties. When using polar monomers, Pakdel et al.[159] found that the addition of 4 wt. % of acrylic acid improved PSA shear strength by 8 h, but by 70 h in the presence of CNCs. This synergistic effect was attributed to the compatibility between acrylic acid and CNCs, between which could from strong hydrogen bonds between the carboxyl and hydroxyl groups.[159] This work further exemplified the necessity for CNC/monomer compatibility in PSA formulations. With more hydrophobic formulations, CNC/polymer incompatibility can affect the dispersion quality of CNCs. This was observed in the case of a CNC-poly(2-ethyl hexyl acrylate-co-butyl acrylate-co-methyl methacrylate) latex, for which the hydrophobicity of 2-ethyl hexyl acrylate resulted in CNC aggregation during the polymerization.[157] While the resulting CNC-polymer latex adhesive still showed improved adhesive properties, it was hypothesized that an improved compatibility between CNCs and the monomers would result in a further improvement.

Table 2.2. Summary of latex-based PSAs containing CNCs in literature to date.

Monomers used	CNC type	CNC addition	Parameters studied	Key conclusions	Refs.
BA/EHA	Unmod. CNC	*In situ*	Effect of CNC loading on PSA properties	-CNC addition up to 4 wt. % could improve PSA peel and shear strength (176 and 518%) -CNC addition up to 2 wt. % could improve probe tack before decreasing due to PSA surface roughness -CNCs can improve all PSA properties	165
BA/MMA	Unmod. CNC	*In situ*/blend	Effect of CNC loading: *in situ* vs blending	-*in situ* addition improved tack, peel strength and shear by 3.8, 6, and 20x respectively and was higher than that of blending (2.4, 1.5, 6.4× for blend) -Increased PSA wettability attributed to addition of CNCs	17
IBA/BA/MMA	Unmod. CNC		Novel formulation	-Addition of CNC improved all PSA properties -Improvement in shear strength due to possible CNC/polymer grafting or hydrogen bonding	158
EHA/BA/MMA	Unmod. CNC	*In situ*/blend	Effect of latex hydrophobicity	-Addition of EHA reduced CNC-particle interactions and lead to poor distribution of aggregation of CNCs in latex and inhibited PSA improvements -Compatibility between monomers and CNCs is important for PSA optimization	157
BA/St/AA	Unmod. CNC	*In situ*	Effect of high (< 2 wt.%) CNC loadings and loading location on PSA properties	-Location of CNC addition (i.e. seed, feed, or both) did not have an significant effect on PSA properties -High CNC loadings improve shear strength but decrease tack and peel strength -CNC concentration in water when added *in situ* must not be too high such that aggregation occurs prior to latex synthesis	160
BA/VAc/AA	Unmod. CNCs	*In situ*	Effect of AA, sodium dodecyl sulfate (SDS) and chain transfer agent (CTA) on PSA properties	-AA strengthened CNC/polymer interactions and improved shear strength -Increasing SDS reduces tack and peel but was exaggerated in the presence of AA -CTA addition at high CNC concentrations drastically reduced shear strength, suggesting CNC/polymer physical interactions	159
BA/EHA/HEA/MMA/AA	Unmod./ γ-MPA CNCs (fCNC)	*In situ*	Effect of fCNCs on PSA performance	-Reactive vinyl groups on γ-MPA incorporated fCNCs into or on polymer particles, improving dispersion in PSA. -PSA tack and peel strength with fCNC was superior to PSAs with unmod. CNC but shear was unchanged	166
BA/VAc/AA	Unmod. CNCs/ Jeffamine-modified CNCS (CNC-103)	*In situ*	Effect of less hydrophobic and surface charged CNCs on PSA properties	-CNC-103s were closely associated with polymer during film formation, improving their dispersion in PSA -Tack and peel of PSAs with CNC-103 was superior to PSAs with unmod. CNCs -Better dispersion of CNC-103 improved film wetting/chain stretching but reduced the elasticity of the PSA (low shear strength)	167

To date, there are only two reports that use "less hydrophilic" CNCs in latex-based pressure sensitive adhesives. Yu et al.[166] modified CNCs with 3-methacryloxypropyltrimethoxysilane coupling agent (γ-MPA) and incorporated them *in situ* into a poly(butyl acrylate-co-2 ethyl hexyl acrylate-co-2 hydroxyethyl acrylate-co-methyl methacrylate-co-acrylic acid) latex. The resulting PSAs containing γ-MPA CNCs exhibited a better tack and peel strength than those with unmodified CNCs, while the improvement in shear was the same for both CNC types. Due to the presence of reactive vinyl groups on γ-MPA, copolymerization between the bulk polymer and γ-MPA occurred, embedding γ-MPA CNCs into polymer particles *via* covalent grafting.[166] Pakdel et al.[167] also explored the use of less hydrophilic CNCs (CNC-103) in latex-based PSA formulations, with CNC-103 addition *in situ* outperforming unmodified CNC (CNC-101)-loaded PSAs in both tack and peel strength. The superior tack and peel was attributed to the improved compatibility between CNC-103 and the polymer by which, upon film formation, CNCs were less aggregated. However, PSAs containing CNC-103 exhibited lower shear strength than PSAs containing CNC-101, with the formation of small CNC-101 aggregates acting as polymer chain anchors to improve cohesive strength.[167] While the use of "less hydrophobic" CNCs were demonstrated in the above studies, the effect of incorporating hydrophobic CNCs into polymer latexes on PSA properties has yet to be investigated. In particular, through the use of polymer grafting, CNCs can be surfaced-modified with the exact same surface chemistry as the polymer latex particles, further offering advantages in improving compatibility and dispersion throughout the polymer matrix.

In this thesis, polymer-grafted CNC-poly(butyl acrylate) latex-based PSAs were produced *via* semi-batch emulsion polymerization. The polymer-grafted CNCs were produced *via* SI-ATRP and added *in situ* at concentrations of 0.5 and 1 wt.% (based on monomer mass) to evaluate the effect of CNC concentration on the adhesive properties. Two polymers commonly used in PSAs but with different T_g values (poly(butyl acrylate) and poly(methyl methacrylate)) were used to evaluate the effect of polymer T_g and compatibility with the bulk latex. Additionally, two chain lengths were used to evaluate the effect of a low and high DP on CNC incorporation and adhesive properties. To our knowledge, this is the first time that polymer-grafted CNCs have been used in a latex-based PSA formulation.

Chapter 3: Effect of Reaction Media on Grafting Hydrophobic Polymers from Cellulose Nanocrystals via Surface-initiated Atom Transfer Radical Polymerization

3.1 Abstract

Hydrophobic polymer-grafted cellulose nanocrystals (CNCs) were produced *via* surface-initiated atom transfer radical polymerization (SI-ATRP) in different solvents to examine the role of reaction media on the extent of surface modification. Poly(butyl acrylate)-grafted CNCs were synthesized in either dimethylformamide (DMF) (D-PBA-*g*-CNCs) or toluene (T-PBA-*g*-CNCs) alongside free polymer from sacrificial initiator, which was analyzed by gel permeation chromatography. UV-visible spectroscopy in transmittance mode was used to evaluate the colloidal stability of unmodified CNCs, initiator-modified CNCs and PBA-*g*-CNCs in suspension in water, DMF, and toluene. The enhanced colloidal stability of initiator-modified CNCs in DMF led to improved accessibility to surface initiator groups during polymer grafting, with D-PBA-*g*-CNCs facilitating up to 30 times more grafted chains relative to T-PBA-*g*-CNCs as determined by thermogravimetric and elemental analysis. Consequently, D-PBA-*g*-CNCs dispersed well in toluene and were hydrophobic, with high molecular weight (>13 kDa) grafted CNCs resulting in a water contact angle of 124^o compared to 25^o for similar CNCs grafted in toluene. X-ray diffraction and transmission electron microscopy confirmed that the cellulose crystal structure was preserved and that individual nanoparticles were retained when grafting was carried out in either solvent. This work highlights that optimizing CNC colloidal stability in a given solvent prior to grafting is a more crucial consideration than solvent–polymer compatibility to obtain high graft densities and highly hydrophobic CNCs *via* SI-ATRP.

3.2 Introduction

Cellulosic materials that have at least one dimension in the nanoscale are referred to as nanocellulose. Nanocellulose is organized into three categories: bacterial nanocellulose (BNC), produced through the fermentation of sugars and plant carbohydrates *via* microorganisms, cellulose nanofibrils (CNFs), produced after mechanically disintegrating cellulose fibers, and cellulose nanocrystals (CNCs), produced *via* chemical hydrolysis or oxidation.[2] Due to their extraction from renewable resources and their potential to replace existing non-renewable materials, nanocelluloses have gained popularity over the last two decades, with their suggested use in a wide range of applications.[2]

Unlike CNFs and BNC, plant-derived CNCs are rigid, rod-like nanoparticles that are nano-sized in all dimensions. CNCs are most commonly produced through a sulfuric acid hydrolysis process that results in sulfate half-ester groups being grafted to the nanoparticle surface, imparting a negative surface charge and colloidal stability in polar solvents. The abundance of hydroxy groups in the cellulose structure additionally makes CNCs highly water compatible and, as such, they are generally considered hydrophilic. However, the arrangement of cellulose chains into the cellulose I crystal structure results in a hydrophobic crystal plane edge void of hydroxy groups which may give CNCs somewhat amphiphilic properties.[153] Furthermore, the rigid and crystalline nature of CNCs gives them exceptional mechanical properties, making them highly-promising as additives for improving the mechanical strength of polymer and cement nanocomposites.[1,13,10]

The colloidal stability of CNCs produced *via* sulfuric acid hydrolysis in aqueous media has been previously studied.[168] CNCs form stable suspensions in water between pH values of 3 and 11; highly acidic conditions can cause further hydrolysis of CNC chains[169] while highly basic conditions are known to desulfate CNCs,[170] causing destabilization of the suspension. The colloidal stability of CNCs in polar organic solvents such as dimethylformamide (DMF) and dimethyl sulfoxide has also been studied, with stable suspensions shown to be possible.[171] However, other organic solvents such as ethanol, chloroform, toluene, and other non-polar organic solvents are not good dispersing media for CNCs, limiting their use in reactions and processes that require such solvents.

To solve the inherent compatibility issues between CNCs and non-polar solvents (and by extension, hydrophobic polymers often used in nanocomposites), a variety of surface modification routes have been employed to improve CNC hydrophobicity. These methods include non-covalent modifications (i.e. adsorption),[13,39] small molecule covalent modifications such as esterification, etherification, silylation, amidation and urethanization,[1,2,38] and polymer grafting.[11,12] The most common non-covalent modification routes involve the adsorption of auto-adsorbing polymers or cationic surfactants. As an example of the adsorption route, Khandal et al.[172] modified CNC surfaces with polyethyleneimine (PEI) *via* physical adsorption to change the rheological properties of CNC suspensions. The modification of CNCs showed no change in nanoparticle morphology, suggesting that a very thin and uniform layer of PEI was present on the surface. As an example of a small molecule functionalization route, Yoo and Youngblood[173] functionalized CNC surfaces with poly(lactic acid) oligomers and various fatty acids though a two-step esterification and demonstrated improved compatibility with solvents such as chloroform and toluene due to their enhanced hydrophobicity. However, polymer grafting serves to covalently attach polymer chains which can lead to a variety of different surface chemistries and morphologies as compared to other methods of CNC modification.

Polymer grafting can be achieved by grafting already synthesized polymer chains to the CNC surface (grafting *to*) or growing new polymers from the CNC surface (grafting *from*). In the work by Araki et al.,[174] polymer grafting *to* was used to sterically stabilize CNCs, pioneering the field of polymer grafting with nanocellulose. Polymer grafting *to* is beneficial since the polymer can be synthesized and characterized before it is attached to the CNCs. However, steric hindrance limits the density of polymer chains that can be grafted.[12] When grafting *from* is used, polymer chains can be grown directly from hydroxy groups on the cellulose surface though free radical or ring-opening polymerizations or through a controlled radical polymerization method in which initiator-bearing chemical groups are first immobilized on the CNC surface. Carlmark and Malmstrom,[98]demonstrated surface-initiated atom transfer radical polymerization (SI-ATRP) grafting of poly(methyl acrylate) from cotton filter paper as the first reported case of controlled radical polymerization from the surface of cellulose. Polymer grafting *from* techniques allow for a much higher density of grafting compared to grafting *to* but often require multiple steps due to the need for initial initiator attachment and lengthy purification protocols; furthermore, characterization of the resulting polymer chain length, grafting density and polymerization kinetics is much more challenging since the reaction occurs directly from the interface rather than in free solution.[104]

SI-ATRP with CNCs has gained popularity in the last two decades.[12] As a controlled radical polymerization, SI-ATRP can produce polymers with low dispersity values that make comparing the effects of polymer molecular properties straightforward. Additionally, the range of solvents that can be used for SI-ATRP allows for a variety of hydrophilic[103,105,120–123,125,127,175–178,107,179,180,110–114,117,118] and hydrophobic[41,101,128,181–185,102,104,106,108,112,116,124,125] polymers to be grafted. The most common hydrophilic and hydrophobic polymers grafted *via* SI-ATRP from CNCs are poly(N-isopropylacrylamide)[105,110–114] (PNIPAM) and polystyrene,[41,102,104,112,124], with PNIPAM employed for its thermoresponsive properties and polystyrene as a model system that has been grafted from a variety of substrates in literature and is capable of enhancing CNC compatibility in polymer composites. The critical first step enabling SI-ATRP is the attachment of an initiator-baring group to produce macroinitiated CNC surfaces. This is typically done in organic solvents like DMF and uses trimethylamine (TEA) and 4-(dimethylamino)pyridine (DMAP) to attached alpha-bromoisobutyryl bromide (BiB) to the CNC surface *via* esterfication.[12] Additionally, the highly crystalline nature of CNCs can withstand the slightly acidic conditions that arise during BiB-modification, despite evidence that suggests minor defects can arise as a result of the reaction.[183] In contrast, the less crystalline nanocelluloses like CNFs can undergo degradation of the amorphous regions present in each nanofibril under such reaction conditions, making SI-ATRP of CNFs challenging.[186]

The effects of CNC properties and SI-ATRP reaction parameters on polymer grafting have been studied previously. CNC properties like BiB grafting density,[105,106] ATRP initiator source,[182] and CNC surface charge[179] have been investigated to optimize polymer grafting *via* SI-ATRP. Studies on BiB grafting density have shown that there is a threshold of BiB groups that can be initiated during SI-ATRP, limiting the number of polymer chains that can be grafted from the surface due to steric hinderances.[105,106] Using a secondary ATRP initiator such as 2-bromopropanoic acid results in larger dispersity values, suggesting that the use of BiB provides better control over the polymerization.[182] Lastly, CNCs with higher anionic sulfate half-ester group densities yield higher grafting efficiencies at the expense of higher polymer dispersities when grafting is performed in aqueous media due to inefficient radical deactivation.[179] The effect of catalyst source can also affect polymer grafting efficiency, with copper wire treated with hydrochloric acid resulting in polymer-grafted CNCs that required little post-synthesis purification.[181] Overall, the number of publications that focus on the optimization of polymer grafting *from* CNCs *via* SI-ATRP is low compared to the total number of papers discussing polymer grafting to CNCs, highlighting the potential for future optimization of this polymerization technique.

A variety of solvents has been used when grafting polymers *from* CNCs, including water,[179] water/methanol,[105,110–114,177] methanol,[103,180] water/DMF,[178] DMF,[106,107,124,125,127,175,108,116–118,120–123] DMSO,[181,183] DMF/THF,[184] THF,[109,185] toluene,[115,128] anisole,[41,104,112,182] and chlorobenzene.[101] When grafting hydrophobic polymers *from* CNCs *via* SI-ATRP, polar solvents such as DMF or non-polar solvents like toluene have most commonly been used but are never compared directly. The choice of solvent can affect multiple parameters of the grafting reaction, with increasing solvent polarity resulting in an increase in the ATRP equilibrium rate constant (thereby accelerating the rate of polymerization[100]) and better dispersion of BiB-modified CNCs prior to grafting; however, if the polymer graft is hydrophobic, non-polar solvents are more compatible with the produced polymer and thus polymer-modified CNCs after the grafting reaction. While solvent polarity can thus have competing effects on the SI-ATRP reaction, the comparative benefits of using more or less polar solvents to graft hydrophobic polymers *from* CNCs have not yet been explored.

In this work, we directly compare the grafting of the hydrophobic polymer poly(butyl acrylate) (PBA) to CNCs using either toluene or DMF as the solvent, keeping all other reaction conditions and purification steps constant. To our knowledge, this is the first known comparison of the effect of reaction solvent on the grafting of a hydrophobic polymer from *any* surface *via* SI-ATRP (not just CNCs). The resulting polymer-grafted CNCs were characterized using a variety of bulk techniques (Fourier-transform infrared spectroscopy, elemental analysis, thermogravimetric analysis, UV/visible spectroscopy, x-ray diffraction, and gel permeation chromatography) and surface characterization methods (transmission electron microscopy, contact angle). The resulting insight into the benefits of using a specific reaction solvent for SI-ATRP with CNCs is beneficial to optimize the grafting of hydrophobic polymers from CNCs and may find broader use in tailoring the compatibility of this and other nanoparticles in polymer composite systems.

3.3 Experimental Section

4.3.1 Materials

α-bromoisobutyryl bromide (BiB), ethyl α-bromoisobutyrate (EBiB), N,N,N′,N″,N″-pentamethyldiethylenetriamine (PMDETA), copper (I) bromide (CuBr), 4-(dimethylamino)pyridine (DMAP), trimethylamine (TEA), dichlorodimethylsilane, aluminum oxide, hydrogen peroxide and ethylenediaminetetraacetic acid (EDTA) were purchased from Sigma Aldrich and used as received. Dimethylformamide (DMF) (anhydrous, 99.8%), toluene (anhydrous, 99.8 %), acetonitrile (ACS reagent, ≥ 99.5%), xylenes (ACS reagent, ≥ 99.5%), ethanol (95%), tetrahydrofuran (THF) (for HPLC, ≥ 99.9%) and sulfuric acid were purchased from Caledon Labs. Polyallyamine hydrochloride (PAH, Mw = 120 000 – 200 000 g/mol) was purchased from Polysciences. Butyl acrylate (BA) was purchased from Sigma Aldrich and passed through a column of basic aluminum oxide prior to use. All water used was purified using a Barnstead GenPure Pro water purification system from ThermoFisher Scientific. Unmodified cellulose nanocrystals were provided as a spray dried powder (in the sodium form) by CelluForce Inc.

3.3.2 Preparation of Initiator-modified CNCs (BiB-CNCs)

Initiator-modified CNCs (BiB-CNCs) were produced by using a similar protocol to Kedzior et al.[164] First, 2 g of dried CelluForce CNCs were re-dispersed in 200 mL of DMF by stirring for 24 h and bath sonicating (Bransonic Ultrasonic MH, Branson) for an additional 2 h in a 500 mL round bottom flask. Under magnetic stirring, 4 mL of TEA was added followed by a catalytic amount (~ 0.5 g) of DMAP. The suspension was sealed with a rubber septum and degassed with argon for 1 h, followed by the addition of 4 mL of BiB added dropwise with continuous argon flow during the addition. The suspension was degassed for an additional 5 min with argon before being placed in a 70°C oil bath for 18 h, after which the reaction was terminated by exposing the suspension to air. The BiB-CNCs were purified through centrifugation (Allegra 64R, Beckman) at 5000 RPM for 15 min at 15°C. The BiB-CNCs were then re-dispersed in ethanol and centrifuged at 7000 RPM for 5 min at 15°C three times before being re-dispersed in water and dialyzed against purified water for 15 x 6 h cycles to remove any unreacted reagents and DMF. Finally, the purified BiB-CNCs were freeze dried (Benchtop Manifold BT85A, MillRock) and stored for further use.

3.3.3 Synthesis of Polymer-grafted CNCs via SI-ATRP in Toluene and DMF

In a typical reaction, 1 g of BiB-CNCs was mixed in 100 g of toluene or DMF for 24 h though magnetic stirring and bath sonicated for 2 h. The suspension was then transferred to a 250 mL round bottom flask, at which point purified monomer was added along with PMDETA and EBiB as sacrificial initiator. The components were added in a molar ratio of x:1:1:1 BA:PMDETA:EBiB:CuBr where x is the desired degree of polymerization (DP) of the grafted polymer. The suspension was sealed with a rubber septum and degassed with argon for 1 h in an ice bath before adding CuBr (catalyst). The suspension was degassed for an additional 15 min before the round bottom flask was moved to a 70°C oil bath with magnetic stirring and left to react for 18 h. The reaction was stopped by exposing the round bottom flask to air. The reaction mixture was centrifuged at 10,000 RPM for 15 min and the first supernatant, containing free polymer dissolved in solvent, was collected. The polymer grafted-CNCs were purified through repeated washing and centrifugation in methanol until the supernatant was clear. The purified polymer grafted-CNCs were redispersed in toluene and added to a separation funnel containing a 0.5 wt. % EDTA mixture in water to remove any residual Cu catalyst before being vacuum dried and collected for use. The free polymer was purified in a column of neutral aluminum oxide and precipitated in cold methanol to remove any remaining Cu catalyst. CNCs with high (H) and low (L) degrees of polymerization (DPs) were synthesized. The target DPs of polymer-grafted CNCs synthesized in toluene (T-PBA-g-CNCs) were 70 (T-PBAL-g-CNCs) and 150 (T-PBAH-g-CNCs), while for those produced in DMF (D-PBA-g-CNCs) the target DPs were 50 (D-PBAL-g-CNCs) and 100 (D-PBAH-g-CNCs).

3.3.4 Fourier-transform Infrared Spectroscopy (FTIR)

Spectra were obtained from KBr pellets containing 10 mg of unmodified CNCs, freeze-dried BiB-CNCs and vacuum-dried polymer grafted-CNCs using a Nicolette 6700 spectrometer operating in absorbance mode. All spectra were collected with a 4 cm-1 resolution and 32 continuous scans.

3.3.5 UV-visible Spectroscopy/transmittance

UV-visible spectroscopy was performed on a Cary 5000 UV-Vis-NIR (Santa Clara, CA) operating in transmittance mode with the wavelength set to 500 nm for all experiments. CNC, BiB-CNC, and PBA-g-CNC suspensions in water, DMF and toluene were evaluated at a concentration of 10 mg/mL. Measurements were taken 30 minutes after shaking samples. Additionally, data points were omitted if the sample was unable to disperse into a given solvent (i.e. high transmittance due to no dispersion). Triplicate measurements of each sample were performed to calculate the average and standard deviation of the transparency for each sample.

3.3.6 Elemental Analysis

Bromine elemental analysis was performed on freeze-dried BiB-CNC samples to obtain the mass percent of Br determined via Schoniger Combustion by Midwest MicroLab (Indianapolis, IN). C/H/N/S combustion elemental analysis (UNICUBE in C/H/N/S mode, Elementar, Langenselbold, Germany) was performed on unmodified CNCs, BiB-CNCs and polymer grafted-CNCs to quantify the mass fractions of carbon and hydrogen. Triplicate measurements of each sample were used to calculate the average and standard deviation of the carbon and hydrogen mass fraction.

3.3.7 Thermogravimetric Analysis (TGA)

Thermogravimetric analysis (TGA) was performed on dried unmodified CNCs, BiB-CNCs, polymer grafted-CNCs and free polymer using a Simultaneous Thermal Analyzer (STA) 6000 from PerkinElmer (Waltham, MA). All CNCs were in the acid form so that comparisons could be made between samples. In each experiment, the dried material (5 mg) was placed in the instrument pan and loaded under argon. The chamber was heated from 30°C to 600°C at a rate of 10°C/min under argon.

3.3.8 Gel Permeation Chromatography (GPC)

Gel permeation chromatography samples were prepared by dissolving a small amount (5-7 mg) of the dried free polymer obtained from the sacrificial initiator added during SI-ATRP from both DMF and toluene reactions in a 1 mg/mL solution in THF. Molecular weight and dispersity were analyzed by a Waters 2695 separations module equipped with a Waters 2414 refractive index detector (Milford, MA) and a Jordi Fluorinated DVB mixed-bed column (Mansfield, MA). Polystyrene standards were used for calibration, with an eluent flow rate of 2 mL/min.

3.3.9 Water Contact Angle

Contact angle samples were produced by drop casting a 1 wt. % suspension of D-PBA-g-CNCs in toluene, T-PBA-g-CNCs in acetonitrile, or unmodified CNCs in water onto a piranha-cleaned silicon wafer 10 times to ensure full coverage of the substrate surface. Measurements were obtained using the sessile drop method on a Future Digital Scientific OCA 20 High Speed Contact Angle Measurer (Westbury, NY). Water contact angle images and measurements were captured both 2-3 s and 1 min after placing the purified water droplet on the sample. Triplicate images were processed using SCA 20 (Filderstadt, Germany) and used to calculate the average and standard deviation of the contact angle for each sample.

3.3.10 X-ray Diffraction (XRD)

XRD measurements were performed using a Bruker D8 DAVINCI diffractometer (Bruker, USA) with a cobalt sealed tube source (λ_{avg}=1.79026 Å), 35 kV, 45 mA with a parallel focus Goebel Mirror, VANTEC 500 area detector and 0.5 mm micro slit and 0.5 mm small collimator over a 2θ range of 8-45º. Si wafer blanks were subtracted from all measurements. Two-dimensional area detector frames were integrated to produce diffraction patterns which underwent Rietveld refinement. Percent crystallinity was calculated though deconvolution using the cellulose I single crystal information file (CIF) with a linear background and a fixed amorphous peak at 24.1º. Samples were prepared by freeze-drying BiB-CNCs, vacuum drying PBA-g-CNCs, or using CelluForce CNCs as received.

3.3.11 Transmission Electron Microscopy (TEM)

TEM images were acquired on a JEOL 1200 EX TEMSCAN microscope operating at 80 kV. Samples were prepared by drop-casting 0.01 wt. % CNC, BiB-CNC, or PBA-g-CNC suspensions onto either Formvar-coated (for CNCs, BiB-CNCs and D-PBA-g-CNCs) or carbon-coated (for T-PBA-g-CNCs) copper TEM grids and air dried until no solvent remained. CNCs and BiB-CNCs were drop-casted from suspensions in water, while PBA-g-CNCs were drop-casted from suspensions in toluene to reduce aggregation after drying. A 1 wt. % uranyl acetate stain was used in order to better visualize the CNCs and BiB-CNCs and to enhance CNC visibility in both PBAH-g-CNC samples.

3.4 Results

To allow for SI-ATRP-mediated polymer grafting from CNCs, the CNCs were first surface modified with the BiB initiator through the esterification of cellulose surface hydroxy groups (Figure 3.1, first step). Two batches of BiB-modified CNCs (BiB-CNCs) were produced by the reaction of BiB with CNCs in DMF. Elemental analysis indicated that both batches had similar bromine contents of 5.8 and 7.4 wt. %, corresponding to 1.05 and 1.40 BiB groups per nm^2 of CNC surface area or 4600 and 6100 BiB groups per CNC respectively (Table 3.1). Details of BiB density calculations based on elemental analysis results are provided in the Supporting Information (Appendix A). These bromine content values are comparable to other reports of BiB-CNCs,[109,118,175,180,181] with only a small fraction of those surface initiator groups normally reported to lead to chain growth[105] due to steric hindrance.

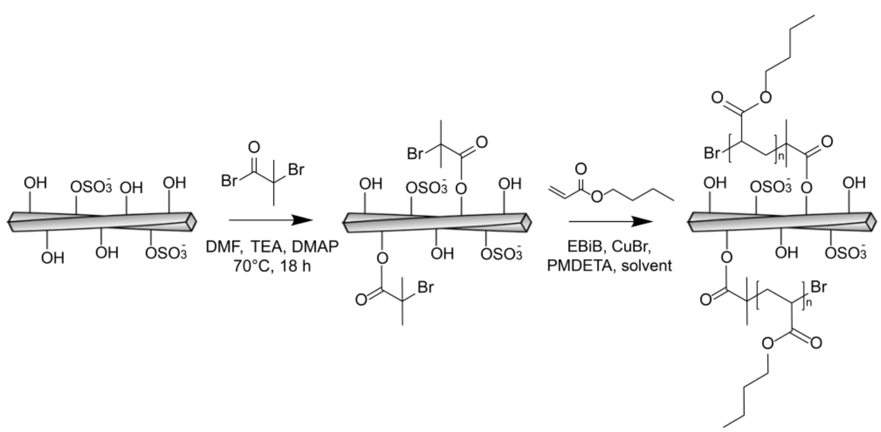

Figure 3.1. Synthesis of poly(butyl acrylate)-grafted CNCs by SI-ATRP by immobilizing the BiB initiator on the CNC surface (step 1) and polymerizing BA from CNCs, where “solvent” is either toluene or DMF (step 2). The EBiB added during the polymerization step is sacrificial initiator that concurrently initiates polymerization in solution to assist with graft polymer characterization.

FTIR was used to assess the successful covalent attachment of the BiB initiator to CNCs, with an increase in the intensity of the C=O peak at 1735 cm^{-1} observed for the BiB-CNCs compared to the unmodified CNCs (Figure 3.2). Due to extensive solvent washing and dialysis prior to characterization, we expect the peak increase at 1735 cm^{-1} to be a result of BiB grafting only. No noticeable change in the OH stretch region was observed in the BiB-CNC spectrum, consistent with the low overall content of grafted BiB content relative to the total number of surface hydroxide groups as well as the signal from internal hydroxyl groups inside the CNCs that are not accessible for initiator attachment.

Table 3.1. Quantification of CNC esterification with BiB initiator based on elemental analysis of two separate batches of BiB-CNCs.

BiB-CNC (Sample number)	Br (mass %)[a]	BiB[b] chains/nm^2	BiB[b] chains/CNC
1	5.80	1.05	4600
2	7.44	1.40	6100

[a] From elemental analysis.
[b]CNC surface area and volume calculated assuming rectangular geometry. CelluForce CNC dimensions taken from reference [29].

Photographs and transmittance measurements using UV-Vis spectrophotometry (Figure 3.3A) indicated that surface modifying CNCs with the BiB initiator allowed for their dispersion in DMF; while the dispersion consisted of smaller aggregates rather than individual CNCs, no sedimentation occurred over time (in contrast to all non-polymer grafted CNCs in toluene, Figure 3.3A). BiB-CNCs were not dispersible in toluene or water, the latter due to the increased interfacial hydrophobicity following BiB grafting. The absence of particle sedimentation in DMF implied that DMF is a better reaction media for BiB-CNCs than toluene and suggests the potential for more CNC uniformity/stability over the course of the polymerization reaction and thus more accessible initiating sites due to the higher available surface area. Additionally, it is suspected that dispersions of BiB-CNCs in DMF could be improved further if the particles were kept in a never-dried state rather than being re-dispersed after freeze drying, as carried out here. The challenge with re-dispersion after freeze-drying may also be amplified due to the fact that BiB-CNCs are in the acid form after initiator attachment (pH ~ 3), which is also known to cause issues for the re-dispersion of unmodified CNCs.[168]

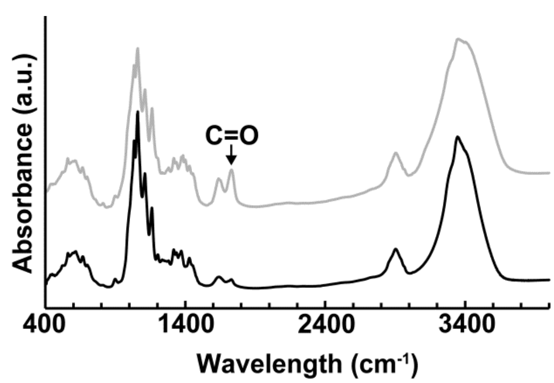

Figure 3.2. FTIR spectra of unmodified CNCs (black) and BiB-CNCs (grey).

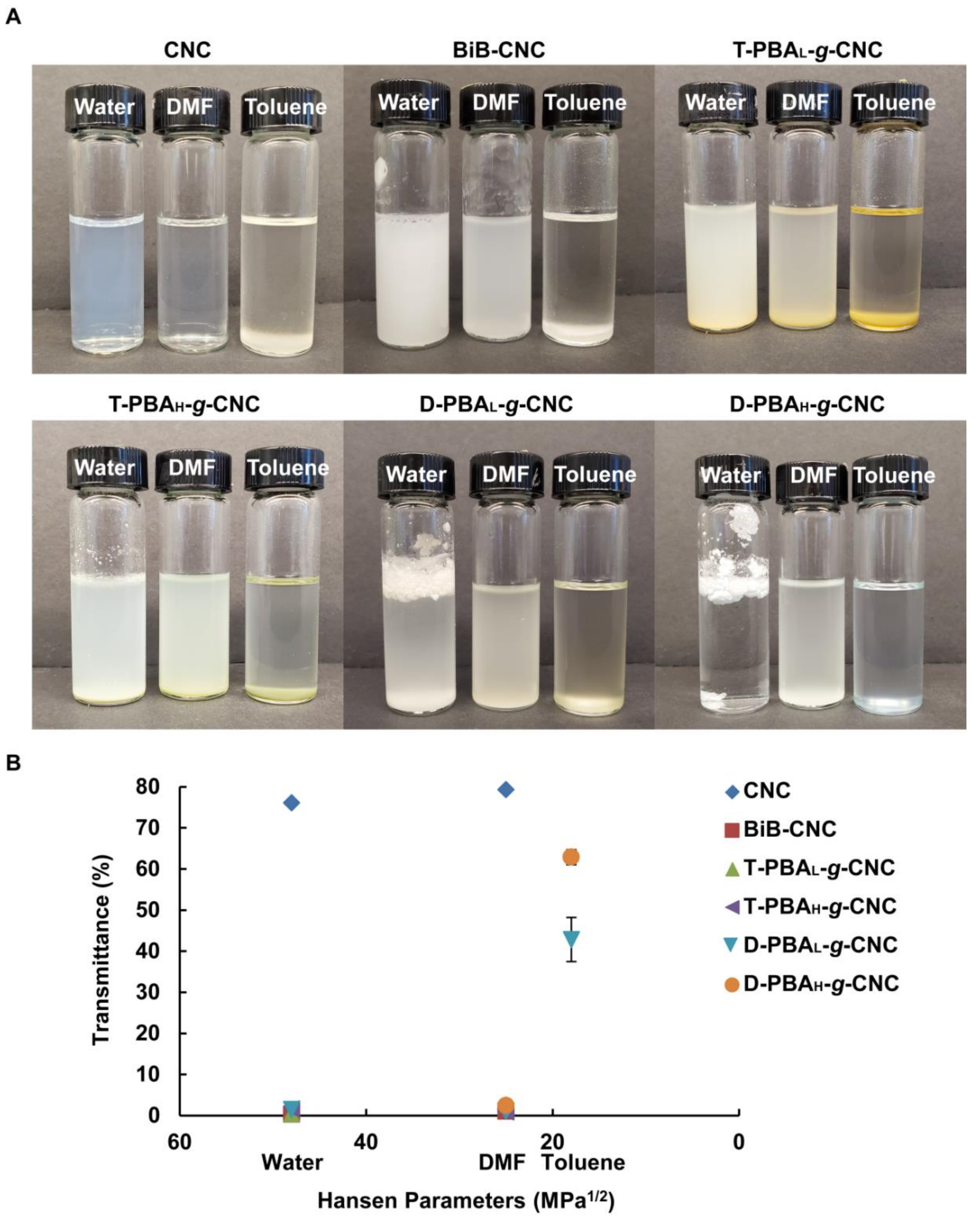

Figure 3.3. Photographs (A) and UV-Vis (transmittance) values (B) of CNC, BiB-CNC and PBA-*g*-CNC suspensions in water, DMF and toluene. All suspensions were kept at a concentration of 10 mg/mL and photos were taken after the samples were allowed to sit for 30 minutes.

The BiB-CNCs were then used as macroinitiators in SI-ATRP (Figure 3.1, second step) using butyl acrylate (BA) as the monomer. BA was chosen due to its hydrophobic nature (compared to the relatively hydrophilic CNCs) and use in polymer latex applications such as adhesives;[156,167] our goal was to evaluate whether the polymerization reaction solvent should be more compatible with the polymer being grafted or the starting CNCs to give the highest grafting densities. The polymerization was conducted with a CuBr/PMDETA catalytic system using either toluene or DMF as the reaction media. EBiB was also added to the reaction mixture as sacrificial initiator. Due to the low concentration of BiB-CNCs used during SI-ATRP (1 wt.%) there are not that many initiator groups, and as a result deactivator species, which can make it difficult to achieve good control over the molecular weight and dispersity of the grafted polymers. The use of a sacrificial initiator allows for a better control over the polymerization kinetics and, ultimately, the polymer properties[104,106] and has been employed for a variety of polymers grafted from CNC surfaces.[104,106,125,127,183,187,188,115] The simultaneous production of free polymer under the same polymerization conditions has the additional benefit of providing an easy route to characterize the properties of the synthesized polymer, with the molecular weight and composition of the polymers formed in solution having been shown to be comparable to surface-grafted polymer.[41,189]

Four different PBA-grafted CNCs (PBA-*g*-CNCs) were then synthesized, the properties of which are summarized in Table 2. PBA-*g*-CNCs synthesized in the two solvents each took on the colour of CuBr when dispersed in their respective solvent, consistent with previous reports of SI-ATRP for CNCs and believed to be related to the presence of adsorbed Cu^{2+}.[128,180]

The molecular weight and dispersity of free polymer was obtained *via* GPC (Table 3.2). In all four cases, dispersity values indicated good control over the polymerization in either solvent (Đ < 1.3). The molecular weights for the low and high DP set are not identical between the polymer grafted-CNCs produced in toluene and DMF due to the slightly different target molecular weights set in the synthetic protocol (i.e. these materials were produced for different purposes at different times); however, in both cases, there is a two-fold difference in molecular weight between the high and low DP (i.e., 9 and 20 kDa for toluene polymerized samples and 6 and 13 kDa for DMF), enabling suitable comparisons to be made with regards to the effect of molecular weight in each case. All molecular weights are maintained to be relatively low (<20 kDa), motivated by previous work indicating that entanglement of polymers can cause complications in dispersing modified CNCs and processing, e.g. in composite and emulsion applications.[115] Instead, given that the goal of polymer grafting is to improve CNC hydrophobicity, polymer graft density is likely to be as much as, or more, influential than the grafted polymer DP.

Table 3.2. Summary of polymer grafted-CNCs and homopolymer properties after polymerization in toluene (T) and DMF (D), including homopolymer molecular weight and dispersity for the targeted low (L) and high (H) molecular weights, polymer mass % in the grafted CNC samples, calculated graft density (chains/CNC) from combining elemental analysis and molecular weight analysis, water contact angle of dried CNC films, and crystallinity index (CrI) from XRD.

		PBA homopolymer			Elemental analysis		TGA		Contact angle (°)		XRD
Sample	Reaction solvent	$\bar{M}_n$ (g mol^{-1})	Đ	DP_n	% PBA (% wt)	PBA chains/ CNC[a]	% PBA (% wt)	PBA chains/ CNC[a]	t = 0 min	t = 1 min	CrI (%)
Unmodified CNC	None	-	-	-	-	-	-	-	20±1	15±1	86
T-PBA$_L$-*g*-CNC	Toluene	9400	1.18	73	7	60	3	30	129±1	~0	73
T-PBA$_H$-*g*-CNC	Toluene	19 900	1.21	155	11	50	10	40	110±1	25±1	59
D-PBA$_L$-*g*-CNC	DMF	6000	1.18	47	48	1170	42	910	134±2	128±2	36
D-PBA$_H$-*g*-CNC	DMF	12 900	1.18	101	64	1040	62	100	130±1	124±5	17

[a] Calculated using elemental analysis, M_n and the CNC specific surface area of 350 m^2/g. CelluForce CNC dimensions taken from reference [29].

FTIR was performed on all PBA-*g*-CNCs (after extensive purification) and compared to the BiB-CNC spectrum to confirm the presence of grafted PBA on the CNCs (Figure 3.4). To make meaningful comparisons between each spectrum, the same CNC mass was used in all FTIR measurements. An increase in the intensity of the peak located at 1735 cm^{-1} confirms the presence of PBA *via* the carbonyl groups present in each monomeric unit, with high DP grafted polymers showing a larger peak than low DP grafted polymers in all cases as expected. Additionally, the intensity of the carbonyl peak for both high and low DP polymer grafted-CNCs polymerized in DMF is significantly higher than that observed for CNCs grafted in toluene, despite the slightly higher molecular weights of the polymers synthesized in toluene, suggesting significantly higher efficiency of grafting when DMF was used as the reaction solvent.

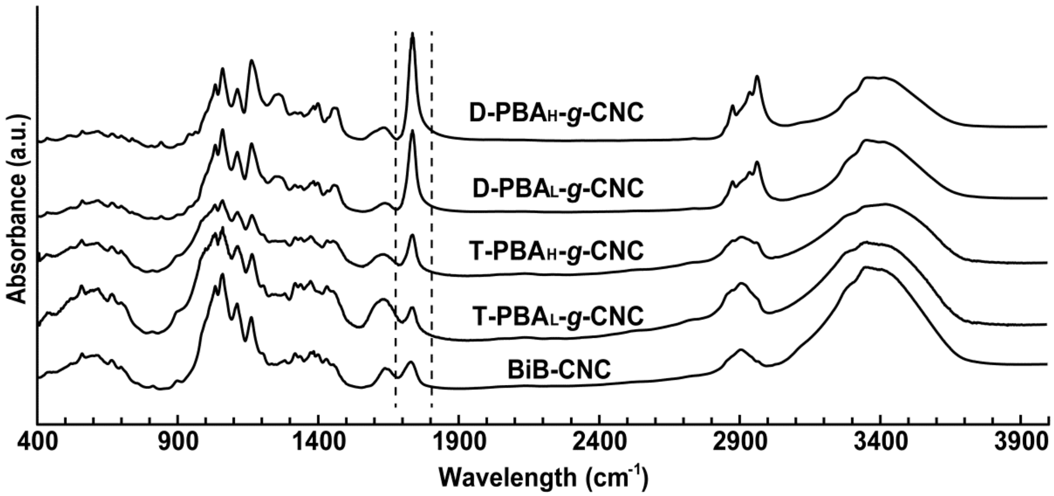

Figure 3.4. FTIR spectra of BiB-CNC and polymer grafted-CNCs.

To confirm the improved grafting efficiency observed using DMF as the solvent, TGA was used to quantify the mass % of polymer grafted to each polymer grafted-CNC (Table 3.2 and Figure 3.5). The presence of a first derivative thermogram DTG peak at ~400^{o}C for all polymer grafted-CNC samples indicated the presence of the PBA polymer, a degradation peak clearly distinct from that of unmodified CNCs (in their acid form) that have an onset of thermal degradation at 175^{o}C. An estimation of the mass % of both CNCs and PBA was made by integrating the curve using the respective regions attributed to each material (details of calculations in Supporting Information, Appendix A). Table 2.2 shows the significantly larger polymer mass obtained when DMF was used as the reaction solvent for polymer grafting, with 42 and 62% of the total mass of the low and high DP D-CNC-g-PBA materials respectively attributable to grafted polymer while only 3 and 10% of the mass of low and high DP T-CNC-g-PBA materials respectively was attributable to grafted polymer. C/H/N/S combustion elemental analysis yielded similar results (Table 3.2), with PBA mass percentages of 7 and 11% observed for low and high DP T-PBA-*g*-CNCs respectively but 48 and 64% for low and high DP D-PBA-*g*-CNCs respectively. The calculated densities of grafted polymer chains for T-PBA-*g*-CNCs are thus significantly lower than D-PBA-*g*-CNCs; however, the calculated chain densities (i.e., 25 – 1041 chains/CNC) are within the range of previous literature on grafting acrylates from CNCs in non-polar solvents.[109,128,182]

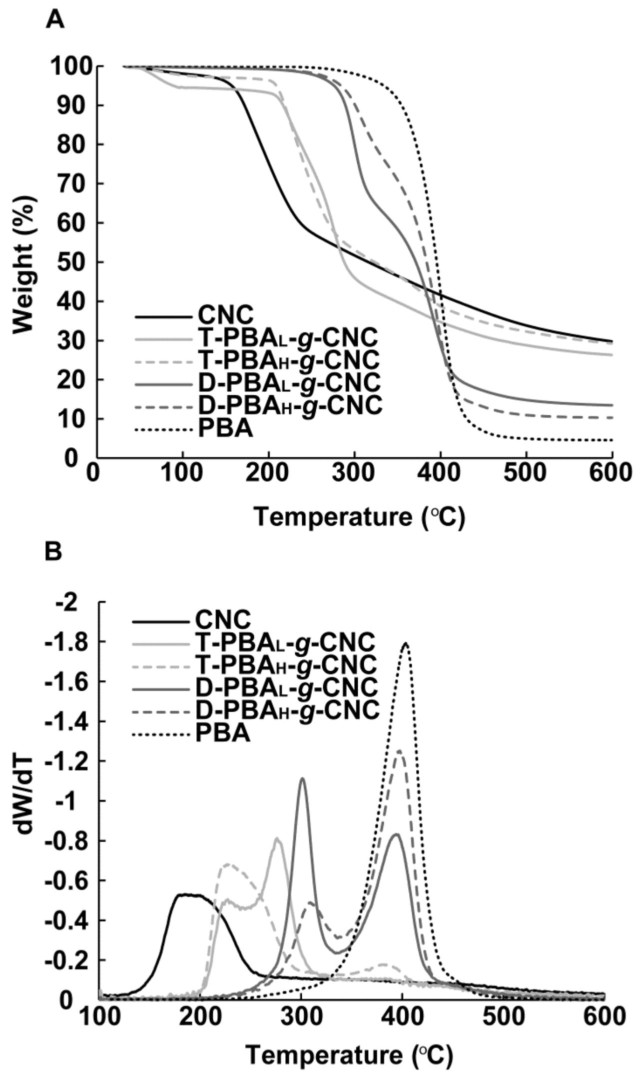

Figure 3.5. Thermogravimetric analysis (A) and first derivative thermogram (B) curves for BiB-CNCs, polymer grafted-CNCs and free PBA homopolymer.

Of note, the TGA curves for all samples containing polymer grafted-CNCs were shifted to the right compared to unmodified CNCs in the onset of cellulose degradation region. Therefore, the grafting of polymers improved the overall thermal stability of polymer-grafted CNC materials, consistent with previous work.[101,102,127,128,182,106,109,111,113,118,120,121,125] The intensity of the shift increased with the mass of polymer grafted. For example, no thermal degradation is observed for the highest graft density material (D-PBA_H-*g*-CNC) until 270^{o}C indicating a substantial improvement in thermal stability. Past work indicates that in some cases a reduced thermal stability of nanocellulose occurs after ATRP initiator attachment, which is attributed to the formation of HBr during heating in TGA experiments.[108,111,120,180,182,183] However, a comparison between the thermal stability of CNCs and BiB-CNCs in their acid forms (Supporting Information, Figure A1) yielded similar degradation profiles, suggesting that the presence of any *in situ* acid formation (either from sulfate half-ester or BiB groups) will reduce the thermal stability of any CNC. Specifically, after neutralizing both the CNCs and BiB-CNCs using NaOH (pH ~ 7), an increase in thermal stability for both was observed (Supporting Information, Figure A1); however, in this state, the sodium salt form of the BiB-CNCs showed reduced thermal stability relative to their CNC counterparts due to the *in situ* acid formation by the BiB groups upon heating. From this, we encourage researchers to be certain that all CNCs (either modified or not) bare the same sulfate half-ester counterion before making thermal stability comparisons.

To assess the affinity of the grafted CNCs for different solvents, water contact angles were measured on films of drop-cast PBA-*g*-CNCs. A significant increase in contact angle was observed between the unmodified CNCs and PBA-*g*-CNCs (Table 3.2) due to the introduction of hydrophobic PBA on the CNC surface, with the D-PBA-*g*-CNCs achieving contact angles as high as 134° compared to only 20° for unmodified CNCs. Of note, the contact angle decreased with time for unmodified CNCs but remained constant for D-PBA-*g*-CNCs, indicating less water penetration and a more hydrophobic surface (Table 3.2 and Supporting Information, Figure A2). In contrast, T-PBA-*g*-CNCs underwent a major reduction in the water contact angle after one minute from 110° to 25° (Table 3.2 and Supporting Information, Figure A2), attributed to the very low PBA graft density around the CNCs. As such, while both T-PBA-*g*-CNCs and D-PBA-*g*-CNCs have improved hydrophobicity as compared to their unmodified counterparts, the higher graft densities in D-PBA-*g*-CNCs result in substantially higher hydrophobicity at the CNC-water interface for CNCs grafted in DMF relative to toluene.

The differences in polymer chain density and polymer chain length grafted to the CNCs in each solvent had significant impacts on the dispersion properties of the different polymer-grafted CNCs. In all cases, we note that dispersions were prepared from dried CNCs/BiB-CNCs/PBA-*g*-CNCs, which reduces dispersibility regardless of the compatibility between CNC type and solvent.[168] CNCs grafted with PBA in toluene (T-PBA-*g*-CNC) could not be dispersed in toluene and formed highly aggregated dispersions in both water and DMF (Figure 3.3). This result is consistent with the low amount of polymer grafted from the surface (Table 3.2), leading to both less compatibility in non-polar solvents and a reduced ability to sterically stabilize the CNCs; indeed the polymer content is sufficiently low that T-PBA-*g*-CNCs could disperse in water similarly to the BiB-CNCs. Conversely, both low and high molecular weight PBA-grafted CNCs in DMF (D-PBA-*g*-CNCs) could be well dispersed in toluene and partially dispersed in DMF but were no longer dispersible in water. Furthermore, D-PBA_H-*g*-CNCs were better dispersed in toluene than D-PBA_L-*g*-CNCs as indicated by their higher transparency observed by UV-Vis spectroscopy (Figure 3.3B, plotted as a function of the solvent Hansen solubility parameter from most to least polar solvent); this result is consistent with the improved steric stabilization and compatibility with the hydrophobic environment achieved with the longer DP grafts[174,190]. Of note, although DMF is not a good solvent for PBA, the compatibility between PBA and DMF was sufficient such that sedimentation did not occur during the reaction.

Finally, XRD and TEM were employed to demonstrate that polymer grafting does not compromise the crystalline cellulose core of the CNCs. XRD demonstrates the clear persistence of cellulose I peaks but increasing amorphous peak scales with the amount of grafted polymer present on the CNC (Supporting Information, Figure A3). Similarly, TEM imaging indicated that the BiB-CNCs remain rod-shaped with similar morphology to their unmodified precursors while PBA-*g*-CNCs have similar lengths but increased width consistent with polymer grafting (Supporting Information, Figure A4). For T-PBA-*g*-CNCs, the change in cross-section was less significant compared to D-PBA-*g*-CNCs, again reflective of the much higher polymer density grafted to CNCs using DMF as the solvent. Of note, individual nanoparticles were observed on the TEM grid for all functionalized CNCs, confirming that the grafting reactions do not induce permanent aggregation of individual CNCs; however, images for PBA-*g*-CNCs contain noticeably less nanoparticles than their unmodified or initiator-modified counterparts, attributed to poor adhesion between the nanoparticles and the TEM grid. Staining the samples with a 1 wt. % uranyl acetate stain (which improves visualization of the CNC core) showed the persistence of the cellulose core of both PBA_H-*g*-CNCs (Supporting Information, Figure A5). Additionally, a noticeable aura of brightfield can be seen around the D-PBA_H-*g*-CNCs, which is indicative of negatively stained polymer and supports the presence of a large polymer shell; no such aura is observed for T-PBA_H-g-CNCs due to the low grafted polymer density.

3.5 Discussion

While ATRP equilibrium constants are higher for polar solvents and can result in faster polymerization kinetics (and thus worse control over the polymerization and chain dispersity),[191] GPC results (Table 3.2) confirm that each reaction reached completion (i.e. the targeted molecular weights of the free polymer were obtained) and maintained good molecular weight control (i.e. similar low dispersity values). Since all other reaction conditions were kept constant between the preparation of T-PBA-*g*-CNCs and D-PBA-*g*-CNCs, the lower grafting densities achieved with toluene-grafted CNCs were attributed to the reduced stability of BiB-CNCs in toluene prior to polymerization (Figure 3.3B), which could limit the number of accessible surface initiator groups during radical initiation. Conversely, D-PBA-*g*-CNCs obtained much higher polymer grafting densities that are comparable to other reports of grafting acrylates from CNC surfaces in polar solvents.[106,127,181,183] Since BiB-CNCs formed more stable suspensions in DMF (Figure 3.3A), the availability of surface initiator groups would be higher than the case of BiB-CNC/toluene suspensions, allowing for more grafted polymer chains. Thus, the graft densities achieved following the grafting of hydrophobic polymers to CNCs appear to be primarily correlated with the colloidal stability of the CNC in the polymerization solvent rather than the potential of the solvent to dissolve the grafted polymer, at least for the shorter polymer grafts targeted herein.

While BiB-CNC sample 1 and 2 (Table 3.1) were used for the synthesis of T-PBA-*g*-CNC and D-PBA-*g*-CNC respectively, the difference in initiator density on the BiB-CNC surface is not expected to have a significant effect on the number of polymer chains grafted. . The idea of a polymer graft threshold for SI-ATRP of CNCs was first identified by Zoppe et al.[105] when attempting to graft the same molecular weight of PNIPAM from BiB-CNCs containing different initiator densities but observing no difference in the polymer content between samples. For PBA specifically, Majoinen et al.[106] reported nearly identical polymer graft densities of poly(*tert*-butyl acrylate) using CNCs containing approximately four times higher initiator concentrations than the ones reported herein. The effect of different initiator densities for both BiB-CNC samples on the density of polymer grafts was therefore considered negligible.

The preservation of CNC morphology and crystallinity after polymer-grafting should be a priority if the desirable properties attributed to CNCs are to be utilized. If either morphology or crystallinity are altered (i.e. rod shape is forfeited or crystal structure is compromised), the intended behavior of the polymer-grafted CNC in an application such as nanocomposite reinforcement or interfacial stabilization may not be maintained. The high aspect ratio of the rod-shaped CNCs facilitates the use of less nanofiller to obtain highly-loaded systems, while the preserved crystallinity of CNCs provides mechanical strength in the resulting nanocomposite.[2,13]

3.6 Conclusions

PBA was grafted from the surface of BiB-modified CNCs *via* SI-ATRP using either toluene or DMF as the reaction medium. TGA and elemental analysis demonstrated that using DMF as the solvent yielded high graft density PBA-*g*-CNCs while using toluene as the solvent resulted in sparsely grafted CNCs. Consequently, D-PBA-*g*-CNCs were highly dispersible in non-polar solvents due to the enhanced compatibility and steric stabilization resulting from the higher number of grafted polymer chains while T-PBA-*g*-CNCs remained dispersible in water. The improvement in polymer-grafting for D-PBA-*g*-CNCs was attributed to the increased number of accessible surface initiator groups due to a more dispersed BiB-CNC suspension prior to polymerization, while BiB-CNCs in toluene were highly aggregated and sedimented. CNC morphology was not compromised during grafting, and the CNC cross-section increased slightly when large amounts of higher molecular weight polymer were grafted.

Overall, the results herein demonstrate that CNC colloidal stability at the beginning of the polymer grafting reaction is the crucial consideration when choosing a solvent for CNC hydrophobic modification, with the colloidal stability/compatibility of the polymer or polymer-grafted CNCs in the solvent being less important for obtaining high densities of surface modification. This result provides insight for the future development of CNCs grafted with hydrophobic polymers and highlights the potential use of more polar solvents for obtaining significantly enhanced graft densities *from* CNCs.

3.7 Acknowledgements

The authors thank CelluForce Inc. for providing the unmodified CNC starting material and Prof. Adronov and Prof. Thompson at McMaster for equipment use. The Biointerfaces Institute at McMaster is acknowledged for equipment use and training. Special thanks to Marcia Reid and the Electron Microscopy Facility in the Health Science Center at McMaster University and Victoria Jarvis at the McMaster Analytical X-ray Diffraction Facility for their time and expertise. E.D.C. is grateful for support and recognition through the Canada Research Chairs program and the University of British Columbia's President's Excellence Chair initiative.

Appendix A: Supporting Information for Chapter 3

BiB CNC Macroinitiator Density Calculation. The method for calculating the degree of substitution of bromine initiator sites (DS) on the BiB-CNCs was adapted from Rosilo et al.[175] and was performed using the following equation:

$$Br = \frac{79.90\ DS}{12.01(6 + 3DS) + 1.008(10 + 5DS) + 16.00(5 + DS) + 79.90DS}$$

where Br is the bromine content as measured by elemental analysis. In the case of BiB-CNC-2 (Br % = 7.44):

$$0.058 = \frac{79.90\ DS}{12.01(6 + 3DS) + 1.008(10 + 5DS) + 16.00(5 + DS) + 79.90DS}$$

$$79.90\ DS = \ 162.14\ (0.0744) + 136.97(0.0744)DS$$

$$DS = 0.17\frac{Br}{AGU}$$

Assuming that 1/3 of the total number of cellulose chains are on the surface,[1] the corrected DS is equal to 0.52 Br/surface AGU. Assuming the CNC has a rectangular geometry and that the density of a CNC is 1.6 x 10^{-21} g/nm^3, the number of AGUs per unit CNC volume (based on CelluForce CNC dimensions from Reid et al.[29]) is calculated as follows:

$$1.6 \times 10^{-21}\frac{g\ AGU}{nm^3} \times (1\ nm\ \times 6\ nm\ \times 6\ nm) \times \frac{mol\ AGU}{162\ g\ AGU}$$

$$= 4 \times 10^{-22}\ mol\ AGU$$

The surface bromine molarity is therefore:

$$4 \times 10^{-22}\ mol\ AGU \times \frac{1}{3}\ surface\ AGU \times 0.52\,\frac{Br}{surface\ AGU} = 6 \times 10^{-23} mol\ Br$$

while the number of bromine groups per unit surface area is:

$$\frac{6 \times 10^{-23} mol\ Br}{24\ nm^2} \times 6.02 \times 10^{23}\,\frac{units}{mol} = \mathbf{1.4.}\frac{\boldsymbol{int.Sites}}{\boldsymbol{nm^2}}$$

PBA-*g*-CNC Chain Density Calculation. The method of calculating PBA surface density was adapted from Wang et al.[181] Assuming a theoretical CNC specific surface area (A_{SSA}) of 350 m^2/g, the density of PBA chains per unit surface area (ρ) can be calculated from the following equation:

$$\boldsymbol{\rho = \frac{m\,N_A}{M_N(1-m)A_{SSA}}}$$

where N_A is Avogadro's number and m and M_N are the mass % and number-average molecular weight of the grafted and free polymer determined by TGA and GPC, respectively. For the case of D-PBA_L-g-CNC:

$$\boldsymbol{\rho = \frac{0.62 \times 6.02\,\frac{units}{mol}}{12\,896\,\frac{g}{mol}(1-0.62)\;3.5 \times 10^{20}\,\frac{nm^2}{g}}}$$

$$\boldsymbol{\rho} = 0.22\ \frac{PBA\ chains}{nm^2}$$

Assuming rectangular CNC geometry and dimensions by Reid et al.,[29] the number of chains per CNC can be calculated:

$$0.22\ \frac{PBA\ chains}{nm^2} \times 4\ sides\ (6\ nm\ \times 183\ nm) = \mathbf{996}\,\frac{\boldsymbol{PBA\ chains}}{\boldsymbol{CNC}}$$

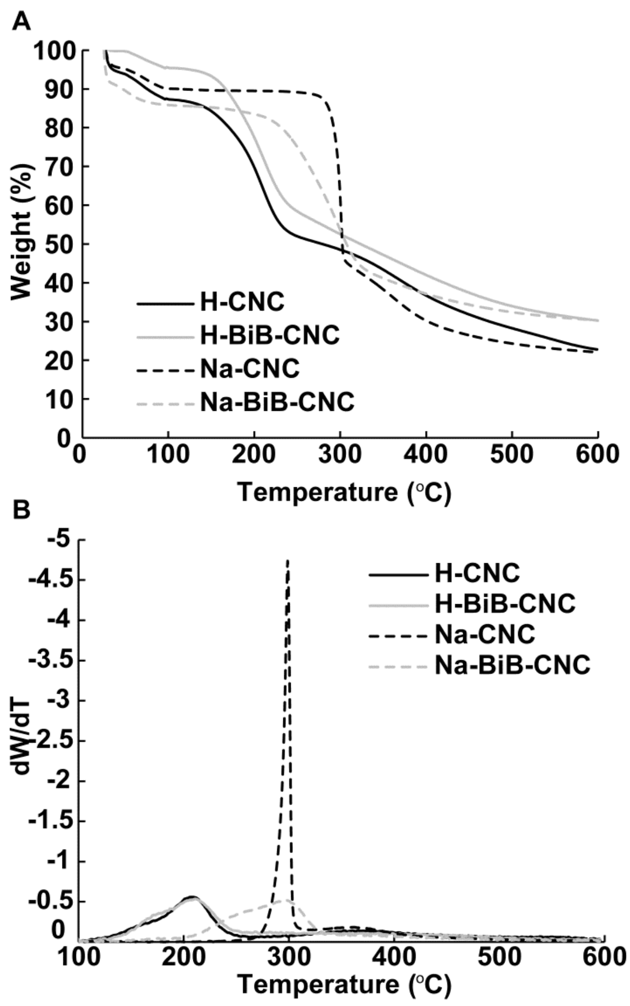

Figure A1. Thermogravimetric analysis (A) and first derivative thermogram (B) curves of CNCs and BiB-CNCs in both acid and sodium-form.

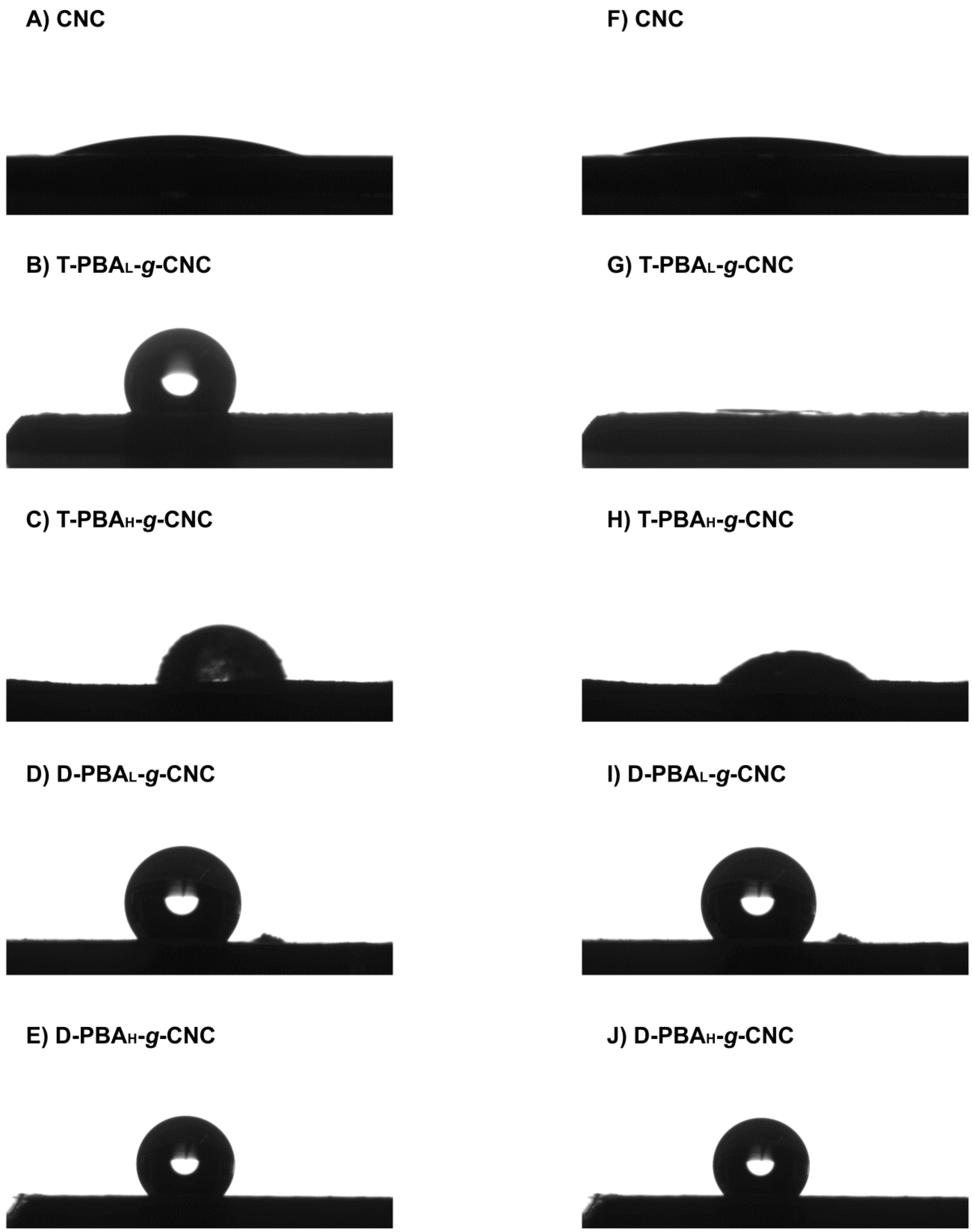

Figure A2. Water contact angle photographs for unmodified and PBA-*g*-CNCs taken immediately (A-E), and after one minute (F-J).

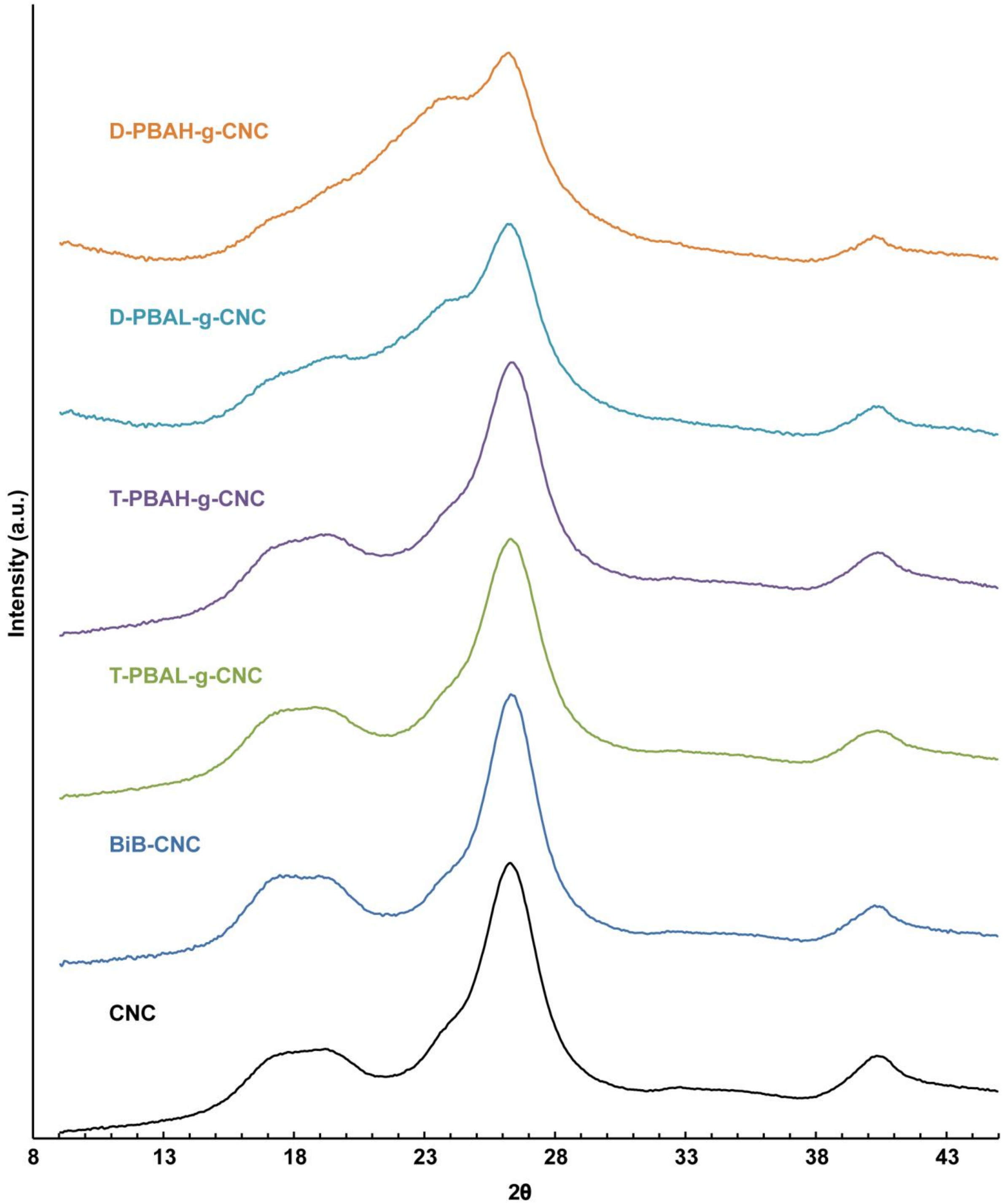

Figure A3. X-ray diffraction (XRD) spectra of CNCs, BiB-CNCs and PBA-*g*-CNCs.

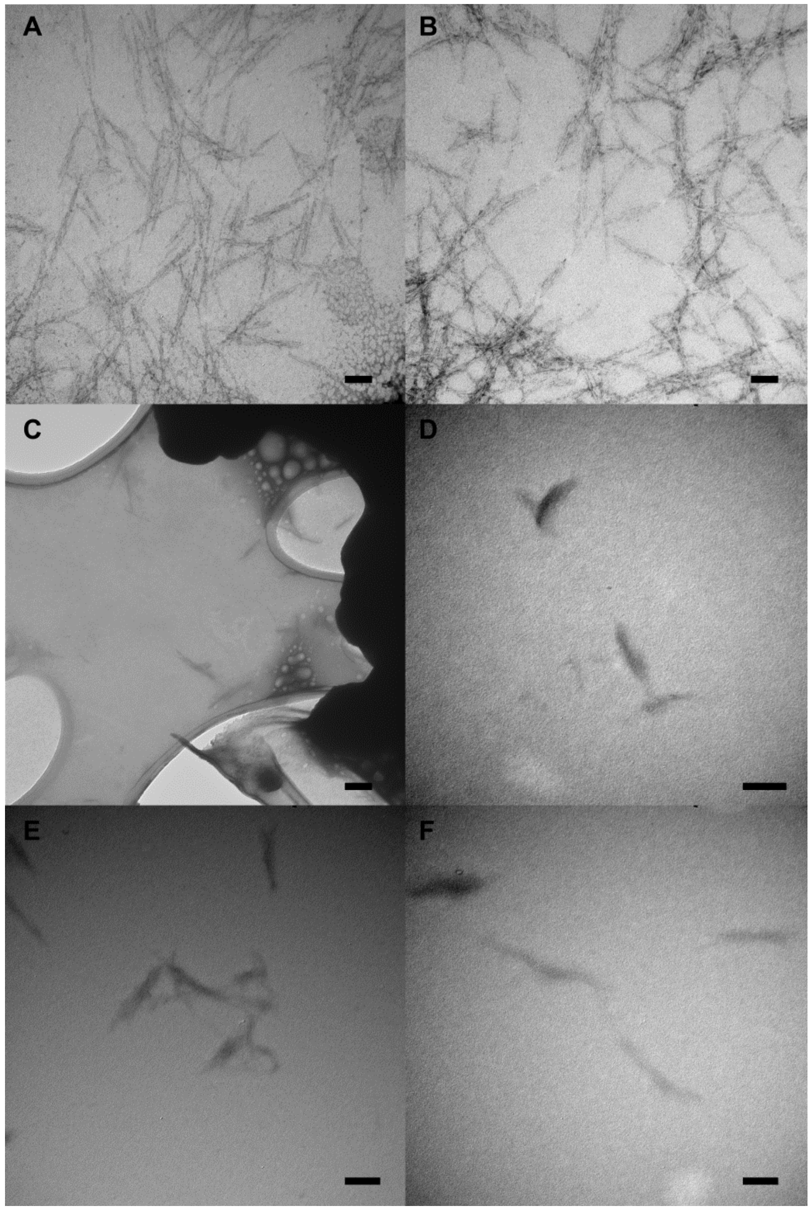

Figure A4. Transmission electron microscopy (TEM) images of A) CNCs, B) BiB-CNCs, C) T-PBA_L-*g*-CNCs, D) T-PBA_H-*g*-CNCs, E) D-PBA_L-*g*-CNCs and F) D-PBA_{H-g}-CNCs. A 1 wt. % uranyl acetate stain was used in the case of a) and b) in order to improve visibility of the CNCs, while no stain was used for the remaining PBA-*g*-CNCs images. All scale bars are too 100 nm.

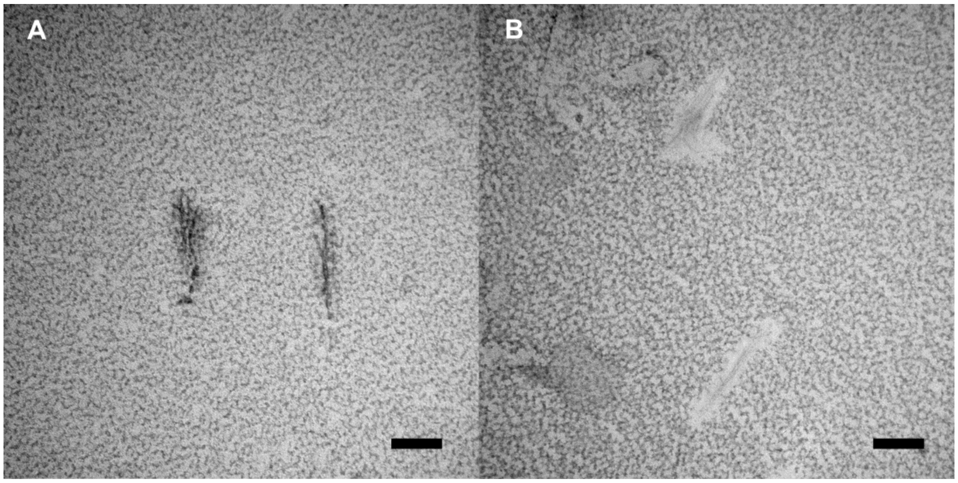

Figure A5. TEM images of A) T-PBA_H-*g*-CNCs and B) D-PBA_H -*g*-CNCs stained with 1 wt. % uranyl acetate. Scale bars = 100 nm.

Chapter 4: Incorporation of Polymer-grafted Cellulose Nanocrystals into Latex-based Pressure Sensitive Adhesives

4.1 Abstract

While the improvement of water-based adhesives containing renewable additives is important for sustainable practices, an understanding of how the compatibility between adhesive additives and polymer formulations affects their performance is currently lacking. Cellulose nanocrystals (CNCs) were functionalized *via* surface-initiated atom transfer radical polymerization with hydrophobic polymers poly(butyl acrylate) and poly(methyl methacrylate) to facilitate their incorporation into latex-based pressure sensitive adhesives (PSAs). Poly(butyl acrylate) latex nanocomposites were then synthesized using a seeded semi-batch emulsion polymerization technique with CNCs or polymer-grafted CNCs added *in situ* at 0.5 or 1 phm (parts per hundred parts monomer by mass) loadings. Viscosity measurements revealed significant differences between latexes prepared with CNCs *versus* polymer-grafted CNCs, with the lower viscosities of the latter suggesting their incorporation inside the polymer particles. PSAs containing CNCs with low number average degree of polymerization (DP) grafts exhibited comparable tack and improved peel strength at 1 phm loadings relative to unmodified CNCs due to their improved distribution throughout the PSA and ability to improve PSA wettability and chain mobility due to the presence of low DP grafts. PSAs containing high DP grafts underperformed due to large CNC aggregates which did not improve PSA wettability or mobility. PSAs containing poly(methyl methacrylate)-grafted CNCs with low DP grafts exhibited the highest tack and peel strength; all PSAs containing polymer-grafted CNCs had poor shear strength compared to PSAs containing unmodified CNCs. These results provide insight into how CNC surface chemistry and the presence of low DP polymer-grafts can affect latex-based PSA properties for future CNC-latex PSA optimization.

4.2 Introduction

Many polymer products, and their manufacturing practices, are currently being redesigned to become more sustainable, with a particular focus on decreasing the environmental footprint of the synthesis method and expanding the use of renewable raw materials.[192] Water-based polymerization techniques satisfy the requirement of a greener polymer production route. In particular, emulsion polymerization is a more sustainable technique than solution polymerization given that it removes the need for volatile and/or toxic organic solvents.[192] An additional advantage is that the resulting polymer is in the form of an aqueous nanoparticle dispersion (a.k.a. a latex) that is highly tuneable, whereby the polymer particle size, colloidal stability and molecular weight can be altered though process alterations (e.g. batch vs. semi-batch systems) and/or the use of additives (e.g. nanofillers, chain-transfer agents).[193] The use of water as a reaction media also acts as a heat sink during the free radical polymerization process, making the process more industrially feasible from a safety perspective.[194,195]

Among renewable material additives, cellulose nanocrystals (CNCs) have gained attention due to their green production process, relatively low cost, and now commercial availability.[29] CNCs are rod-shaped nanoparticles produced though the degradation of the amorphous (or disordered) regions of cellulose *via* acid hydrolysis or oxidation, leaving behind highly-ordered crystalline cellulose regions.[26] These particles can vary in size (2-20 nm in width and 100 nm-2 μm in length) depending on the cellulose source used, with cotton or wood pulp being the most common.[36] CNCs have a large surface area, high aspect ratio,[1] and are considered non-toxic,[196] making them an ideal candidate for renewable and cost-effective additives in polymer-based products.

The use of CNCs in polymer nanocomposites to-date has not only improved product sustainability but also offered enhanced mechanical, rheological, thermal and barrier properties.[14] Favier et al.[154] were the first to blend CNCs with soft polymer latexes in suspension, observing a drastic increase in the measured shear storage modulus of a cast latex film upon loading a concentration above the CNC percolation threshold of 1.5 wt. %.[197] Since then, researchers have mixed CNCs with variety of polymer latexes though post-synthesis blending or *in situ* addition techniques where CNCs do not act as stabilizers but are dispersed throughout the continuous (water) phase.[14] When CNCs have been used directly as Pickering stabilizers for emulsions and emulsion/suspension polymerization, they often produce micron-sized droplets/particles.[33,152] However, a recent study by Jiménez-Saelices et al.[143] showed the presence of latex (nano) particles with a sparse coating of CNCs when monomers with some water solubility were used, despite the formation of micron-sized monomer droplets prior to polymerization. Additionally, Glasing et al.[145] has shown that the initiator solubility in water can also influence the formation of latex particles when CNCs or polymer-grafted CNCs (g-CNCs) act as Pickering stabilizers, with more water soluble initiators inducing homogeneous nucleation and producing latex particles with few CNCs on the surface.

Pressure sensitive adhesives (PSAs) are composed of mostly low glass transition temperature (T_g < -30°C) polymers. When produced from polymer latexes, the evaporation of water and formation of a polymer film yields a sticky surface that, upon the application of a force, can bond to another surface but can be easily removed without any residue for some applications such as masking tapes or sticky notes.[15] Due to the favourable properties observed when combining CNCs with latex particles, recent interest has emerged in using CNCs as a reinforcing and/or viscosity modifying agent in PSA production. Dastjerdi et al.[156] were the first to incorporate CNCs in a seeded semi-batch emulsion polymerization to form CNC–polymer nanocomposite PSAs, reporting significant improvements in both adhesive (i.e. tack and peel strength) and cohesive (i.e. shear strength) properties for *in situ* addition of CNCs at a 1 wt. % loading. Shamsabadi and Moghbeli[165] incorporated CNCs into a PSA formulation produced *via* miniemulsion polymerization and found that both peel and shear strength could be improved with CNC loadings up to 4 wt. %, with tack remaining constant. However, the total solids contents of these latexes were 25 wt. %, which is low for industrially produced PSA formulations (typically 35-40 wt. % is the minimum). Gabriel et al.[160] loaded CNCs into a seeded semi-batch emulsion polymerized PSA at concentrations up to 4 wt. % obtaining a total solids content of 40 wt. %. Results showed that CNC loadings higher that 2 wt. % did not improve tack or peel strength but could improve shear strength. Furthermore, the local concentration of CNCs prior to polymerization (i.e. the CNC concentration in the water phase during the seed or feed stage) was the key to forming stable latexes; above a critical concentration of 13.85 and 17.87 $g_{CNC}\ L^{-1}{}_{water}$ in the seed and feed stage respectively, CNC aggregation reduced the adhesive properties of the PSA.[160] Pakdel et al.[159] studied the effect of polar monomer acrylic acid (AA), sodium dodecyl sulfate (SDS) concentration and the use of chain transfer agent 1-dodecanethiol (NDM) on PSA properties of CNC–latex nanocomposites using a sequential design approach. Interactions between AA and CNCs provided a synergistic effect whereby shear strength was improved by 70 h as compared to a PSA with no CNCs. Additionally, increasing the SDS concentration had a negative effect on PSA properties which was minimized when AA was not used. Lastly, the incorporation of NDM in the presence of CNCs could improve tack and peel strength up to 1.5 and 5× respectively but at the cost of shear strength. Since NDM reduces polymer molecular weight, the reduction in shear strength was attributed to the lack of physical interactions between CNCs and polymer chains. Collectively, these results suggest promise around the use of CNCs for improving adhesive properties but also some cautionary data around how PSA chemical composition and aggregation state can undo or even reverse these positive effects, making further studies to better understand the fundamentals of PSA-CNC interactions important to enable the practical use of CNCs in PSAs.

While the colloidal stability of CNCs in water generally makes them useful in water-based systems, surface modification of CNCs to better improve the compatibility between CNCs and the more hydrophobic PSA latexes enables tuning of the location of CNCs in the polymer latex and thus the ultimate performance observed. The importance of CNC–polymer compatibility was exemplified by Ouzas et al.,[157] who incorporated 2-ethylhexyl acrylate (EHA) (a monomer that has a low water solubility < 0.001 g L^{-1}) into a latex-based PSA formulation and observed extensive CNC aggregation during film formation and thus poor PSA properties. On the other hand, Yu et al.[166] incorporated CNCs modified with 3-methacryloxypropyltrimethoxysilane coupling agent (fCNCs) *in situ* into EHA-containing latexes and observed significantly improved adhesive properties relative to unmodified CNCs, attributable to the ability of fCNCs to copolymerize with the bulk polymer due to the presence of reactive vinyl groups on 3-methacryloxypropyltrimethoxysilane and thus compatibilize the CNC-PSA interface.[166] Similarly, Pakdel et al.[167] demonstrated that "less hydrophilic" CNCs (produced by CelluForce, product grade: CNC-103) of lower surface charge density and higher surface activity resulted in reduced CNC aggregation during PSA film formation and consequently improved tack and peel strength compared to unmodified CNCs. While Kedzior et al.[164] have demonstrated that the location of CNCs within high T_g poly(methyl methacrylate) (PMMA) latex particles produced *via* miniemulsion polymerization can be tuned based on the surface grafting of the PSA-relevant polymer poly(butyl acrylate) (PBA) on the CNCs, the effect of CNCs with a hydrophobic surface modification on latex-based PSA properties has not yet been reported.

Herein, highly modified, hydrophobic CNCs were synthesized *via* surface-initiated atom transfer radical polymerization (SI-ATRP) and incorporated into PBA latex polymers for PSA production. Both PBA-grafted CNCs (PBA-*g*-CNCs) and PMMA-grafted CNCs (PMMA-*g*-CNCs) were synthesized, each with two different degrees of polymerization (DP) denoted as low DP (PBA_L and $PMMA_L$) and high DP (PBA_H and $PMMA_H$), and used to produce CNC–PBA latex nanocomposites (40 wt. % solids) using seeded semi-batch emulsion polymerization. The type and length of polymer grafted to the CNCs is correlated to the resulting adhesive properties of cast films, providing insight into how CNC surface chemistry and its consequent effect on the CNC distribution inside the polymer latex can influence the adhesive properties of PSAs.

4.3 Experimental Section

4.3.1 Materials

α-Bromoisobutyryl bromide (BiB), ethyl α-bromoisobutyrate (EBiB), N,N,N′,N″,N″-pentamethyldiethylenetriamine (PMDETA), copper (I) bromide (CuBr), 4-(dimethylamino)pyridine (DMAP), trimethylamine (TEA), aluminum oxide, hydrogen peroxide, sodium dodecyl sulfate (SDS), potassium persulfate (KPS), ethylenediaminetetraacetic acid (EDTA), and dimethylformamide (DMF) were purchased from Sigma Aldrich and used as received. Toluene, ethanol (95%), and sulfuric acid were purchased from Caledon Labs. Butyl acrylate (BA) and methyl methacrylate (MMA) were purchased from Sigma Aldrich and passed through a column of basic aluminum oxide prior to use. All water used was purified using a Barnstead GenPure Pro water purification system from ThermoFisher Scientific. Unmodified cellulose nanocrystals were provided as a spray dried powder (in the sodium-salt form) by CelluForce Inc.

4.3.2 Preparation of Initiator-modified CNCs (BiB-CNCs)

Initiator-modified CNCs (BiB-CNCs) were produced as outlined in Chapter 3. First, 2 g of dried CelluForce CNCs were redispersed in 200 mL of DMF by stirring for 24 h and bath sonicating (Bransonic Ultrasonic MH, Branson) for an additional 2 h in a 500 mL round bottom flask. Under magnetic stirring, 4 mL of TEA was added followed by a catalytic amount of DMAP. The suspension was sealed with a rubber septum and degassed with argon for 1 h, followed by the addition of 4 mL of BiB added dropwise with continuous argon flow during the addition. The suspension was degassed for an additional 5 min with argon before being placed in a 70°C oil bath for 18 h, after which the reaction was terminated by exposing the suspension to air. The BiB-CNCs were purified through centrifugation (Allegra 64R, Beckman) at 5000 RPM for 15 min at 15°C. The BiB-CNCs were then redispersed in ethanol and centrifuged at 7000

RPM for 5 min at 15°C three times before being redispersed in water and dialyzed against purified water for 15 × 6 h cycles to remove any unreacted reagents and DMF. Finally, the purified BiB-CNCs were freeze dried (Benchtop Manifold BT85A, MillRock) and stored for further use.

4.3.3 Synthesis of g-CNCs via SI-ATRP

Poly(butyl acrylate)-grafted CNCs (PBA-*g*-CNCs) and poly(methyl methacrylate)-grafted CNCs (PMMA-*g*-CNCs) were produced using the protocol as outlined in Chapter 3 where DMF was used as the reaction solvent. In a typical reaction, 1 g of BiB-CNCs was mixed in 100 g of toluene or DMF for 24 h though magnetic stirring and bath sonicated for 2 h. The suspension was transferred to a 250 mL round bottom flask, to which purified monomer, PMDETA, and EBiB (as sacrificial initiator) were added. The components were added in a molar ratio of x:1:1:1 BA:PMDETA:EBiB:CuBr, where x is the desired number average degree of polymerization (DP) of the grafted polymer; CNCs with low (DP = 50) and high (DP = 100) DP were targeted for both PBA-*g*-CNCs and PMMA-*g*-CNCs. The suspension was sealed with a rubber septum and degassed with argon for 1 h in an ice bath before adding CuBr (catalyst). Following, the suspension was degassed for an additional 15 min before the round bottom flask was moved to a 70°C oil bath with magnetic stirring and left to react for 18 h, after which the reaction was stopped by exposing the round bottom flask to air. The reaction mixture was centrifuged at 10,000 RPM for 15 min and the first supernatant, containing free polymer dissolved in solvent, was collected. The g-CNCs were purified through extensive washing and centrifugation in methanol until the supernatant was clear. The purified g-CNCs were redispersed in toluene and added to a separation funnel containing a 0.5 wt. % EDTA mixture in water to remove any residual Cu catalyst before being vacuum dried and collected for use. The free polymer was purified in a column of neutral aluminum oxide and precipitated in cold methanol to remove any remaining Cu catalyst.

4.3.4 *In situ* Semi-batch Emulsion Polymerization for Latex Synthesis.

Prior to synthesis, unmodified CNCs, PBA-g-CNCs or PMMA-g-CNCs were re-dispersed into either the available water (unmodified CNCs only) or PBA monomer (all CNC types) for the seed and feed emulsions. Re-dispersion was achieved by stirring CNCs in the appropriate medium overnight followed by probe sonication with a Qsonica Q700 sonicator (Qsonica, CT) for 5 minutes (50 A, pulse mode 2 s on/1 s off) in an ice bath. The resulting CNC suspension was then added to the rest of the emulsion components and emulsified via probe sonication (50 A, 5-10 min, pulse mode 2 s on/1 s off) in an ice bath. The resulting seed emulsion was added to a 500 mL three-necked round bottom flask and degassed for 1 h under argon under 250 RPM mechanical stirring. The seed emulsion was then placed in a 60°C oil bath and, after 5 minutes of heating, an initiator solution (0.01 g mL^{-1} in water) was injected, with the seed stage proceeding over the next hour. In parallel, the feed emulsion and feed initiator solutions were degassed for 30 min. in separate 100 mL round bottom flasks and, after the one hour seed stage, were injected using a Chemyx Fusion 4000 syringe pump (Chemyx, TX) at rates of 1.2 and 0.2 mL/min for the feed emulsion and initiator solution, respectively. Upon completion of the feeding process, the latex was left to react for an additional hour, after which the reaction was ended by exposing the latex to air. A general recipe to produce the latex is shown in Table 4.1.

4.3.5 Partitioning Experiments

Partitioning experiments were performed to assess the compatibility between g-CNCs and BA prior to polymerization. For each g-CNC type, a 1 wt. % suspension of g-CNCs in BA was produced by bath sonication for 4 h (Branson MH Series 5800, Danbury, CT) and added to water at a BA:water mass ratio of 40:60 in order to simulate polymerization conditions. The resulting monomer–water mixtures containing g-CNCs were then vortexed, and the partitioning of g-CNC was assessed qualitatively via visual inspection. The monomer and water phases were then removed and weighed before and after drying to estimate the extent of g-CNC in the monomer phase. This experiment was also repeated using unmodified CNCs as a control.

4.3.6 Fourier-transform Infrared Spectroscopy (FTIR)

Spectra of unmodified CNCs, freeze-dried BiB-CNCs, and vacuum-dried polymer grafted-CNCs were obtained from KBr pellets containing 10 mg of material using a Nicolette 6700 spectrometer operating in absorbance mode. All spectra were collected using a 4 cm^{-1} resolution and 32 continuous scans.

4.3.7 Elemental Analysis

Elemental analysis was performed on freeze-dried BiB-CNC samples to obtain the mass percent of Br *via* Schoniger combustion by Midwest MicroLab (Indianapolis, IN).

4.3.8 Gel Permeation Chromatography (GPC)

Gel permeation chromatography samples were prepared by dissolving a small amount of the dried free polymer obtained from the sacrificial initiator added during SI-ATRP in a 1 mg/mL solution in THF. Molecular weight and dispersity were analyzed using a Waters 2695 separations module equipped with a Waters 2414 refractive index detector (Milford, MA) and a Jordi Fluorinated DVB mixed-bed column (Mansfield, MA) operating at an eluent flow rate of 2 mL/min. Polystyrene standards were used for calibration.

4.3.9 X-ray Diffraction (XRD)

XRD measurements were performed using a Bruker D8 DAVINCI diffractometer (Bruker, USA) operating with a cobalt sealed tube source (λ_{avg}=1.79026 Å) at an accelerating voltage of 35 kV (current 45 mA) with a parallel focus Goebel Mirror, VANTEC 500 area detector, 0.5 mm micro slit and 0.5 mm small collimator over a 2θ range of 8-45º. Si wafer blanks were subtracted from all measurements. Two-dimensional area detector frames were integrated to produce diffraction patterns which underwent Rietveld refinement. Percent crystallinity was calculated though deconvolution using the cellulose I single crystal information file (CIF) with a linear background and a fixed amorphous peak at 24.1º. Samples were prepared by freeze-drying BiB-CNCs, vacuum drying g-CNCs, or using CelluForce CNCs as received.

4.3.10 Thermogravimetric Analysis (TGA)

Thermogravimetric analysis (TGA) was performed on all CNC types and dried polymer latex nanocomposites using a Simultaneous Thermal Analyzer (STA) 6000 from PerkinElmer (Waltham, MA). In each experiment, the dried material (5 mg) was placed in the instrument pan and loaded under argon. The chamber was heated to 600°C at a rate of 10°C/min under argon, and the residual weight % as a function of temperature was recorded. Grafted polymer mass was quantified by integrating the area under the first derivative thermogram (DTG) curve associated with the degradation of the grafted polymer (350-450°C) and cellulose (150-300°C) respectively.

4.3.11 Dynamic Light Scattering (DLS).

DLS was used to calculate the mean particle diameter and polydispersity index (PDI) of polymer latexes. Latexes were diluted to 0.1 wt. % and measured on a NanoBrook 90Plus PALS (Brookhaven, NY) with a 90° backscattering angle at 25°C. Reported data is an average of three measurements with standard deviation reported as error.

4.3.12 Differential Scanning Calorimetry (DSC)

DSC measurements were obtained on polymer latex nanocomposites using a Q200 differential scanning calorimeter (TA Instruments, DE) to determine the T_g of each sample. 10-15 mg of each latex were placed in TZero hermetic sealed aluminum pans and measured under a nitrogen atmosphere. For the first heat cycle, samples were heated from 20 to 100°C (10°C/min) and then cooled to -70°C (10°C/min) to erase the thermal history of the polymer. Next, the sample was heated from -70 to 100°C (10°C/min), with the inflection point of the reverse heatflow curve reported as T_g.

4.3.13 Rheology

Viscosity measurements of the final latexes were obtained from dynamic flow sweep experiments on a dynamic hybrid rheometer 2 (DHR-2) (TA Instruments) at a shear rate of 10 s^{-1} using a cone (diameter = 40 mm, angle = 1.004°) and plate geometry. Five measurements were taken per sample at 25°C, and the data was processed by TRIOS version 4.4.1. (TA Instruments).

4.3.14 Water Contact Angle

Contact angle samples were produced by drop casting g-CNCs or polymer latex on a piranha-cleaned silicon wafer. Measurements were obtained *via* the sessile drop method using a Future Digital Scientific OCA 20 High Speed Contact Angle Measurer (Westbury, NY). Water contact angle images and measurements were captured 60 times over a one minute period. Triplicate images were processed using SCA 20 (Filderstadt, Germany) and used to calculate the standard deviation of the contact angle for each sample.

4.3.15 UV-visible Spectroscopy

UV-visible spectroscopy was performed on a Cary 5000 UV-Vis-NIR spectrophotometer (Santa Clara, CA) operating in transparency mode at an operating wavelength of 500 nm. Dry latex discs were produced by drop casting latexes onto glass slides overlaid with silicone molds (diameter = 1.5 cm, thickness = 1 mm) to ensure the thickness of each film was constant.

4.3.16 Transmission Electron Microscopy (TEM)

TEM images were acquired on a JEOL 1200 EX TEMSCAN microscope operating at 80 kV. Samples were prepared by drop-casting 0.01 wt. % CNC, BiB-CNC and g-CNC suspensions onto Formvar-coated TEM grids and air drying until no solvent remained. CNCs and BiB-CNCs were drop-casted from suspensions in water, while g-CNCs were drop-casted from suspensions in toluene to reduce aggregation after drying. A 1 wt. % uranyl acetate stain was used to better visualize the CNCs and BiB-CNCs. Latexes were diluted to 0.1 wt. % and prepared using the same technique as CNC suspensions for imaging.

4.3.17 PSA Properties

Pressure Sensitive Tape Council standards (PSTC) including PSTC16, PSTC101 and PSTC107A for tack, 180° peel, and shear strength respectively were followed for sample preparation and testing.[136] Final latexes were cast on 50 μm corona-treated Mylar sheets using either a #50 Meyer rod for samples containing 0 or 0.5 phm (parts per hundred parts monomer by mass) CNCs/g-CNC or a #20 Meyer rod for samples containing 1 phm CNCs/g-CNCs and dried under controlled conditions (temperature = 25°C, relative humidity (RH) = 50±5) for 48 h. An Instron 3000 Universal tester and Bluehill 2 Materials Testing Software were used to measure the tack and peel strength as the force per unit width require for removing the PSA from the substrate. All tests were performed 6 times, with the average results and standard deviations were reported.

Tack measurements: Tack strips were 1” × 6” and formed into a drop loop by taping 1” of each end of the strip that was then secured under the grip of the Instron. The upper grip was moved downward at a rate of 1 mm/s until an area of 1” × 1” of a stainless steel substrate mounted on the lower grip was fully covered. The upper grip was then pulled up at 5 mm/s, and the maximum force require for removal was recorded as tack.

Peel strength measurements: A 180° peel strength test was employed. PSA strips of 1” x 5” were cut and adhered to a stainless steel substrate *via* the application of a 2040 g roll coater. Next, the PSA and the substrate were fixed in the lower and upper grips, with the latter pulled upward at a rate of 5 mm/s. The average force required for peeling (N/m) was reported as the peel strength.

Shear strength measurements: Shear testing was performed using a home-made tester in order to see how long a PSA strip can hold against a constant vertical force. Strips of 0.5” × 5” were cut and one strip end was laminated on a stainless steel substrate, similarly to that described for the peel strength (0.5” × 0.5” area of contact). A c-clamp was then used to hand a 500 g weight to the other end of the strip. The time required (h) until the covered area was removed was reported as shear strength.

Table 4.1. General formulation for *in situ* seeded semi-batch emulsion polymerization.

Component	Seed stage (phm)	Feed stage (phm)	Total (phm)
Monomer	20	80	100
Surfactant	0.3	1.2-1.7	1.5-2.0
Initiator	0.06	0.26	0.32
CNC	0.1-0.2	0.4-0.8	0.5-1.0
Water	70.6	86.6	157.2

4.4 Results and Discussion

4.4.1 g-CNC Characterization

CNCs were surface modified *via* SI-ATRP to improve the compatibility between CNCs and hydrophobic monomers/polymers. The reaction can be divided into two parts: 1) immobilizing bromine-bearing initiator groups on the CNC surface though the esterification of surface hydroxy groups; and 2) covalently grafting polymer, either PBA or PMMA, from the CNC surface (Figure 4.1).

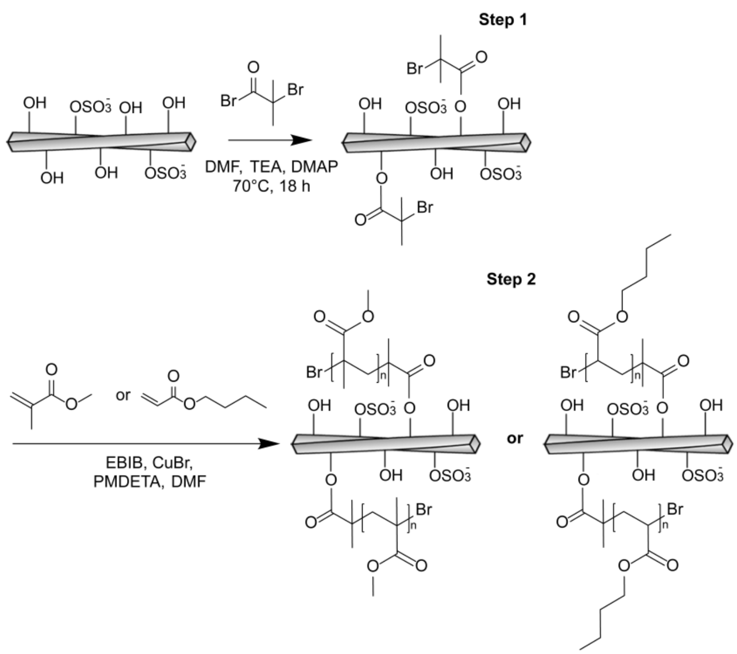

Figure 4.1. Two-step process of grafting polymers from CNCs with 1) the immobilization of an ATRP initiator, and 2) synthesis of either PBA or PMMA-grafted CNCs *via* SI-ATRP in DMF.

FTIR spectra confirmed the covalent attachment of both the BiB initiator groups and the grafted polymers (Figure 4.2). The absorption peak located at 1730 cm^{-1} is assigned to the stretching vibrations of C=O in both the BiB initiator and the polymer backbones. An increase in absorbance at 1730 cm^{-1} is observed after the addition of polymer; due to the extensive purification of all PBA-*g*-CNCs and PMMA-*g*-CNCs to remove unbound polymer, this increased absorbance can be attributed to the covalent attachment of polymer and not free polymer or contamination.

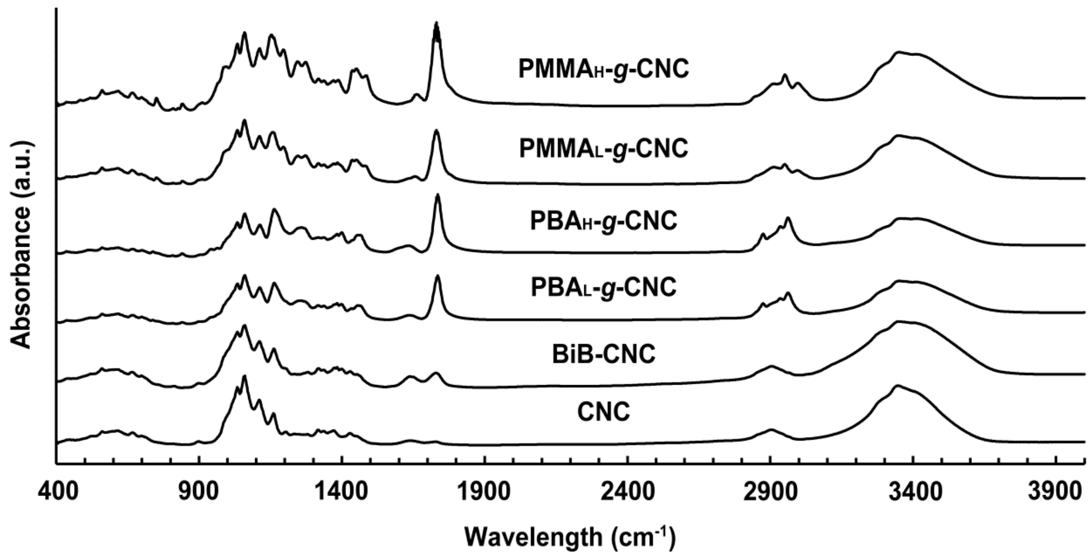

Figure 4.2. FTIR spectra of CNCs, BiB-CNCs and g-CNCs.

TGA was performed to evaluate the thermal stability of the modified CNCs and quantify the amount of polymer-grafted for each CNC type. CNC degradation (in acid form) is observed starting at 158°C (Figure 4.3), consistent with previous reports (onset 160-180°C).[31] The initial degradation is attributed to the self-catalyzed desulfation of sulfate half-ester groups on the CNC surface, a reaction that produces localized acid that, coupled with available bound water, catalyzes further de-esterification, hydrolysis, and ultimately depolymerization of cellulose.[31] Figure 4.3A and 4.3C show a right shift in the TGA curve for all g-CNCs, indicative of an improvement in the overall thermal stability of the hybrid material. This improved thermal stability is due to the abundance of PBA or PMMA at the CNC surface, which acts as an insulator and delays thermally-induced desulfation.[198] This phenomenon has also been observed for other g-CNCs in the cases where the grafted polymer is more thermally stable than cellulose.[101,102,127,128,182,106,109,111,113,118,120,121,125] For the case of PBA-*g*-CNCs, there is a clear distinction between the degradation of cellulose (200-300°C) and PBA (350-400°C), allowing a first derivative thermogram (DTG) to provide a good estimation of the wt. % of both components (Figure 4.3B). For PMMA-*g*-CNCs, the PMMA and CNC components degrade over a similar temperature range, complicating such an analysis; however, the wt. % of PMMA can still be estimated through integration of the cellulose and PMMA degradation that occurs separately with an understanding that the ratio of PMMA to cellulose is likely underestimated (Figure 4.3D). A summary of TGA analysis results are shown in Table 4.2.

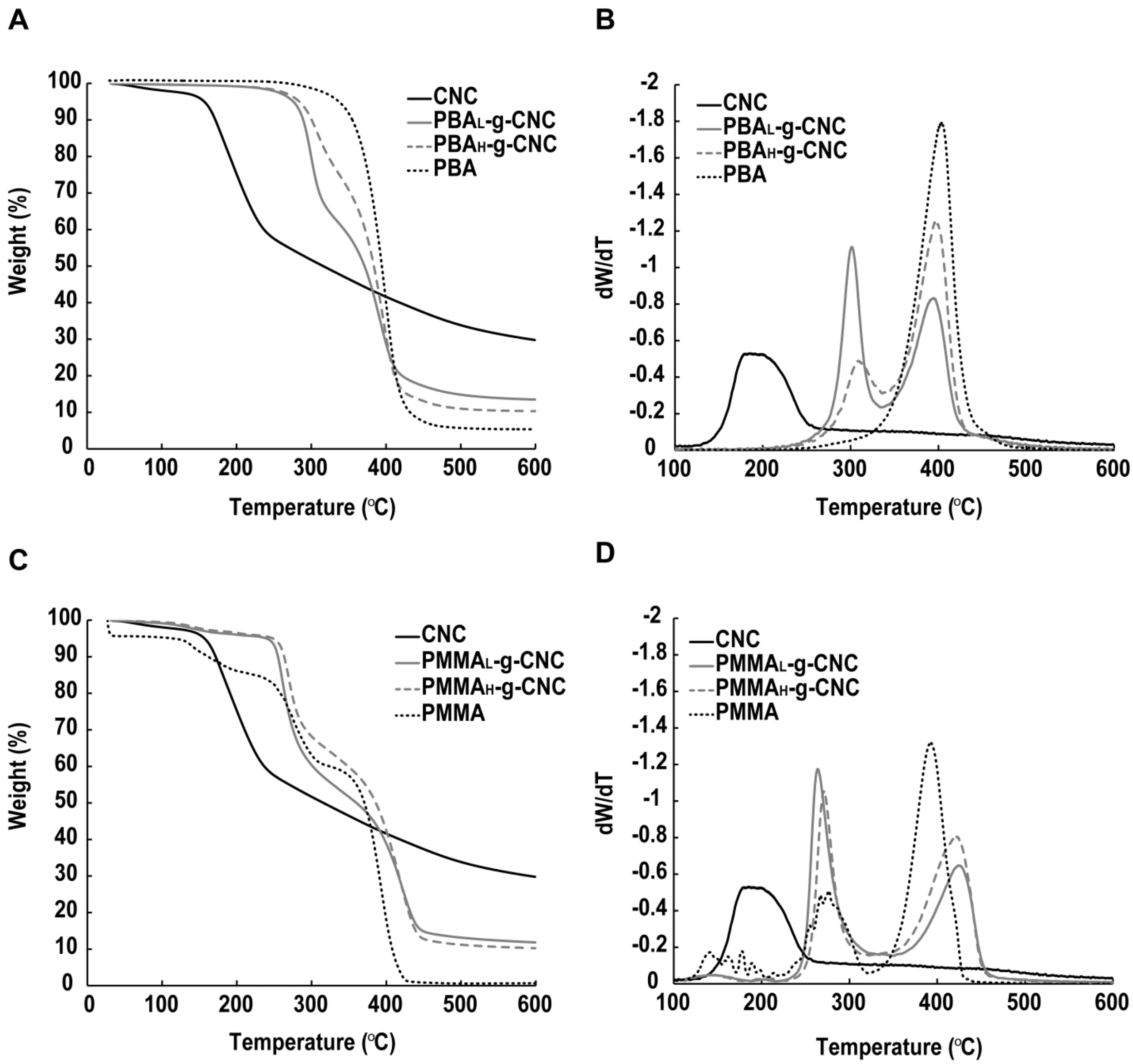

Figure 4.3. Thermogravimetric analysis (A and C) and first derivative thermograms (B and D) curves for PBA-*g*-CNCs (A and B) and PMMA-*g*-CNCs C and D).

GPC was performed on the free polymer produced from sacrificial initiator during each SI-ATRP reaction to estimate the molecular weight (M_n) and DP of grafted polymer (Table 4.2). Using the free polymer is not as accurate as de-grafting surface polymers for characterization, but has been validated as a method for grafted polymer characterization[41] and is often used in cases where the de-grafting of hydrophobic polymers is difficult.[104] The dispersity index of all the grafted polymers is <1.2, indicating good control over the polymerization.

Table 4.2. Summary of g-CNC characterization including free polymer molecular weight, TGA analysis results, water contact angle and crystallinity index (CrI).

	PBA homopolymer			TGA		Contact angle (°)		XRD
Sample	$\bar{M}_n$ (g mol^{-1})	Đ	DP_n	% PBA (% wt)	PBA chains /CNC	t = 0 m	t = 1 m	CrI (%)
Unmodified CNC	-	-	-	-	-	20±1	15±1	86
PBA_L-*g*-CNC	6000	1.18	47	42	900	134±2	128±2	36
PBA_H-*g*-CNC	12 900	1.18	101	62	1000	130±1	124±5	17
$PMMA_L$-*g*-CNC	4400	1.26	44	41	1200	131±1	130±1	Tbd[a]
$PMMA_H$-*g*-CNC	7500	1.24	75	53	1150	133±1	130±1	Tbd[a]

[a] analysis of XRD spectra is pending

The particle morphology for CNCs, BiB-CNCs and all g-CNCs was visualized though TEM imaging (Figure 4.4). CNCs and BiB-CNCs were found to have a comparable morphology, indicating that there is no significant alteration of the CNC structure as a result of initiator attachment. XRD measurements confirm that there is no change in the crystallinity index (CrI) of the CNCs when BiB was added (Table 4.2). Images of PBA-*g*-CNCs and PMMA-*g*-CNCs indicated that the grafted CNCs, while similar in length, had a significantly increased width compared to their un-grafted counterparts. PBA-*g*-CNCs were found to have the largest width (~ 50 nm), consistent with the low T_g of PBA (~ -48°C) allowing for spreading of the grafted polymer on the TEM grid that is not possible with the high T_g (~100°C) PMMA-*g*-CNCs. XRD confirmed that the primary crystalline cellulose I peak was unchanged as a result of all grafting reactions, suggesting that the underlying CNCs remain intact after polymer-grafting (Supporting Information, Appendix B, Figure B1); however, the overall CrI for all g-CNCs was reduced due to the presence of amorphous polymer chains on the nanoparticle surface (Table 4.2).

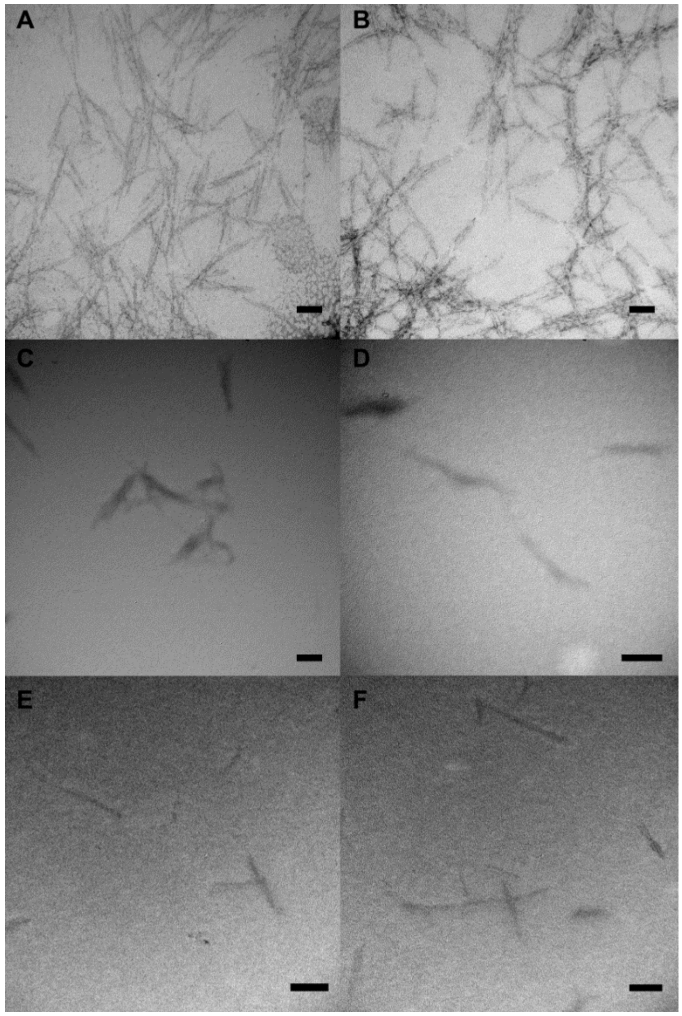

Figure 4.4. Transmission electron microscopy images of A) CNCs, B) BiB-CNCs, C) PBA_L-*g*-CNCs, D) PBA_H-*g*-CNCs, E) $PMMA_L$-*g*-CNCs and F) $PMMA_H$-*g*-CNCs. Scale bars = 100 nm.

To assess the effect of polymer grafting on the hydrophilicity of CNCs, a CNC partitioning experiment was performed in which CNCs and g-CNCs were dispersed in BA monomer, added to water (monomer:water 40:60 wt. %) and vortexed to see where the nanoparticles partition. When g-CNC suspensions in BA were added to water and agitated, they preferred to stay in the monomer phase; in contrast, unmodified CNCs transferred into the aqueous phase (Figure 4.5). Additionally, PMMA-*g*-CNCs with both low and high DP were observed to partition closer to the monomer–water interface after agitation, indicative of the higher surface activity of PMMA-grafted CNCs relative to PBA-grafted CNCs. While the water contact angles of both PBA-*g*-CNCs and PMMA-*g*-CNCs are similar at ca. 130^o (Table 4.2), pure PMMA is more hydrophilic than PBA and thus PMMA-*g*-CNCs are more likely to migrate to the monomer–water interface, suggesting their potential role as particle stabilizers (i.e., Pickering emulsifiers) during emulsion polymerization. While the contact angle measurements act as an indication of improved hydrophobicity of g-CNCs when cast as films the partitioning study provides additional information that is crucial for understanding g-CNC/monomer compatibility in relevant liquid environments. Gravimetric analysis of the monomer phases confirmed that the extent of g-CNC retention in the monomer phase after agitation was much higher than that observed with unmodified CNCs (Supporting Information, Appendix B, Table B1), while the retention of PMMA-*g*-CNCs in the monomer phase was lower than that of PBA-*g*-CNCs due to their partitioning more at the monomer–water interface.

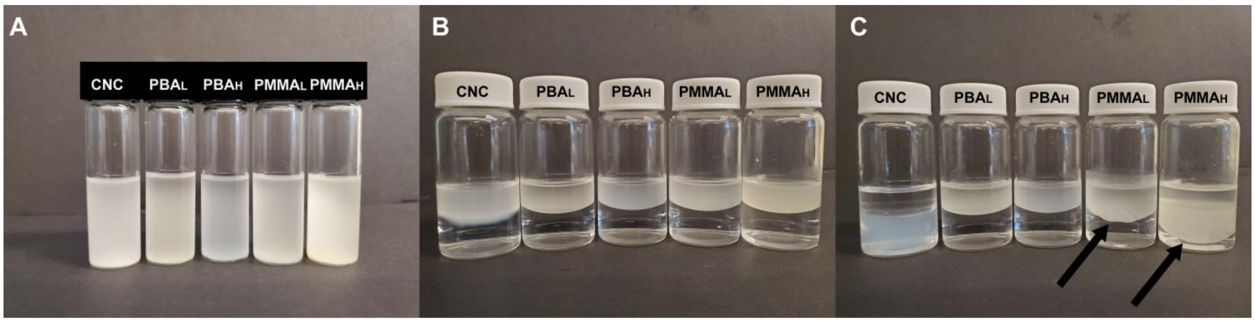

Figure 4.5. Partitioning experiment for g-CNCs. A) Photographs of all CNCs tested after 4 h of bath sonication in the monomer, BA; B) Photographs of all CNCs tested following the addition of the BA-suspended CNCs into the water phase (40:60 wt. % BA:water); C) Photographs of all CNCs tested following 1 min of vortex mixing of the BA/water mixture from (B), showing the partitioning of unmodified CNCs into the water phase while all g-CNCs remained in the monomer phase (as shown through the enhanced turbidity). Arrows point to g-CNCs partitioning at a monomer–water interface.

4.4.2 Characterization of Latexes and PSAs

Seeded semi-batch emulsion polymerization of PBA with *in situ* addition of CNCs and g-CNCs produced 13 stable latexes (one base case with no CNCs, four unmodified CNC containing latexes, and eight latexes with g-CNCs). Table 4.3 provides a summary of the final latex properties for all 13 samples. For latexes containing any CNC type, loadings were normalized to total cellulose mass to ensure that the number of CNCs in each sample was consistent. Latexes containing 0.5 phm of any CNC type had a larger average particle size measured by DLS than their 1 phm counterparts (~10-15 nm). This difference is likely due to the fact that a lower SDS concentration was employed to prepare latexes with 0.5 phm CNCs/g-CNC (1.5 phm SDS) as compared to those with 1 phm CNCs/g-CNCs (2 phm SDS), and less surfactant is known to lead to bigger particles.[193] The minimization of the total amount of surfactant needed to obtain stable latexes was prioritized over the use of a constant SDS concentration in order to maximize product sustainability. Furthermore, recent work by Pakdel et al. showed that the range of SDS concentrations used here has no major effect on PSA properties but in general more surfactant decreases adhesive performance.[159]

Latexes containing PMMA-*g*-CNCs exhibited a much smaller average particle size than those prepared with PBA-*g*-CNCs as determined by DLS (Table 4.3); this result is consistent with the tendency of PMMA-*g*-CNCs to partition at the monomer–water interface (Figure 4.5) and thus potentially stabilize the growth of more (and thus overall smaller) particles during the seeded emulsion polymerization process. Overall, latexes containing g-CNCs or CNC dispersed in the water phase (CNC-W) have relatively low polydispersities (PDI, $\leq$ 0.1) while latexes containing unmodified CNCs initially dispersed into the monomer phase (CNC-M) contain higher PDI values consistent with the relatively poor dispersion of CNCs into BA that likely results in persistent CNC aggregates during the polymerization process.

Table 4.3. PBA latex properties as a function of different CNC types and loadings.

Sample ID	CNC type	CNC loading (phm)	CNC dispersion location	Solids (wt. %)	Particle Size (nm)	PDI	Viscosity (mPa-s)	T_g (°C)	Contact Angle (°)
1	No CNCs	0	n/a	38	187±1	0.03±0.02	11±2	-48.4	94±1
2	CNC-W	0.5	Water	40	193±2	0.09±0.02	386±25	-47.3	90±1
3	CNC-M	0.5	Monomer	40	218±3	0.12±0.01	Unstable	-46.9	91±1
4	PBA_L-*g*-CNC	0.5	Monomer	39	193±2	0.04±0.04	11±1	-47.6	91±1
5	PBA_H-*g*-CNC	0.5	Monomer	40	201±1	0.07±0.04	14±2	-49.0	91±1
6	$PMMA_L$-*g*-CNC	0.5	Monomer	38	135±1	0.10±0.04	17±4	-46.7	90±1
7	$PMMA_H$-*g*-CNC	0.5	Monomer	38	142±2	0.11±0.03	11±3	-47.8	90±1
8	CNC-W	1	Water	40	182±3	0.03±0.02	485±12	-47.1	70±4
9	CNC-M	1	Monomer	39	187±1	0.13±0.02	287±9	-48.1	70±11
10	PBA_L-*g*-CNC	1	Monomer	37	182±1	0.01±0.01	13±2	-47.7	91±1
11	PBA_H-*g*-CNC	1	Monomer	37	187±2	0.04±0.05	12±1	-47.8	91±1
12	$PMMA_L$-*g*-CNC	1	Monomer	37	159±3	0.10±0.01	12±3	-46.8	88±3
13	$PMMA_H$-*g*-CNC	1	Monomer	37	180±1	0.04±0.05	15±5	-47.9	84±4

Rheological measurements were performed on final latexes to assess the effect of CNC type on latex viscosity (Table 4.3). Samples containing unmodified CNCs exhibited higher viscosities than any of the other latexes produced regardless of which phase was used to initially disperse the CNCs. Increasing the CNC concentration in water is known to increase the solution viscosity in conjunction with a phase transition from the isotropic (random orientation) to a bi-phasic (random and ordered) and ultimately a gel structure.[199,200] While concentration of CNCs in the water phase for all latexes produced is not high enough to induce gel formation, the increased viscosity of latexes containing unmodified CNCs is attributable to the increased volume fraction of suspended particles and possible interactions between CNCs and the polymer particles. Conversely, the viscosities of latexes prepared with g-CNCs showed no significant increase compared to latexes prepared without CNCs, suggesting that g-CNCs are not dispersed in the water phase but rather incorporated into (or onto) the latex particles. This observation is consistent with that of Yu et al. with silane-modified CNCs, which were found to be located either at the water–polymer interface or inside the latex particles and thus induced minimal impacts on the overall latex viscosity.[166]

DSC was used to measure the (T_g) of the CNC-modified latexes (Table 4.3), an important factor influencing the tack, peel strength, and shear strength of PSAs.[131] Overall, a slight increase in T_g (2.1°C or less) was observed for all latexes containing CNCs or g-CNCs, suggesting potential interactions between the polymer particles and nanocrystals that may cause small interfacial reduction in the chain mobility at the CNC-PBA interface within the PBA latex. However, all latexes maintained a very low T_g value consistent with their intended utility as a PSA, independent of the type or concentration of CNC incorporated. Additionally, the presence of a T_g related to PMMA for PSAs containing PMMA-*g*-CNC was not observed likely due to the small amount of g-CNCs added relative to bulk polymer (i.e. < 1g in total latex).

The effect of CNC and g-CNC loading on the water contact angle of PSA films was measured to gain an understanding of the resulting PSA wettability (Table 4.3). Previous work has shown that CNCs improve the hydrophilicity and thus wettability of hydrophobic polymer films, which can greatly improve both tack and peel strength;[157] however, higher loadings of CNCs (≥ 1 phm) have also been demonstrated to improve the elasticity of PSAs, simultaneously improving shear strength while decreasing tack and peel strength.[15] The contact angle of PSAs containing unmodified CNCs decreases with increasing CNC content, consistent with the addition of more CNCs increasing PSA hydrophilicity. However, the largest variability (standard deviation ± 11°) was found for CNC-M at a 1 phm loading, likely attributable to CNC aggregation creating a more heterogeneous interface in which the contact angle would strongly depend on the location of the water droplet used to measure the contact angle. For all PSAs containing g-CNCs, a decrease in the water contact angle was also observed but to a significantly lesser extent than their unmodified CNC-loaded counterparts. PMMA-*g*-CNCs exhibited a larger water contact reduction given that PMMA is more hydrophilic than PBA; however, the ability for PBA-g-CNCs to at least minimally decrease the contact angle may suggest that some CNCs are not fully or uniformly modified and thus could still impart some hydrophilicity to the PSA.

Transmission electron microscopy was used to image PSAs containing no CNCs and 1 phm CNCs/g-CNCs to visualize the location of CNCs within the polymer matrix. Latexes were diluted to 0.01 wt. % before being cast onto TEM grids for imaging so that individual particles could be observed. For PSAs containing CNC-W, CNC aggregates were observed around some of the latex particles (Figure 4.6B), indicating the ability of CNCs to physically (i.e.

physisorption) or chemically (i.e. crosslinking *via* initiation of CNC surface hydroxy groups by KPS) interact with, and ultimately bridge upon film formation, the latex particles. The same was found for PSAs prepared with CNC-M (Figure 4.6C); however, very large CNC aggregates were also present which were likely formed in the monomer phase prior to being expelled to the water phase during the reaction. In contrast, PSAs prepared with low DP g-CNCs showed the presence of relatively few CNCs between the latex particles, with those that were visible consistently observed near the particle interface and appearing to bend around the latex particles (Figures 4.6D and 4.6F). A study by Chen et al.[201] demonstrated that CNCs are able to bend up to a critical bending limit of 60°; the apparent bending of g-CNCs here (Figure 4.6D and 4.6F) is consistent with previous observations of the bending of both unmodified[143] and polymer-grafted[145] CNCs on latex particle surfaces.

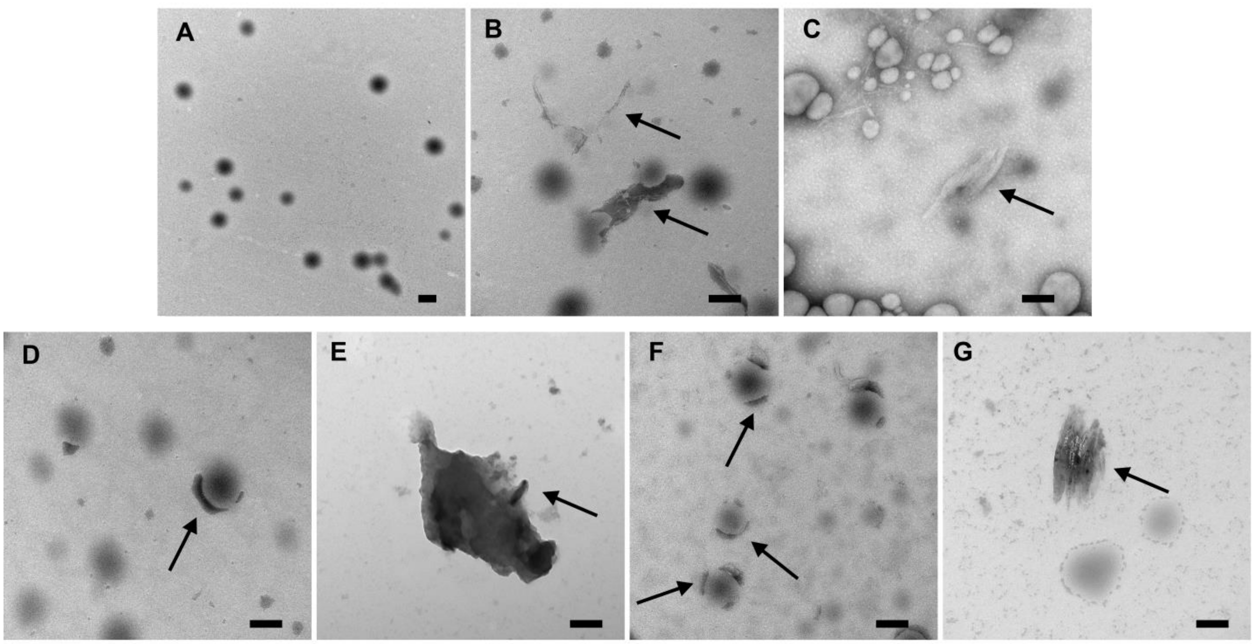

Figure 4.6. Transmission electron microscopy images of PSAs diluted to 0.01 wt. % containing A) no CNCs, B) CNC-W (unmodified CNCs loaded into the emulsion polymerization through the water phase), C) CNC-M (unmodified CNCs loaded into the emulsion polymerization through the monomer phase, D) PBA_L-*g*-CNC, E) PBA_H-*g*-CNCs, F) $PMMA_L$-*g*-CNCs and G) $PMMA_H$-*g*-CNCs. Arrows indicate the location of CNCs or g-CNCs. All scale bars are to 200 nm.

On the other hand, PSAs containing high DP g-CNCs had large CNC aggregates throughout the continuous phase of the PSA or associated with polymer coagulum (Figures 4.6E and 4.6G). It is unclear if the aggregates formed in the monomer phase (from grafted chain entanglement) or if the larger size of the high DP g-CNCs inhibited their incorporation into the latex particles forcing them into the continuous phase and inducing aggregation due to their incompatibility with water. To a minor extent, it may also be possible that these high DP g-CNCs act as secondary seeds of nucleation during the emulsion polymerization. Irrespective of the mechanism, large CNCs and CNC aggregated were found to be less well-integrated into the latex particles. Overall, the low DP g-CNCs appear to produce the most consistent and CNC-incorporated latex particles among those analyzed.

Latexes were then cast into PSA films as described in Appendix B to evaluate their adhesive properties. Films were cast using Mayer rods to control film thickness and roughness, with more viscous latexes requiring Mayer rods of a higher number (e.g. 50) and less viscous latexes requiring a lower number (e.g. 20). The first PSA set (0.5 phm unmodified CNCs and the no-CNC "base case" latex) was cast using a Mayer rod #50 (wet film thickness = 127 μm); however, latexes containing PMMA-*g*-CNCs could not be cast using this same technique due to the low viscosity and smaller particle size of the base latex. For the 1 phm latex set, Mayer rod #20 (wet film thickness = 50.8 μm) was used so that all latexes could be cast into uniform films and compared directly. Since a thicker PSA film will increase both tack and peel strength but reduce shear strength, using different Mayer rods for different formulations means that at present, we cannot compare PSA properties between the 0.5 and 1 phm CNC loaded latexes; instead, the following discussion is limited to comparing latexes prepared with the same CNC/g-CNC loading in which the films have the same thickness (and thus differences in adhesion properties are attributed to the composition of the latex itself). Future work will redo the PSA film casting and measure tack, peel and shear strength on films with the same thickness.

Figures 4.7 and Figure 4.8 summarize the tack, peel and shear strength for adhesive films prepared from latexes with PBA-g-CNCs and PMMA-g-CNCs (compared to the no-CNC and unmodified CNC controls) at 0.5 and 1 phm loading, respectively. ANOVA and post-hoc analysis details can be found in Appendix B.

Tack Results

The addition of 0.5 phm CNC-W significantly improved the tack of PSAs relative to the no-CNC latex; however, there was no significant difference in tack between any PSAs containing CNCs or g-CNCs (Figure 4.7A). We attribute this result to the addition of CNCs (even if grafted with a hydrophobic polymer) imparting a degree of hydrophilicity on the PSA films consistent with the lower contact angles observed for these films (Table 4.3), leading to higher work of adhesion and increased tack.[17] While g-CNCs lower the contact angle and thus improve hydrophilicity to a lesser degree than CNCs (Table 4.3), the polymer grafts in this case may be behaving analogously to low molecular weight polymers which interact with the bulk polymer chains. When lower molecular weight polymer chains are present, the mobility of the polymer matrix (i.e. flowability) will increase to improve tack; this is particularly true at the CNC–latex interface, of which there is more overall in films prepared with low DP polymers (Figure 4.6D and 4.6F). This hypothesis is further supported by the 1 phm loading data (Figure 4.8A), in which the high DP g-CNC PSAs significantly underperform in terms of tack relative to low DP g-CNC PSAs.

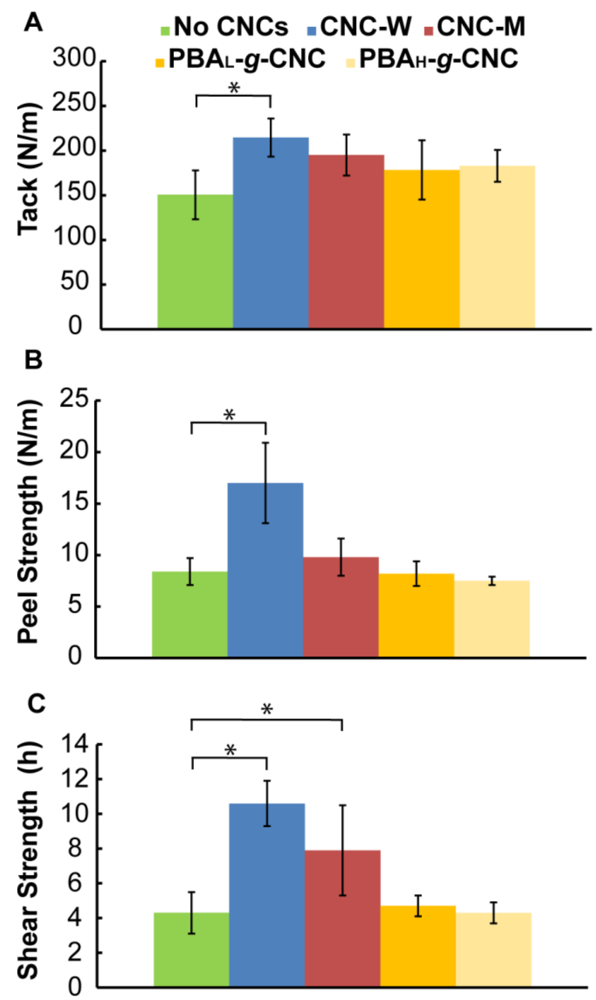

Figure 4.7. PSA film performance testing for latexes containing no CNCs and 0.5 phm CNCs and PBA-*g*-CNCs: A) tack, B) peel strength, and C) shear strength. Bars containing an asterisk (*) signifies a significant difference from the PSA containing no CNCs as determined by Tukey post-hoc analysis.

A significant reduction in tack was also observed for CNC-M at the 1 phm loading due to the presence of large CNC aggregates in the film, consistent with their initial poor dispersion into the monomer phase prior to polymerization (Figure 4.6C); both g-CNCs with a high DP were also more aggregated at a 1 phm loading (Figures 4.6E and 4.6F), which may also contribute to the lower tack observed for these fillers. Additionally, since the numerical values of tack for PSAs containing 1 phm CNCs/g-CNCs are similar to those with 0.5 phm despite being significantly thinner films, we can infer that the PSAs with 1 phm CNCs/g-CNCs have enhanced tack.[15] Unfortunately, there are no generalized models that exist to correct for film thickness, making direct numerical comparisons out of the scope of this thesis

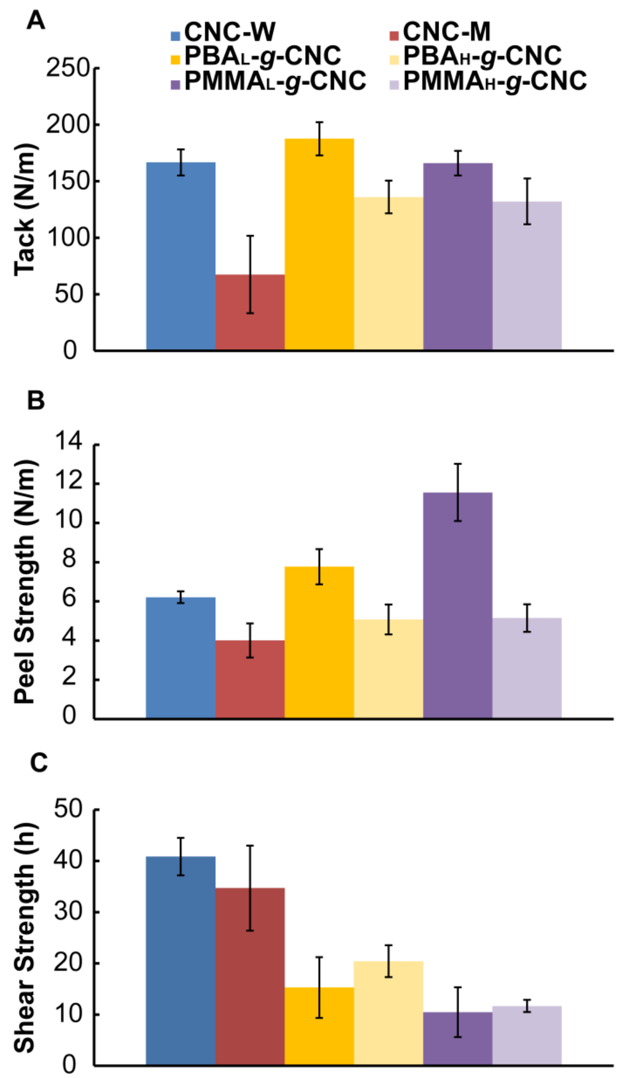

Figure 4.8. PSA film performance testing for latexes containing 1 phm CNCs and PBA and PMMA *g*-CNCs: A) tack, B) peel strength, and C) shear strength. Statistical significance relative to the PSA containing no CNCs could not be determined due to film thickness differences between it and latexes containing 1 phm CNCs/g-CNCs.

Peel Strength Results

Peel strength is also directly correlated with the wettability and polymer chain mobility of a PSA film, with the addition of hydrophilic CNCs expected to improve peel by increasing PSA wetting.[17,157–160,167] Consistent with this hypothesis, Figure 4.7B shows that CNC-W significantly improved peel strength compared to the no-CNC PSA, attributed to the good dispersion of CNCs in the continuous (aqueous) phase of the latex and therefore improved wettability of the PSA. However, PSAs containing 1 phm of unmodified CNCs underperformed compared to low DP g-CNCs and were observed to aggregate around the polymer particles by TEM (Figure 4.6B). Long CNC aggregates are known to improve the elasticity of PSAs by acting as anchoring points for polymer adsorption, thus forming a nanoparticle-reinforced polymer network;[159,165] peel strength is attributed to the ability of a PSA to dissipate energy by deformation as it is peeled off a surface (i.e. when the film is less elastic).[202] Thus, the presence of CNC aggregates are likely improving PSA elasticity as indicated by the large shear strength observed at 1 phm (Figure 4.7C and 4.8Cc). Peel strength was also improved using low DP g-CNCs at higher loadings (Figure 4.8B) despite the significantly higher hydrophilicity (as estimated *via* contact angle, Table 4.2) of PSAs with unmodified CNCs. Given the high interfacial dispersion of CNCs achieved with the low DP CNC latex (Figure 4.6D and 4.6F), we attribute this improved peel performance to the higher dispersion and thus interfacial area between the CNCs and the PBA within the latex (and ultimately within the film), enhancing polymer chain mobility at these interfaces to dissipate internal stresses. $PMMA_L$-*g*-CNCs have the highest peel strength at the 1 phm loading likely due to the presence of "hard" MMA monomers (i.e. high T_g) improving the peel strength up to a maximum point (i.e. until the polymer is too hard to function as a PSA).[15]

Shear Strength Results

In terms of shear strength, PSAs prepared using unmodified CNCs resulted in significantly higher shear strength (Figures 4.7C and 4.8C), consistent with previous literature reports indicating that CNCs improve film coalescence[203] and interact with the latex polymer either as physical anchors for polymer chain entanglement or through chemical grafting thus improving the gel network and film cohesion.[17,156–160,165–167] However, no significant increase in shear strength was observed between the no-CNC PSA and those prepared with 0.5 phm PBA-*g*-CNCs. A similar overall trend was observed at a 1 phm loading, with PSAs containing unmodified CNCs exhibiting a much higher shear strength relative to PSAs prepared using g-CNCs. A recent study by Pakdel et al.[167] suggests that CNC aggregation may be playing a much larger role with respect to shear strength. The incorporation of either sulfated CNCs or "less hydrophilic" CNCs into latex-based PSAs yielded similar gel contents (i.e. percentage of crosslinked material) at all CNC loadings; however, the more aggregated sulfated CNCs after film formation exhibited a higher PSA shear strength at all loadings. This improvement in shear strength was attributed to the presence of longer CNC aggregates, which could expand the area through which polymer chains were immobilized (*via* physical interactions) to a greater extent, therefore increasing shear strength.[167] In the case of adding g-CNCs, the ability for physical adsorption between the CNC and the polymer chains is likely reduced due to the presence of grafts on the surface. Therefore, shear strength will not increase in the presence of g-CNCs as observed in Figures 4.7C and 4.8C, regardless of the degree of dispersion of the CNCs in the latex.

Summary

Overall, the adhesion results suggest that there are both benefits and drawbacks to using CNCs or g-CNCs as additives to latex-based PSAs. A summary of the key findings is provided in Table 4.4. With tack, the incorporation of either unmodified CNCs or g-CNCs with a low DP of grafted polymer will yield similar results, attributed to the improved wettability and/or capacity of the grafted CNC fillers to create deformable CNC-PBA interfaces (and thus displace PBA-PBA interactions) within the PSA phase. However, the improved dispersion of low DP g-CNCs within the polymer film significantly enhanced peel strength at higher g-CNC loadings, while more aggregated CNCs could still improve peel strength but to a lesser extent. Additionally, the use of PMMA as the CNC modification resulted in higher peel strength PSA films relative to PBA-grafted CNCs, likely due to the positive effect of higher T_g polymers on peel strength. Lastly, the shear strength was highest for PSAs containing unmodified CNCs due to the potential for physical crosslinking *via* CNC–polymer physical or chemical interactions not possible when the CNC surface is already grafted with a like polymer.

Table 4.4. Summary of results from PSA testing.

PSA Property	Optimal CNC type	Explanation
Tack	Unmodified CNCs or low DP g-CNCs	Improved PSA wettability (with unmodified and g-CNCs) or increased local chain mobility at g-CNC/PBA latex interface (with g-CNCs)
Peel strength	$PMMA_L$-*g*-CNCs	Improved wettability, increased chain mobility at g-CNC-PBA latex interface, higher T_g of grafted polymer
Shear strength	Unmodified CNCs	CNC-polymer interactions lead to physical/chemical crosslinks and improve film coalescence. When CNCs are polymer grafted and localized inside/at the latex particle interface they cannot help in network formation during film casting to the same extent as CNCs dispersed in the continuous phase

4.5 Conclusions

Stable *in situ* g-CNC–latex nanocomposites were synthesized through a seeded semi-batch emulsion polymerization process and tested as PSAs. PBA-*g*-CNCs and PMMA-*g*-CNCs were synthesized *via* SI-ATRP and were re-dispersible in BA monomer prior to latex synthesis, as determined by partitioning experiments. g-CNC-based latexes did not significantly enhance the solution viscosity of the latex while the addition of unmodified CNCs dispersed in the water resulted in much higher viscosities at all loadings, suggesting the successful incorporation of g-CNCs into the latex particles.

TEM indicated that unmodified CNCs introduced in the water prior to latex synthesis aggregated near the latex particles, similarly CNCs introduced in the monomer phase prior to emulsion polymerization also aggregated in the continuous phase; in contrast, low DP g-CNCs were found in much smaller quantities individually attached to the surface of PBA particles (with virtually none in the continuous phase) while high DP g-CNCs were observed to be highly aggregated with their PSAs containing a high fraction of coagulum. Correspondingly, an improvement in both tack and peel was seen for PSAs containing 1 phm of low DP g-CNCs, with peel strength of the resulting nanocomposite PSA exceeding that achievable using unmodified CNCs.

The improvement in both tack and peel was attributed to a well-dispersed g-CNC *inside* the polymer particles, which would in turn disrupt inter-polymer interactions and improve film formation despite their less significant contribution toward improving the overall PSA wettability compared to unmodified CNCs. In contrast, shear strength was not significantly improved with the addition of g-CNCs while PSAs prepared with unmodified CNCs that could adsorb the PSA polymer enabled significantly higher shear stresses. The nanocomposite materials produced in this work thus provide insight into how CNC surface chemistry and the presence of low DP graft polymers, which improve PSA mobility, can improve tack and peel strength of latex-based PSAs.

While the work presented here uses a homopolymer system of PBA as the bulk latex polymer, the findings suggest that the use of g-CNCs in more hydrophobic PSA formulations (i.e. using monomers with lower water solubility than BA) may be beneficial to PSA property enhancement. In the study by Ouzas et al.[157] in which 2-ethyl hexyl acrylate was used in a PSA formulation, severe CNC aggregation occurred during film formation and no significant enhancements in either peel or shear strength were achieved. While CNC aggregation herein led to improved shear strength of the PSA films, extreme incompatibility between CNCs and the PSA monomer can result in too much aggregation and thus no PSA improvement. In cases like these, the use of hydrophobic additives like the g-CNCs presented here may be of particular benefit, with the better dispersions of g-CNCs achieved after film formation offsetting the lower wettability of the g-CNCs relative to unmodified CNCs.

4.6 Acknowledgements

The authors thank CelluForce Inc. for providing the unmodified CNC starting material and Prof. Adronov and Prof. Thompson at McMaster for equipment use. The Biointerfaces Institute at McMaster is acknowledged for equipment use and training. Special thanks to Marcia Reid and the Electron Microscopy Facility in the Health Science Center at McMaster University and Victoria Jarvis at the McMaster Analytical X-ray Diffraction Facility for their time and expertise. E.D.C. is grateful for support and recognition through the Canada Research Chairs program and the University of British Columbia's President's Excellence Chair initiative.

Appendix B: Supporting Information for Chapter 4

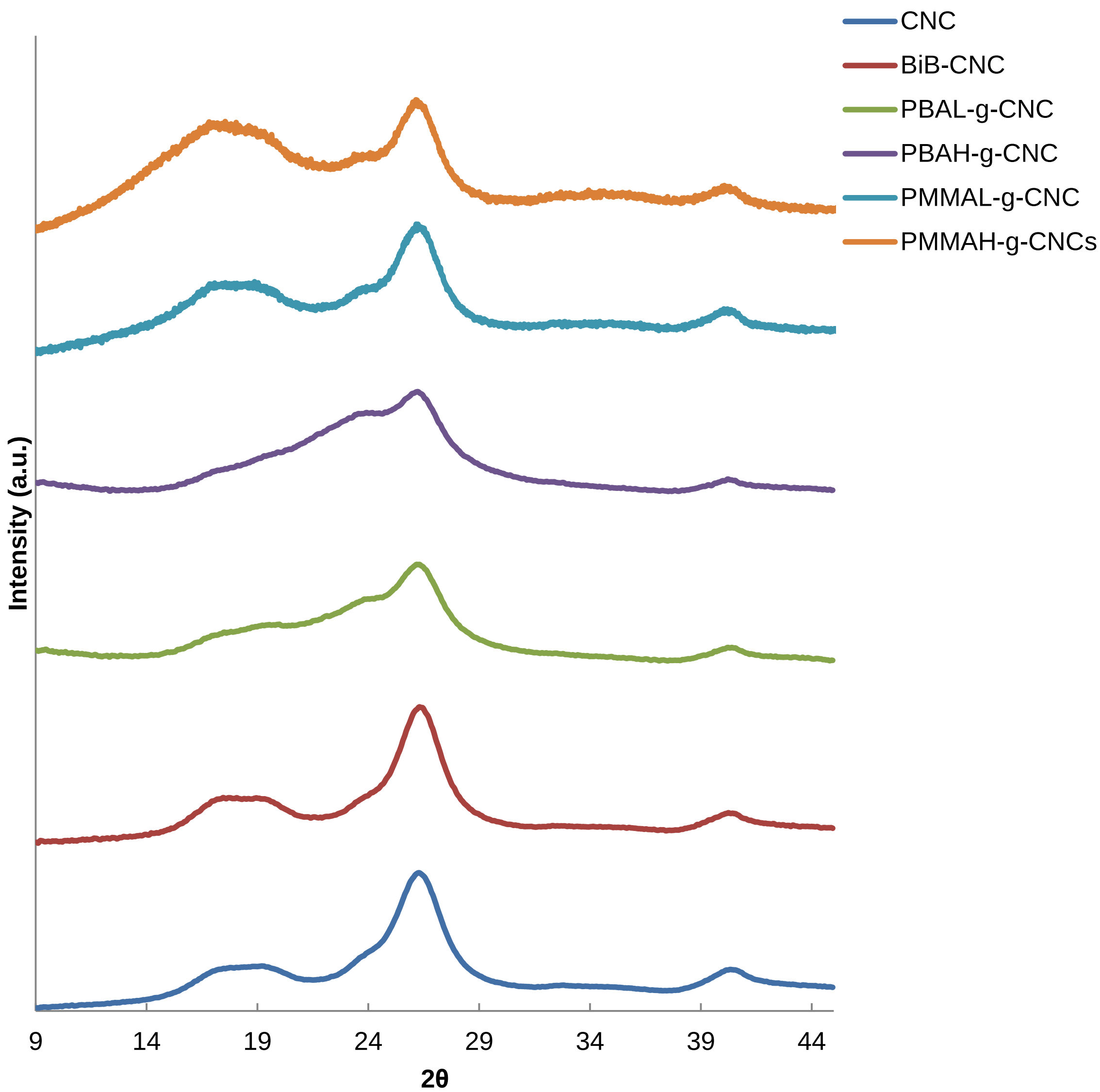

Figure B1. XRD spectra for CNC, BiB-CNC and g-CNC.

Table B1. Mass recovered from the BA monomer phase during the partitioning experiments.

Component	% Mass in Monomer Phase
CNC	<1
PBA_L-*g*-CNC	75
PBA_H-*g*-CNC	92
$PMMA_L$-*g*-CNC	63
$PMMA_H$-*g*-CNC	40

Statistical analysis of PSA testing

To evaluate statistically significant differences between PSA testing results, ANOVA was used on each sample set (i.e. comparing the no-CNC latex with the 0.5 phm g-CNC loaded latexes (set 1) and the 1 phm g-CNC loaded latexes (set 2)). A significance level of 5% was used, and the resulting *p*-values were compared to assess the null hypothesis (i.e. all population means are equal).

Table B2. ANOVA charts for latex set 1 (tack analysis).

SUMMARY

Groups	*Count*	*Sum*	*Average*	*Variance*
No CNCs	6	903.16	150.5267	749.1703
CNC-W	6	1287.4	214.5667	459.7772
CNC-M	6	1170.47	195.0783	529.6905
PBA_L-*g*-CNC	6	1070.59	178.4317	1099.665
PBA_H-*g*-CNC	6	1097.15	182.8583	319.9229

ANOVA

Source of Variation	*SS*	*df*	*MS*	*F*	*P-value*	*F crit*
Between Groups	13256.38	4	3314.096	5.246768	0.003294	2.75871
Within Groups	15791.13	25	631.6452			
Total	29047.51	29				

Table B3. ANOVA chart for latex set 1 (peel strength).

SUMMARY

Groups	*Count*	*Sum*	*Average*	*Variance*
No CNCs	6	50.38189	8.396982	1.712148
CNC-W	6	101.9252	16.98753	15.33395
CNC-M	6	58.62205	9.770341	3.292279
PBA_L-*g*-CNC	6	49.30709	8.217848	1.41791
PBA_H-*g*-CNC	6	45.23228	7.538714	0.167682

ANOVA

Source of Variation	*SS*	*df*	*MS*	*F*	*P-value*	*F crit*
Between Groups	363.0953	4	90.77383	20.70196	1.23E-07	2.75871
Within Groups	109.6198	25	4.384793			
Total	472.7151	29				

Table B4. ANOVA chart for latex set 1 (shear strength analysis).

SUMMARY

Groups	*Count*	*Sum*	*Average*	*Variance*
No CNCs	6	25.59389	4.265648	1.380161
CNC-W	6	63.3175	10.55292	1.641361
CNC-M	6	47.23611	7.872685	6.68386
PBA_L-*g*-CNC	6	28.36611	4.727685	0.310698
PBA_H-*g*-CNC	6	25.85722	4.309537	0.346042

ANOVA

Source of Variation	*SS*	*df*	*MS*	*F*	*P-value*	*F crit*
Between Groups	186.7374	4	46.68435	22.52645	5.54E-08	2.75871
Within Groups	51.81061	25	2.072424			
Total	238.548	29				

Table B5. ANOVA chart from latex set 2 (tack).

SUMMARY

Groups	Count	Sum	Average	Variance
CNC-W	6	1000.32	166.72	133.8901
CNC-M	6	560.77	93.46167	1004.413
PBA_L-*g*-CNC	6	996.72	166.12	118.5217
PBA_H-*g*-CNC	6	793.35	132.225	411.3101
$PMMA_L$-*g*-CNC	6	1125.82	187.6367	215.8003
$PMMA_H$-*g*-CNC	6	816.77	136.1283	209.6975

ANOVA

Source of Variation	SS	df	MS	F	P-value	F crit
Between Groups	33651.75	5	6730.349	19.28805	1.44E-08	2.533555
Within Groups	10468.16	30	348.9387			
Total	44119.91	35				

Table B6. ANOVA chart for latex set 2 (peel strength).

SUMMARY

Groups	Count	Sum	Average	Variance
CNC-W	6	37.25189	6.208649	0.087228
CNC-M	6	24.08657	4.014428	0.75267
PBA_L-*g*-CNC	6	69.35813	11.55969	2.140276
PBA_H-*g*-CNC	6	30.92514	5.154189	0.495524
$PMMA_L$-*g*-CNC	6	46.64951	7.874919	0.80951
$PMMA_H$-*g*-CNC	6	30.49994	5.083323	0.573929

ANOVA

Source of Variation	SS	df	MS	F	P-value	F crit
Between Groups	223.2096492	5	44.64193	55.12328	3.23E-14	2.533555
Within Groups	24.29568474	30	0.809856			
Total	247.505334	35				

Table B7. ANOVA chart for latex set 2 (shear strength).

SUMMARY

Groups	*Count*	*Sum*	*Average*	*Variance*
CNC-W	6	245.1378	40.8563	13.28354
CNC-M	6	208.1514	34.6919	68.82639
PBA_L-*g*-CNC	6	62.94917	10.49153	1.411511
PBA_H-*g*-CNC	6	70.12028	11.68671	23.59231
$PMMA_L$-*g*-CNC	6	122.5814	20.43023	9.581672
$PMMA_H$-*g*-CNC	6	91.73417	15.28903	35.16636

ANOVA

Source of Variation	*SS*	*df*	*MS*	*F*	*P-value*	*F crit*
Between Groups	4815.636	5	963.1272	38.05278	4.13E-12	2.533555
Within Groups	759.3089	30	25.3103			
Total	5574.945	35				

Based on the results of ANOVA, the null hypothesis was rejected in all cases (i.e. the p-value < significance value). From this, post-hoc analysis was performed to determine which means were statistically different for each ANOVA analysis. Tukey tests were then used to compare all possible pairs of means based on the studentized range distribution (q). The test is as follows:

$$q_{crit} > q_{\alpha}$$

$$q_{crit} = \frac{\bar{x}_{max} - \bar{x}_{min}}{\sqrt{\frac{MS_W}{n}}}$$

where q_{α} is taken for the studentized range q table for a given number of groups and degrees of freedom, n is the number of samples within a group, and MS_W is the pooled variance. In the case where the above condition is true (i.e. q_{crit} larger than the q_{α} value from the studentized range distribution), than a significant difference between the two compared groups is present. The following tables summarize the findings of a post-hoc Tukey test for all ANOVA groups.

Table B8. Critical value q_α from the studentized range distribution. 16

	Latex set 1	**Latex set 2**
q_α	4.17	4.30

Table B9. Summary of Tukey HSD for latex set 1.

	Tack		**Peel strength**		**Shear strength**	
Comparisons	q_{crit}	$q_{crit} > q_\alpha$	q_{crit}	$q_{crit} > q_\alpha$	q_{crit}	$q_{crit} > q_\alpha$
No CNC/CNC-W	6.24	yes	10.05	yes	10.70	yes
No CNC/CNC-M	4.34	yes	1.61	no	6.14	yes
No CNC/PBA_L-*g*-CNC	2.72	no	0.21	no	0.79	no
No CNC/PBA_H-*g*-CNC	3.15	no	1.00	no	0.07	no
CNC-W/CNC-M	1.90	no	8.44	yes	4.56	yes
CNC-W/ PBA_L-*g*-CNC	3.52	no	10.26	yes	9.91	yes
CNC-W/ PBA_H-*g*-CNC	3.09	no	11.05	yes	10.62	yes
CNC-M/ PBA_L-*g*-CNC	1.62	no	1.82	no	5.35	yes
CNC-M/ PBA_H-*g*-CNC	1.19	no	2.61	no	6.06	yes
PBA_L-*g*-CNC/ PBA_H-*g*-CNC	0.43	no	0.79	no	0.71	no

Table B10. Summary of Tukey HSD for latex set 2.

	Tack		**Peel strength**		**Shear strength**	
Comparisons	q_{crit}	$q_{crit} > q_\alpha$	q_{crit}	$q_{crit} > q_\alpha$	q_{crit}	$q_{crit} > q_\alpha$
CNC-W/CNC-M	9.61	yes	5.97	yes	3.00	no
CNC-W/$PMMA_L$-*g*-CNC	0.08	no	14.56	yes	14.78	yes
CNC-W/$PMMA_H$-*g*-CNC	4.52	yes	2.87	no	14.20	yes
CNC-W/PBA_L-*g*-CNC	2.74	no	4.54	yes	9.95	yes
CNC-W/PBA_H-*g*-CNC	4.01	no	3.06	no	12.45	yes
CNC-M/$PMMA_L$-*g*-CNC	9.53	yes	20.54	yes	11.78	yes
CNC-M/$PMMA_H$-*g*-CNC	5.08	yes	3.10	no	11.20	yes
CNC-M/ PBA_L-*g*-CNC	12.35	yes	10.51	yes	6.94	yes
CNC-M/ PBA_H-*g*-CNC	5.59	yes	2.91	no	9.45	yes
$PMMA_L$-*g*-CNC	4.44	yes	17.44	yes	0.58	no
$PMMA_L$-*g*-CNC	2.82	no	10.03	yes	4.84	yes
$PMMA_L$-*g*-CNC	3.93	no	17.63	yes	2.34	no
$PMMA_H$-*g*-CNC/	7.27	yes	7.41	yes	4.26	no
$PMMA_H$-*g*-CNC/	0.51	no	0.19	no	1.75	no
PBA_L-*g*-CNC/PBA_H-*g*-CNC	6.75	yes	7.60	yes	2.50	no

Chapter 5: Conclusions & Future Work

5.1 Conclusions

The incorporation of CNCs into latex-based PSAs prior to this work has enable improvements in adhesive tack, peel strength and shear strength; however, the effects of CNC surface chemistry and location within a latex on PSA properties had yet to be fully understood. This work provides a method of producing highly-modified polymer-grafted CNCs using the controlled radical polymerization technique SI-ATRP. These polymer-grafted CNCs were then added *in situ* into a seeded semi-batch emulsion polymerization to produce CNC/latex nanocomposites that were cast as films and tested as PSAs.

In Chapter 3, a comparison between grafting the hydrophobic polymer PBA from CNC surfaces *via* SI-ATRP in either a polar solvent (DMF) or a non-polar solvent (toluene) was performed. Grafting in either solvent produced surface-modified CNCs, but polymer-grafted CNCs synthesized in DMF contained up to 6 times more polymer grafts on a mass basis. This improved grafting efficiency was attributed to the higher colloidal stability of BiB-CNCs in DMF, by which a better dispersion maximized the number of available surface initiator groups during the polymerization. In contrast, BiB-CNCs dispersed in toluene succumbed to severe aggregation, which reduced the number of accessible initiating sites during polymerization. PBA-*g*-CNCs produced in DMF were colloidally stable in toluene (due to steric stabilization and improved solvent compatibility), while PBA-*g*-CNCs produced in toluene were aggregated, consistent with the low grafted polymer chain surface coverage on those CNCs. This work highlighted the importance of reaction media when grafting polymers *from* CNCs *via* SI-ATRP, specifically emphasizing that BiB-CNC colloidal stability is more important than maximizing polymer/solvent compatibility in terms of achieving high graft densities. While SI-ATRP is a powerful tool for modifying CNCs with polymers, this work provides a deeper understanding of what affects the graft density, and thus dispersion of polymer-grafted CNCs, which to-date has not been extensively studied.[41,104,105,179,182]

In Chapter 4, PBA-g-CNCs and PMMA-g-CNCs of a low and high DP were synthesized and introduced *in situ* into a seeded semi-batch emulsion polymerization to produce PBA latexes to be employed as PSAs. Polymer-grafted CNCs were loaded into the polymerization through the monomer phase. The location of CNCs/g-CNCs was determined by TEM, with low DP grafted-CNCs found to be in/on the surface of the latex particles. Conversely, high DP grafted-CNCs were highly aggregated in the continuous phase, and coagulum was found throughout the samples prepared for TEM. Latexes containing unmodified CNCs introduced either in the water or monomer phase during emulsion polymerization were also synthesized, and the CNCs were found to be localized in the continuous water phase but aggregated nearby the latex particles. PSA testing of all produced latexes showed that the incorporation of low DP grafted-CNCs achieved higher peel strength than all other PSAs due to improved wettability and improved PSA flowability; PSAs with low DP grafted-CNCs had comparable tack to PSAs with unmodified CNCs introduced to the polymerization through the water phase. Lastly, the polymer-grafted CNC containing latexes tested did not significantly improve PSA shear strength, while PSAs prepared with unmodified CNCs that could adsorb to polymer chains significantly improved cohesive strength. This work provided insight into the importance of CNC surface chemistry, dispersibility, and location within latex systems on the performance of latex-based PSA properties. While the PSAs containing polymer-grafted CNCs were not able to improve shear strength, the learnings here may be useful for other latex-based products such as coatings in which enhanced incorporation of CNCs inside the latex particles (but without aggregation) may be desired.

5.2 Future Work

While Chapter 3 of this thesis compared the effect of the reaction medium on the extent of grafting hydrophobic polymers from CNC surfaces, a more in-depth understanding of how CNC grafting occurs in non-polar media should be investigated. A future study would evaluate the extent of grafting and changes in CNC morphology/colloidal stability as a function of reaction time. Specifically, if BiB-CNCs are highly aggregated in toluene prior to grafting, we expect that these aggregates will start to break up as polymer chains grow from the surface. Additionally, the same comparison study between polar and non-polar solvents could be performed for different hydrophobic polymers in order to determine if the effect of solvent is independent of the polymer synthesized.

We also recognize that the large-scale implementation of SI-ATRP for CNC surface modification would not be feasible due to purification constraints and the use of toxic solvents. As such, the results from Chapter 3 aim to provide insight into what a “hydrophobic” CNC should look like if the aim is to incorporate them into the polymer phase of a latex. Here, hydrophobic CNCs with high water contact angles (i.e. ~ 130°), a high degree of surface coverage, and highly retained morphology and crystallinity were synthesized. Developing methods to synthesize hydrophobic CNCs using easier (i.e. no catalyst removal) and greener (i.e. no solvents) one-step methods like polymer adsorption may be beneficial, with adsorption having been shown to completely cover CNC surfaces but without the headache of strenuous post-synthesis characterization;[204-172] however, the utility of such methods for producing hydrophobic CNCs (like the ones presented here) is still an open question. Additionally, water-based grafting techniques to produce hydrophobic CNCs, such as grafting tannic acid/decylamine[205] in the absence of synthetic polymer grafts, may reduce the effects seen here in Chapter 4 where interactions between grafted and bulk polymer could improve tack and peel strength. Ultimately, while there is clear potential for the use of hydrophobic CNCs in latex-based PSAs or coating applications, the development of new, safer, and easier methods of production should be prioritized.

When PSA adhesive properties are improved with the addition of CNCs, there is also a corresponding change in their mechanical properties. In general, PSAs with better adhesive properties (tack and peel strength) are less elastic and thus result in a lower Young's modulus. Dynamic mechanical analysis (DMA) is often used to evaluate the storage and loss modulus of free-standing PSA films, but sample preparation can be inconsistent and requires a lot of material (i.e., 15- 20 mL of 40 wt.% latex per sample). Due to material synthesis constraints (i.e., 60 mL total of latex produced) other methods of mechanical testing are required to evaluate the mechanical properties of latex-CNC films. The proposed method for these measurements is nanoindentation, which requires only sub-millimetre thick films cast on a substrate and thus significantly less test material than is needed compared with DMA or other tensile testing methods. An optimized film formation protocol for nanoindentation experiments must be developed in order to produce flat films with a thickness of 100-200 μm. A hydrophobic substrate should be used (e.g. polystyrene), and films should be produced *via* spin-coating to minimize surface roughness. Additionally, PSA testing on latex set 1 (i.e., no CNCs and 0.5 phm loaded PSAs) should be performed again at the lower thickness such that direct comparisons with latex set 2 (i.e., 1 phm loaded PSAs) can be made. Another consideration for future work to build off of Chapter 4 include incorporating polymer grafted CNCs into copolymer latexes that more closely resemble commercial PSA formulations like BA/MMA, EHA/BA/MMA or BA/VAc (since only BA homopolymer latexes were tested so far).

References

(1) Habibi, Y.; Lucia, L. A.; Rojas, O. J. Cellulose Nanocrystals : Chemistry, Self-Assembly, and Applications. *Chem. Rev.* **2010**, *110* (6), 3479–3500.

(2) Klemm, D.; Cranston, E. D.; Fischer, D.; Gama, M.; Kedzior, S. A.; Kralisch, D.; Kramer, F.; Kondo, T.; Lindström, T.; Nietzsche, S.; Petzold-Welcke, K.; Rauchfuß, F. Nanocellulose as a Natural Source for Groundbreaking Applications in Materials Science: Today's State. *Mater. Today* **2018**, *21* (7), 720–748. https://doi.org/10.1016/j.mattod.2018.02.001.

(3) Charreau, H.; Cavallo, E.; Foresti, M. L. Patents Involving Nanocellulose : Analysis of Their Evolution since 2010. *Carbohydr. Polym.* **2020**, *237* (December 2019), 116039. https://doi.org/10.1016/j.carbpol.2020.116039.

(4) Charreau, H.; Foresti, M. L.; Vázquez, A. Nanocellulose Patents Trends : A Comprehensive Review on Patents on Cellulose Nanocrystals , Microfibrillated and Bacterial Cellulose. *Recent Pat. Nanotechnol.* **2013**, *7*, 56–80.

(5) Shatkin, J. A.; Wegner, T. H.; Bilek, T.; Cowie, J. Market Projections of Cellulose Nanomaterial-Enabled Products- Part 1: Applications. *TAPPI J.* **2014**, *13* (5), 9–16.

(6) Cowie, J.; Bilek, T.; Wegner, T. H.; Shatkin, J. A. Market Projecttions of Cellulose Nanomaterial-Enabled Products - Part 2: Volume Estimates. *TAPPI J.* **2014**, *13* (6), 57–69.

(7) Blanco, A.; Monte, M. C.; Campano, C.; Balea, A.; Merayo, N.; Negro, C. *Nanocellulose for Industrial Use: Cellulose Nanofibers (CNF), Cellulose Nanocrystals (CNC), and Bacterial Cellulose (BC)*; Elsevier Inc., 2018. https://doi.org/10.1016/B978-0-12-813351-4.00005-5.

(8) Nickerson, R. F.; Habrle, J. A. Cellulose Intercrystalline Structure. *Ind. Eng. Chem.* **1947**, *39* (11), 1507–1512. https://doi.org/10.1021/ie50455a024.

(9) Revol, J. F.; Bradford, H.; Giasson, J.; Marchessault, R. H.; Gray, D. G. Helicoidal Self-Ordering of Cellulose Microfibrils in Aqueous Suspension. *Int. J. Biol. Macromol.* **1992**, *14* (3), 170–172. https://doi.org/10.1016/S0141-8130(05)80008-X.

(10) Dufresne, A. Nanocellulose Processing Properties and Potential Applications. *Curr. For. Reports* **2019**, *5*, 76–89.

(11) Wohlhauser, S.; Delepierre, G.; Labet, M.; Morandi, G.; Thielemans, W.; Weder, C.; Zoppe, J. O. Grafting Polymers from Cellulose Nanocrystals: Synthesis, Properties, and Applications. *Macromolecules* **2018**, *51* (16), 6157–6189. https://doi.org/10.1021/acs.macromol.8b00733.

(12) Kedzior, S. A.; Zoppe, J. O.; Berry, R. M.; Cranston, E. D. Recent Advances and an Industrial Perspective of Cellulose Nanocrystal Functionalization through Polymer Grafting. *Curr. Opin. Solid State Mater. Sci.* **2019**, *23* (2), 74–91.

https://doi.org/10.1016/j.cossms.2018.11.005.

(13) Moon, R. J.; Martini, A.; Nairn, J.; Simonsen, J.; Youngblood, J. Cellulose Nanomaterials Review: Structure, Properties and Nanocomposites. *Chem. Soc. Rev.* **2011**, *40*, 3941–3994. https://doi.org/10.1039/c0cs00108b.

(14) Kedzior, S. A.; Gabriel, V. A.; Dubé, M. A.; Cranston, E. D. Nanocellulose in Emulsions and Heterogeneous Water-Based Polymer Systems: A Review. *Adv. Mater.* **2020**, 2002404. https://doi.org/10.1002/adma.202002404.

(15) Jovanović, R.; Dubé, M. A. Emulsion-Based Pressure-Sensitive Adhesives: A Review. *J. Macromol. Sci. Part C* **2004**, *44* (1), 1–51. https://doi.org/10.1081/MC-120027933.

(16) Dastjerdi, Z.; Cranston, E. D.; Berry, R.; Fraschini, C.; Dubé, M. A. Polymer Nanocomposites for Emulsion-Based Coatings and Adhesives. *Macromol. React. Eng.* **2018**, *13* (2), 1–15. https://doi.org/10.1002/mren.201800050.

(17) Dastjerdi, Z.; Cranston, E. D.; Dubé, M. A. Pressure Sensitive Adhesive Property Modification Using Cellulose Nanocrystals. *Int. J. Adhes. Adhes.* **2018**, *81*, 36–42. https://doi.org/10.1016/j.ijadhadh.2017.11.009.

(18) Dufresne, A. *Handbook of Nanocellulose and Cellulose Nanocomposites*; 2017. https://doi.org/10.1002/9783527689972.

(19) Dufresne, A. *Nanocellulose: From Nature to High Performance Tailored Materials, 2. Edition*; 2017. https://doi.org/10.1515/9783110480412.

(20) Medronho, B.; Romano, A.; Miguel, M. G.; Stigsson, L.; Lindman, B. Rationalizing Cellulose (in)Solubility: Reviewing Basic Physicochemical Aspects and Role of Hydrophobic Interactions. *Cellulose* **2012**, *19* (3), 581–587. https://doi.org/10.1007/s10570-011-9644-6.

(21) Lindman, B.; Karlström, G.; Stigsson, L. On the Mechanism of Dissolution of Cellulose. *J. Mol. Liq.* **2010**, *156* (1), 76–81. https://doi.org/10.1016/j.molliq.2010.04.016.

(22) Ha, M.; Apperley, D. C.; Evans, B. W.; Huxham, I. M.; Jardine, W. G.; Vie, R. J.; Vian, B.; Jarvis, M. C. Fine Structure in Cellulose Microfibrils: NMR Evidence from Onion and Quince. *Plant J.* **1998**, *16* (June), 183–190.

(23) Elazzouzi-hafraoui, S.; Nishiyama, Y.; Putaux, J.; Heux, L.; Dubreuil, F.; Rochas, C. The Shape and Size Distribution of Crystalline Nanoparticles Prepared by Acid Hydrolysis of Native Cellulose. *Biomacromolecules* **2008**, *9*, 57–65. https://doi.org/10.1021/bm700769p.

(24) Mariano, M.; El Kissi, N.; Dufresne, A. Cellulose Nanocrystals and Related Nanocomposites: Review of Some Properties and Challenges. *J. Polym. Sci. Part B Polym. Phys.* **2014**, *52* (12), 791–806. https://doi.org/10.1002/polb.23490.

(25) Klemm, D.; Kramer, F.; Moritz, S.; Lindström, T.; Ankerfors, M.; Gray, D.; Dorris, A. Nanocelluloses: A New Family of Nature-Based Materials. *Angew. Chemie - Int. Ed.*

2011, *50* (24), 5438–5466. https://doi.org/10.1002/anie.201001273.

(26) Rånby, B. G.; Banderet, A.; Sillén, L. G. Aqueous Colloidal Solutions of Cellulose Micelles. *Acta Chemica Scandinavica*. 1949, pp 649–650. https://doi.org/10.3891/acta.chem.scand.03-0649.

(27) Matos Ruiz, M.; Cavaillé, J. Y.; Dufresne, A.; Gèrard, J. F.; Graillat, C. Processing and Characterization of New Thermoset Nanocomposites Based on Cellulose Whiskers. *Compos. Interfaces* **2000**, *7* (2), 117–131. https://doi.org/10.1163/156855400300184271.

(28) Anglès, M. N.; Dufresne, A. Plasticized Starch/Tunicin Whiskers Nanocomposite Materials. 2. Mechanical Behavior. *Macromolecules* **2001**, *34* (9), 2921–2931. https://doi.org/10.1021/ma001555h.

(29) Reid, M. S.; Villalobos, M.; Cranston, E. D. Benchmarking Cellulose Nanocrystals: From the Laboratory to Industrial Production. *Langmuir* **2017**, *33* (7), 1583–1598. https://doi.org/10.1021/acs.langmuir.6b03765.

(30) Camarero-Espinosa, S.; Kuhnt, T.; Foster, E. J.; Weder, C. Isolation of Thermally Stable Cellulose Nanocrystals by Phosphoric Acid Hydrolysis. *Biomacromolecules* **2013**, *14* (4), 1223–1230. https://doi.org/10.32604/jrm.2020.07940.

(31) Vanderfleet, O. M.; Reid, M. S.; Bras, J.; Heux, L.; Godoy-Vargas, J.; Panga, M. K. R.; Cranston, E. D. Insight into Thermal Stability of Cellulose Nanocrystals from New Hydrolysis Methods with Acid Blends. *Cellulose* **2018**, *7*. https://doi.org/10.1007/s10570-018-2175-7.

(32) Vanderfleet, O. M.; Cranston, E. D. Production Routes to Tailor the Performance of Cellulose Nanocrystals. *Nat. Rev. Mater.* **2020**. https://doi.org/10.1038/s41578-020-00239-y.

(33) Kalashnikova, I.; Bizot, H.; Bertoncini, P.; Cathala, B.; Capron, I. Cellulosic Nanorods of Various Aspect Ratios for Oil in Water Pickering Emulsions. *Soft Matter* **2013**, *9* (3), 952–959. https://doi.org/10.1039/c2sm26472b.

(34) Wu, Q.; Meng, Y.; Wang, S.; Li, Y.; Fu, S.; Ma, L.; Harper, D. Rheological Behavior of Cellulose Nanocrystal Suspension: Influence of Concentration and Aspect Ratio. *J. Appl. Polym. Sci.* **2014**, *131* (15), 40525. https://doi.org/10.1002/app.40525.

(35) Rusli, R.; Shanmuganathan, K.; Rowan, S. J.; Weder, C.; Eichhorn, S. J. Stress Transfer in Cellulose Nanowhisker Composites-Influence of Whisker Aspect Ratio and Surface Charge. *Biomacromolecules* **2011**, *12* (4), 1363–1369.

(36) Beck-Candanedo, S.; Roman, M.; Gray, D. G. Effect of Reaction Conditions on the Properties and Behavior of Wood Cellulose Nanocrystal Suspensions. *Biomacromolecules* **2005**, *6* (2), 1048–1054. https://doi.org/10.1021/bm049300p.

(37) Domingues, R. M. A.; Gomes, M. E.; Reis, R. L. The Potential of Cellulose Nanocrystals in Tissue Engineering Strategies. *Biomacromolecules* **2014**, *15* (7), 2327–2346. https://doi.org/10.1021/bm500524s.

(38) Habibi, Y. Key Advances in the Chemical Modification of Nanocelluloses. *Chem. Soc. Rev.* **2014**, *43* (5), 1519–1542. https://doi.org/10.1039/c3cs60204d.

(39) Kargarzadeh, H.; Mariano, M.; Gopakumar, D.; Ahmad, I.; Thomas, S.; Dufresne, A.; Huang, J.; Lin, N. Advances in Cellulose Nanomaterials. *Cellulose* **2018**, *25* (4), 2151–2189. https://doi.org/10.1007/s10570-018-1723-5.

(40) Habibi, Y.; Dufresne, A. Highly Filled Bionanocomposites from Functionalized Polysaccharide Nanocrystals. *Biomacromolecules* **2008**, *9* (7), 1974–1980. https://doi.org/10.1021/bm8001717.

(41) Morandi, G.; Thielemans, W. Synthesis of Cellulose Nanocrystals Bearing Photocleavable Grafts by ATRP. *Polym. Chem.* **2012**, *3* (6), 1402–1407. https://doi.org/10.1039/c2py20069d.

(42) Liu, Y.; Zhou, L.; Wang, L.; Pan, X.; Wang, K.; Shu, J.; Liu, L.; Zhang, H.; Lin, L.; Shi, X.; Schlarb, A. K.; Zhang, J. Air-Dried Porous Powder of Polymethyl Methacrylate Modified Cellulose Nanocrystal Nanocomposite and Its Diverse Applications. *Compos. Sci. Technol.* **2020**, *188*, 107985. https://doi.org/10.1016/j.compscitech.2019.107985.

(43) Brinatti, C.; Akhlaghi, S. P.; Pires-Oliveira, R.; Bernardinelli, O. D.; Berry, R. M.; Tam, K. C.; Loh, W. Controlled Coagulation and Redispersion of Thermoresponsive Poly Di(Ethylene Oxide) Methyl Ether Methacrylate Grafted Cellulose Nanocrystals. *J. Colloid Interface Sci.* **2019**, *538*, 51–61. https://doi.org/10.1016/j.jcis.2018.11.071.

(44) Farnia, F.; Fan, W.; Dory, Y.; Zhao, Y. Making Nanocomposites of Hydrophilic and Hydrophobic Polymers Using Gas-Responsive Cellulose Nanocrystals. *Macromol. Rapid Commun.* **2019**, *40* (12), 1900114. https://doi.org/10.1002/marc.201900114.

(45) Pracella, M.; Haque, M. M. U.; Puglia, D. Morphology and Properties Tuning of PLA/Cellulose Nanocrystals Bio-Nanocomposites by Means of Reactive Functionalization and Blending with PVAc. *Polymer (Guildf).* **2014**, *55* (16), 3720–3728. https://doi.org/10.1016/j.polymer.2014.06.071.

(46) Kan, K. H. M.; Li, J.; Wijesekera, K.; Cranston, E. D. Polymer-Grafted Cellulose Nanocrystals as PH-Responsive Reversible Flocculants. *Biomacromolecules* **2013**, *14* (9), 3130–3139. https://doi.org/10.1021/bm400752k.

(47) Tang, J.; Berry, R. M.; Tam, K. C. Stimuli-Responsive Cellulose Nanocrystals for Surfactant-Free Oil Harvesting. *Biomacromolecules* **2016**, *17* (5), 1748–1756. https://doi.org/10.1021/acs.biomac.6b00144.

(48) Kedzior, S. A.; Graham, L.; Moorlag, C.; Dooley, B. M.; Cranston, E. D. Poly(Methyl Methacrylate)-Grafted Cellulose Nanocrystals: One-Step Synthesis, Nanocomposite Preparation, and Characterization. *Can. J. Chem. Eng.* **2016**, *94*, 811–822. https://doi.org/10.1002/cjce.22456.

(49) Liu, S.; Jin, M.; Chen, Y.; Gao, H.; Shi, X.; Cheng, W.; Ren, L.; Wang, Y. High Internal Phase Emulsions Stabilised by Supramolecular Cellulose Nanocrystals and Their

Application as Cell-Adhesive Macroporous Hydrogel Monoliths. *J. Mater. Chem. B* **2017**, *5* (14), 2671–2678. https://doi.org/10.1039/c7tb00145b.

(50) Anirudhan, T. S.; Rejeena, S. R.; Binusree, J. Adsorptive Separation of Myoglobin from Aqueous Solutions Using Iron Oxide Magnetic Nanoparticles Modified with Functionalized Nanocrystalline Cellulose. *J. Chem. Eng. Data* **2013**, *58* (5), 1329–1339. https://doi.org/10.1021/je400088g.

(51) Ma, Z. K.; Han, X. Y.; Liu, H.; Ji, J. C.; Qin, S. Y.; Li, X. D.; Lei, X. Lyotropic Liquid Crystal to Measure Residual Dipolar Couplings in Dimethyl Sulfoxide Based on Modified Cellulose Nanocrystals. *New J. Chem.* **2020**, *44* (11), 4262–4265. https://doi.org/10.1039/c9nj06031f.

(52) Yang, J.; Han, C. R.; Duan, J. F.; Ma, M. G.; Zhang, X. M.; Xu, F.; Sun, R. C. Synthesis and Characterization of Mechanically Flexible and Tough Cellulose Nanocrystals-Polyacrylamide Nanocomposite Hydrogels. *Cellulose* **2013**, *20* (1), 227–237. https://doi.org/10.1007/s10570-012-9841-y.

(53) Yang, J.; Han, C. R.; Duan, J. F.; Ma, M. G.; Zhang, X. M.; Xu, F.; Sun, R. C.; Xie, X. M. Studies on the Properties and Formation Mechanism of Flexible Nanocomposite Hydrogels from Cellulose Nanocrystals and Poly(Acrylic Acid). *J. Mater. Chem.* **2012**, *22* (42), 22467–22480. https://doi.org/10.1039/c2jm35498e.

(54) Zhou, C.; Wu, Q.; Yue, Y.; Zhang, Q. Application of Rod-Shaped Cellulose Nanocrystals in Polyacrylamide Hydrogels. *J. Colloid Interface Sci.* **2011**, *353* (1), 116–123. https://doi.org/10.1016/j.jcis.2010.09.035.

(55) Zhou, C.; Wu, Q.; Zhang, Q. Dynamic Rheology Studies of in Situ Polymerization Process of Polyacrylamide-Cellulose Nanocrystal Composite Hydrogels. *Colloid Polym. Sci.* **2011**, *289* (3), 247–255. https://doi.org/10.1007/s00396-010-2342-3.

(56) Espino-Pérez, E.; Gilbert, R. G.; Domenek, S.; Brochier-Salon, M. C.; Belgacem, M. N.; Bras, J. Nanocomposites with Functionalised Polysaccharide Nanocrystals through Aqueous Free Radical Polymerisation Promoted by Ozonolysis. *Carbohydr. Polym.* **2016**, *135*, 256–266. https://doi.org/10.1016/j.carbpol.2015.09.005.

(57) Wu, Y.; Wang, L.; Qing, Y.; Yan, N.; Tian, C.; Huang, Y. A Green Route to Prepare Fluorescent and Absorbent Nano-Hybrid Hydrogel for Water Detection. *Sci. Rep.* **2017**, *7* (4380), 1–11. https://doi.org/10.1038/s41598-017-04542-7.

(58) Chen, Y.; Abdalkarim, S. Y. H.; Yu, H. Y.; Li, Y.; Xu, J.; Marek, J.; Yao, J.; Tam, K. C. Double Stimuli-Responsive Cellulose Nanocrystals Reinforced Electrospun PHBV Composites Membrane for Intelligent Drug Release. *Int. J. Biol. Macromol.* **2020**, *155*, 330–339. https://doi.org/10.1016/j.ijbiomac.2020.03.216.

(59) Alharthi, S.; Grishkewich, N.; Berry, R. M.; Tam, K. C. Functional Cellulose Nanocrystals Containing Cationic and Thermo-Responsive Polymer Brushes. *Carbohydr. Polym.* **2020**, *246*, 116651. https://doi.org/10.1016/j.carbpol.2020.116651.

(60) Zubik, K.; Singhsa, P.; Wang, Y.; Manuspiya, H.; Narain, R. Thermo-Responsive Poly(N-Isopropylacrylamide)-Cellulose Nanocrystals Hybrid Hydrogels for Wound Dressing. *Polymers (Basel).* **2017**, *9* (4), 119. https://doi.org/10.3390/polym9040119.

(61) Tang, J.; Lee, M. F. X.; Zhang, W.; Zhao, B.; Berry, R. M.; Tam, K. C. Dual Responsive Pickering Emulsion Stabilized by Poly[2-(Dimethylamino)Ethyl Methacrylate] Grafted Cellulose Nanocrystals. *Biomacromolecules* **2014**, *15* (8), 3052–3060. https://doi.org/10.1021/bm500663w.

(62) Habibi, Y.; Goffin, A. L.; Schiltz, N.; Duquesne, E.; Dubois, P.; Dufresne, A. Bionanocomposites Based on Poly(ε-Caprolactone)-Grafted Cellulose Nanocrystals by Ring-Opening Polymerization. *J. Mater. Chem.* **2008**, *18* (41), 5002–5010. https://doi.org/10.1039/b809212e.

(63) Chen, G.; Dufresne, A.; Huang, J.; Chang, P. R. A Novel Thermoformable Bionanocomposite Based on Cellulose Nanoerystal-Graft-Poly(ε-Caprolactone). *Macromol. Mater. Eng.* **2009**, *294* (1), 59–67. https://doi.org/10.1002/mame.200800261.

(64) Lin, N.; Chen, G.; Huang, J.; Dufresne, A.; Chang, P. R. Effects of Polymer-Grafted Natural Nanocrystals on the Structure and Mechanical Properties of Poly(Lactic Acid): A Case of Cellulose Whisker-Graft-Polycaprolactone. *J. Appl. Polym. Sci.* **2009**, *113*, 3417–3425. https://doi.org/10.1002/app.

(65) Labet, M.; Thielemans, W. Improving the Reproducibility of Chemical Reactions on the Surface of Cellulose Nanocrystals: ROP of ε-Caprolactone as a Case Study. *Cellulose* **2011**, *18* (3), 607–617. https://doi.org/10.1007/s10570-011-9527-x.

(66) Goffin, A. L.; Raquez, J. M.; Duquesne, E.; Siqueira, G.; Habibi, Y.; Dufresne, A.; Dubois, P. From Interfacial Ring-Opening Polymerization to Melt Processing of Cellulose Nanowhisker-Filled Polylactide-Based Nanocomposites. *Biomacromolecules* **2011**, *12* (7), 2456–2465. https://doi.org/10.1021/bm200581h.

(67) Goffin, A. L.; Raquez, J. M.; Duquesne, E.; Siqueira, G.; Habibi, Y.; Dufresne, A.; Dubois, P. Poly(ε-Caprolactone) Based Nanocomposites Reinforced by Surface-Grafted Cellulose Nanowhiskers via Extrusion Processing: Morphology, Rheology, and Thermo-Mechanical Properties. *Polymer (Guildf).* **2011**, *52* (7), 1532–1538. https://doi.org/10.1016/j.polymer.2011.02.004.

(68) Labet, M.; Thielemans, W. Citric Acid as a Benign Alternative to Metal Catalysts for the Production of Cellulose-Grafted-Polycaprolactone Copolymers. *Polym. Chem.* **2012**, *3* (3), 679–684. https://doi.org/10.1039/c2py00493c.

(69) Goffin, A. L.; Habibi, Y.; Raquez, J. M.; Dubois, P. Polyester-Grafted Cellulose Nanowhiskers: A New Approach for Tuning the Microstructure of Immiscible Polyester Blends. *ACS Appl. Mater. Interfaces* **2012**, *4* (7), 3364–3371. https://doi.org/10.1021/am3008196.

(70) Braun, B.; Dorgan, J. R.; Hollingsworth, L. O. Supra-Molecular EcoBioNanocomposites Based on Polylactide and Cellulosic Nanowhiskers: Synthesis and Properties.

Biomacromolecules **2012**, *13*, 2013–2019.

(71) Bitinis, N.; Fortunati, E.; Verdejo, R.; Bras, J.; Kenny, J. M.; Torre, L.; López-Manchado, M. A. Poly(Lactic Acid)/Natural Rubber/Cellulose Nanocrystal Bionanocomposites. Part II: Properties Evaluation. *Carbohydr. Polym.* **2013**, *96* (2), 621–627. https://doi.org/10.1016/j.carbpol.2013.03.091.

(72) Tehrani, A. D.; Neysi, E. Surface Modification of Cellulose Nanowhisker throughout Graft Polymerization of 2-Ethyl-2-Oxazoline. *Carbohydr. Polym.* **2013**, *97* (1), 98–104. https://doi.org/10.1016/j.carbpol.2013.04.082.

(73) Habibi, Y.; Aouadi, S.; Raquez, J. M.; Dubois, P. Effects of Interfacial Stereocomplexation in Cellulose Nanocrystal-Filled Polylactide Nanocomposites. *Cellulose* **2013**, *20* (6), 2877–2885. https://doi.org/10.1007/s10570-013-0058-5.

(74) Bitinis, N.; Verdejo, R.; Bras, J.; Fortunati, E.; Maria, J.; Torre, L.; López-manchado, M. A. Poly (Lactic Acid)/Natural Rubber/Cellulose Nanocrystal Bionanocomposites Part I . Processing and Morphology. *Carbohydr. Polym.* **2013**, *96*, 611–620.

(75) Peltzer, M.; Pei, A.; Zhou, Q.; Berglund, L.; Jiménez, A. Surface Modification of Cellulose Nanocrystals by Grafting with Poly(Lactic Acid). *Polym. Int.* **2014**, *63* (6), 1056–1062. https://doi.org/10.1002/pi.4610.

(76) Tian, C.; Fu, S.; Chen, J.; Meng, Q.; Lucia, L. A. Graft Polymerization of ε-Caprolactone to Cellulose Nanocrystals and Optimization of Grafting Conditions Utilizing a Response Surface Methodology. *Nord. Pulp Pap. Res. J.* **2014**, *29* (1), 58–68. https://doi.org/10.3183/npprj-2014-29-01-p058-068.

(77) Lizundia, E.; Vilas, J. L.; León, L. M. Crystallization, Structural Relaxation and Thermal Degradation in Poly(l-Lactide)/Cellulose Nanocrystal Renewable Nanocomposites. *Carbohydr. Polym.* **2015**, *123*, 256–265. https://doi.org/10.1016/j.carbpol.2015.01.054.

(78) Ma, P.; Jiang, L.; Xu, P.; Dong, W.; Chen, M.; Lemstra, P. J. Rapid Stereocomplexation between Enantiomeric Comb-Shaped Cellulose-g-Poly(l-Lactide) Nanohybrids and Poly(d-Lactide) from the Melt. *Biomacromolecules* **2015**, *16* (11), 3723–3729. https://doi.org/10.1021/acs.biomac.5b01135.

(79) Fu, S.; Habibi, Y.; Lucia, L. A. Polymerization Topochemistry of Cellulose Nanocrystals: A Function of Surface Dehydration Control. *Langmuir* **2014**, *30*, 14670–14679.

(80) Miao, C.; Hamad, W. Y. In-Situ Polymerized Cellulose Nanocrystals (CNC)—Poly(L-Lactide) (PLLA) Nanomaterials and Applications in Nanocomposite Processing. *Carbohydr. Polym.* **2016**, *153*, 549–558. https://doi.org/10.1016/j.carbpol.2016.08.012.

(81) Lizundia, E.; Fortunati, E.; Dominici, F.; Vilas, J. L.; León, L. M.; Armentano, I.; Torre, L.; Kenny, J. M. PLLA-Grafted Cellulose Nanocrystals: Role of the CNC Content and Grafting on the PLA Bionanocomposite Film Properties. *Carbohydr. Polym.* **2016**, *142*, 105–113. https://doi.org/10.1016/j.carbpol.2016.01.041.

(82) de Paula, E. L.; Roig, F.; Mas, A.; Habas, J. P.; Mano, V.; Pereira, F. V.; Robin, J. J.

Effect of Surface-Grafted Cellulose Nanocrystals on the Thermal and Mechanical Properties of PLLA Based Nanocomposites. *Eur. Polym. J.* **2016**, *84*, 173–187. https://doi.org/10.1016/j.eurpolymj.2016.09.019.

(83) Bellani, C. F.; Pollet, E.; Hebraud, A.; Pereira, F. V.; Schlatter, G.; Avérous, L.; Bretas, R. E. S.; Branciforti, M. C. Morphological, Thermal, and Mechanical Properties of Poly(ε-Caprolactone)/Poly(ε-Caprolactone)-Grafted-Cellulose Nanocrystals Mats Produced by Electrospinning. *J. Appl. Polym. Sci.* **2016**, *133* (21), 43445. https://doi.org/10.1002/app.43445.

(84) Wu, H.; Nagarajan, S.; Zhou, L.; Duan, Y.; Zhang, J. Synthesis and Characterization of Cellulose Nanocrystal-Graft-Poly(D-Lactide) and Its Nanocomposite with Poly(L-Lactide). *Polymer (Guildf).* **2016**, *103*, 365–375. https://doi.org/10.1016/j.polymer.2016.09.070.

(85) Simão, J. A.; Bellani, C. F.; Branciforti, M. C. Thermal Properties and Crystallinity of PCL/PBSA/Cellulose Nanocrystals Grafted with PCL Chains. *J. Appl. Polym. Sci.* **2017**, *134* (8), 44493. https://doi.org/10.1002/app.44493.

(86) Muiruri, J. K.; Liu, S.; Teo, W. S.; Kong, J.; He, C. Highly Biodegradable and Tough Polylactic Acid-Cellulose Nanocrystal Composite. *ACS Sustain. Chem. Eng.* **2017**, *5* (5), 3929–3937. https://doi.org/10.1021/acssuschemeng.6b03123.

(87) Hou, L.; Fang, J.; Wang, W.; Xie, Z.; Dong, D.; Zhang, N. Indocyanine Green-Functionalized Bottle Brushes of Poly(2-Oxazoline) on Cellulose Nanocrystals for Photothermal Cancer Therapy. *J. Mater. Chem. B* **2017**, *5* (18), 3348–3354. https://doi.org/10.1039/c7tb00812k.

(88) Chen, J.; Wu, D.; Tam, K. C.; Pan, K.; Zheng, Z. Effect of Surface Modification of Cellulose Nanocrystal on Nonisothermal Crystallization of Poly(β-Hydroxybutyrate) Composites. *Carbohydr. Polym.* **2017**, *157*, 1821–1829. https://doi.org/10.1016/j.carbpol.2016.11.071.

(89) Ma, P.; Shen, T.; Lin, L.; Dong, W.; Chen, M. Cellulose-g-Poly(D-Lactide) Nanohybrids Induced Significant Low Melt Viscosity and Fast Crystallization of Fully Bio-Based Nanocomposites. *Carbohydr. Polym.* **2017**, *155*, 498–506. https://doi.org/10.1016/j.carbpol.2016.09.003.

(90) Sessini, V.; Navarro-Baena, I.; Arrieta, M. P.; Dominici, F.; López, D.; Torre, L.; Kenny, J. M.; Dubois, P.; Raquez, J. M.; Peponi, L. Effect of the Addition of Polyester-Grafted-Cellulose Nanocrystals on the Shape Memory Properties of Biodegradable PLA/PCL Nanocomposites. *Polym. Degrad. Stab.* **2018**, *152*, 126–138. https://doi.org/10.1016/j.polymdegradstab.2018.04.012.

(91) Kasyapi, N.; Dinesh Kumar, K.; Bhowmick, A. K. Sustainable Bionanocomposite from d,l-Lactide/δ-Valerolactone Triblock and Bionanowhiskers: Preparation, Characterization, and Properties. *J. Appl. Polym. Sci.* **2018**, *135* (13), 46035. https://doi.org/10.1002/app.46035.

(92) Lin, W.; Hu, X.; You, X.; Sun, Y.; Wen, Y.; Yang, W.; Zhang, X.; Li, Y.; Chen, H. Hydrophobic Modification of Nanocellulose via a Two-Step Silanation Method. *Polymers (Basel).* **2018**, *10* (9), 1035. https://doi.org/10.3390/POLYM10091035.

(93) Xie, Q.; Wang, S.; Chen, X.; Zhou, Y.; Fang, H.; Li, X.; Cheng, S.; Ding, Y. Thermal Stability and Crystallization Behavior of Cellulose Nanocrystals and Their Poly(l-Lactide) Nanocomposites: Effects of Surface Ionic Group and Poly(d-Lactide) Grafting. *Cellulose* **2018**, *25* (12), 6847–6862. https://doi.org/10.1007/s10570-018-2086-7.

(94) Wang, Y.; Zhu, P.; Li, G.; Zhu, S.; Liu, K.; Liu, Y.; He, J.; Lei, J. Amphiphilic Carboxylated Cellulose-g-Poly(L-Lactide) Copolymer Nanoparticles for Oleanolic Acid Delivery. *Carbohydr. Polym.* **2019**, *214*, 100–109. https://doi.org/10.1016/j.carbpol.2019.03.033.

(95) Fang, H.; Chen, X.; Wang, S.; Cheng, S.; Ding, Y. Enhanced Mechanical and Oxygen Barrier Performance in Biodegradable Polyurethanes by Incorporating Cellulose Nanocrystals with Interfacial Polylactide Stereocomplexation. *Cellulose* **2019**, *26* (18), 9751–9764. https://doi.org/10.1007/s10570-019-02742-0.

(96) Zoppe, J. O.; Ataman, N. C.; Mocny, P.; Wang, J.; Moraes, J.; Klok, H. A. Surface-Initiated Controlled Radical Polymerization: State-of-the-Art, Opportunities, and Challenges in Surface and Interface Engineering with Polymer Brushes. *Chem. Rev.* **2017**, *117* (3), 1105–1318. https://doi.org/10.1021/acs.chemrev.6b00314.

(97) Wang, J. S.; Matyjaszewski, K. Controlled/“Living” Radical Polymerization. Atom Transfer Radical Polymerization in the Presence of Transition-Metal Complexes. *J. Am. Chem. Soc.* **1995**, *117* (20), 5614–5615. https://doi.org/10.1021/ja00125a035.

(98) Carlmark, A.; Malmstrom, E. Atom Transfer Radical Polymerization from Cellulose Fibers at Ambient Temperature. *J. Am. Chem. Soc.* **2002**, *124* (6), 900–901.

(99) Boujemaoui, A.; Mongkhontreerat, S.; Malmström, E.; Carlmark, A. Preparation and Characterization of Functionalized Cellulose Nanocrystals. *Carbohydr. Polym.* **2015**, *115*, 457–464. https://doi.org/10.1016/j.carbpol.2014.08.110.

(100) Matyjaszewski, K. Atom Transfer Radical Polymerization (ATRP): Current Status and Future Perspectives. *Macromolecules* **2012**, *45* (10), 4015–4039. https://doi.org/10.1021/ma3001719.

(101) Xu, Q.; Yi, J.; Zhang, X.; Zhang, H. A Novel Amphotropic Polymer Based on Cellulose Nanocrystals Grafted with Azo Polymers. *Eur. Polym. J.* **2008**, *44* (9), 2830–2837. https://doi.org/10.1016/j.eurpolymj.2008.06.010.

(102) Yi, J.; Xu, Q.; Zhang, X.; Zhang, H. Chiral-Nematic Self-Ordering of Rodlike Cellulose Nanocrystals Grafted with Poly(Styrene) in Both Thermotropic and Lyotropic States. *Polymer (Guildf).* **2008**, *49*, 4406–4412. https://doi.org/10.1016/j.polymer.2008.08.008.

(103) Yi, J.; Xu, Q.; Zhang, X.; Zhang, H. Temperature-Induced Chiral Nematic Phase Changes of Suspensions of Poly (N,N-Dimethylaminoethyl Methacrylate)-Grafted Cellulose

Nanocrystals. *Cellulsoe* **2009**, *16*, 989–997. https://doi.org/10.1007/s10570-009-9350-9.

(104) Morandi, G.; Heath, L.; Thielemans, W. Cellulose Nanocrystals Grafted with Polystyrene Chains through Surface-Initiated Atom Transfer Radical Polymerization (SI-ATRP). *Langmuir* **2009**, *25* (14), 8280–8286. https://doi.org/10.1021/la900452a.

(105) Zoppe, J. O.; Habibi, Y.; Rojas, O. J.; Venditti, R. A.; Johansson, L. S.; Efimenko, K.; Österberg, M.; Laine, J. Poly(N-Isopropylacrylamide) Brushes Grafted from Cellulose Nanocrystals via Surface-Initiated Single-Electron Transfer Living Radical Polymerization. *Biomacromolecules* **2010**, *11* (10), 2683–2691. https://doi.org/10.1021/bm100719d.

(106) Majoinen, J.; Walther, A.; Mckee, J. R.; Kontturi, E.; Aseyev, V.; Malho, J. M.; Ruokolainen, J.; Ikkala, O. Polyelectrolyte Brushes Grafted from Cellulose Nanocrystals Using Cu-Mediated Surface-Initiated Controlled Radical Polymerization. *Biomacromolecules* **2011**, *12* (8), 2997–3006.

(107) Morits, M.; Hynninen, V.; Nonappa; Niederberger, A.; Ikkala, O.; Gröschel, A. H.; Müllner, M. Polymer Brush Guided Templating on Well-Defined Rod-like Cellulose Nanocrystals. *Polym. Chem.* **2018**, *9* (13), 1650–1657. https://doi.org/10.1039/c7py01814b.

(108) Zhang, Z.; Sèbe, G.; Wang, X.; Tam, K. C. UV-Absorbing Cellulose Nanocrystals as Functional Reinforcing Fillers in Poly(Vinyl Chloride) Films. *ACS Appl. Nano Mater.* **2018**, *1* (2), 632–641. https://doi.org/10.1021/acsanm.7b00126.

(109) Yu, J.; Wang, C.; Wang, J.; Chu, F. In Situ Development of Self-Reinforced Cellulose Nanocrystals Based Thermoplastic Elastomers by Atom Transfer Radical Polymerization. *Carbohydr. Polym.* **2016**, *141*, 143–150. https://doi.org/10.1016/j.carbpol.2016.01.006.

(110) Hemraz, U. D.; Lu, A.; Sunasee, R.; Boluk, Y. Structure of Poly(N-Isopropylacrylamide) Brushes and Steric Stability of Their Grafted Cellulose Nanocrystal Dispersions. *J. Colloid Interface Sci.* **2014**, *430*, 157–165. https://doi.org/10.1016/j.jcis.2014.05.011.

(111) Zoppe, J. O.; Dupire, A. V. M.; Lachat, T. G. G.; Lemal, P.; Rodriguez-Lorenzo, L.; Petri-Fink, A.; Weder, C.; Klok, H. A. Cellulose Nanocrystals with Tethered Polymer Chains: Chemically Patchy versus Uniform Decoration. *ACS Macro Lett.* **2017**, *6* (9), 892–897. https://doi.org/10.1021/acsmacrolett.7b00383.

(112) Risteen, B.; McBride, M.; Gonzalez, M.; Khau, B.; Zhang, G.; Reichmanis, E. Functionalized Cellulose Nanocrystal-Mediated Conjugated Polymer Aggregation. *ACS Appl. Mater. Interfaces* **2019**, *11* (28), 25338–25350. https://doi.org/10.1021/acsami.9b06072.

(113) Risteen, B.; Delepierre, G.; Srinivasarao, M.; Weder, C.; Russo, P.; Reichmanis, E.; Zoppe, J. Thermally Switchable Liquid Crystals Based on Cellulose Nanocrystals with Patchy Polymer Grafts. *Small* **2018**, *14* (46), 1–10. https://doi.org/10.1002/smll.201802060.

(114) Zoppe, J. O.; Venditti, R. A.; Rojas, O. J. Pickering Emulsions Stabilized by Cellulose Nanocrystals Grafted with Thermo-Responsive Polymer Brushes. *J. Colloid Interface Sci.* **2012**, *369* (1), 202–209. https://doi.org/10.1016/j.jcis.2011.12.011.

(115) Kedzior, S. A.; Kiriakou, M.; Niinivaara, E.; Dubé, M. A.; Fraschini, C.; Berry, R. M.; Cranston, E. D. Incorporating Cellulose Nanocrystals into the Core of Polymer Latex Particles via Polymer Grafting. *ACS Macro Lett.* **2018**, *7* (8), 990–996. https://doi.org/10.1021/acsmacrolett.8b00334.

(116) Wang, Z.; Zhang, Y.; Yuan, L.; Hayat, J.; Trenor, N. M.; Lamm, M. E.; Vlaminck, L.; Billiet, S.; Du Prez, F. E.; Wang, Z.; Tang, C. Biomass Approach toward Robust, Sustainable, Multiple-Shape-Memory Materials. *ACS Macro Lett.* **2016**, *5* (5), 602–606. https://doi.org/10.1021/acsmacrolett.6b00243.

(117) Zhang, J.; Wu, Q.; Li, M. C.; Song, K.; Sun, X.; Lee, S. Y.; Lei, T. Thermoresponsive Copolymer Poly(N-Vinylcaprolactam) Grafted Cellulose Nanocrystals: Synthesis, Structure, and Properties. *ACS Sustain. Chem. Eng.* **2017**, *5* (8), 7439–7447. https://doi.org/10.1021/acssuschemeng.7b02033.

(118) Zhang, X.; Zhang, J.; Dong, L.; Ren, S.; Wu, Q.; Lei, T. Thermoresponsive Poly(Poly(Ethylene Glycol) Methylacrylate)s Grafted Cellulose Nanocrystals through SI-ATRP Polymerization. *Cellulose* **2017**, *24* (10), 4189–4203. https://doi.org/10.1007/s10570-017-1414-7.

(119) Malho, J.; Pecastaings, G.; Ruokolainen, J.; Garanger, E. Multifunctional Stimuli-Responsive Cellulose Nanocrystals via Dual Surface Modi Fi Cation with Genetically Engineered Elastin-Like Polypeptides and Poly(Acrylic Acid). **2018**. https://doi.org/10.1021/acsmacrolett.8b00321.

(120) Li, M.; Liu, X.; Liu, N.; Guo, Z.; Singh, P. K.; Fu, S. Effect of Surface Wettability on the Antibacterial Activity of Nanocellulose-Based Material with Quaternary Ammonium Groups. *Colloids Surfaces A Physicochem. Eng. Asp.* **2018**, *554* (June), 122–128. https://doi.org/10.1016/j.colsurfa.2018.06.031.

(121) Yuan, W.; Wang, C.; Lei, S.; Chen, J.; Lei, S.; Li, Z. Ultraviolet Light-, Temperature- and PH-Responsive Fluorescent Sensors Based on Cellulose Nanocrystals. *Polym. Chem.* **2018**, *9* (22), 3098–3107. https://doi.org/10.1039/c8py00613j.

(122) Zhang, Z.; Sèbe, G.; Wang, X.; Tam, K. C. Gold Nanoparticles Stabilized by Poly(4-Vinylpyridine) Grafted Cellulose Nanocrystals as Efficient and Recyclable Catalysts. *Carbohydr. Polym.* **2018**, *182* (October 2017), 61–68. https://doi.org/10.1016/j.carbpol.2017.10.094.

(123) Zhou, L.; He, H.; Li, M. C.; Huang, S.; Mei, C.; Wu, Q. Grafting Polycaprolactone Diol onto Cellulose Nanocrystals via Click Chemistry: Enhancing Thermal Stability and Hydrophobic Property. *Carbohydr. Polym.* **2018**, *189* (January), 331–341. https://doi.org/10.1016/j.carbpol.2018.02.039.

(124) Zhang, Z.; Tam, K. C.; Sèbe, G.; Wang, X. Convenient Characterization of Polymers

Grafted on Cellulose Nanocrystals via SI-ATRP without Chain Cleavage. *Carbohydr. Polym.* **2018**, *199* (April), 603–609. https://doi.org/10.1016/j.carbpol.2018.07.060.

(125) Zhang, Z.; Wang, X.; Tam, K. C.; Sèbe, G. A Comparative Study on Grafting Polymers from Cellulose Nanocrystals via Surface-Initiated Atom Transfer Radical Polymerization (ATRP) and Activator Re-Generated by Electron Transfer ATRP. *Carbohydr. Polym.* **2019**, *205* (September 2018), 322–329. https://doi.org/10.1016/j.carbpol.2018.10.050.

(126) Chen, J.; Mao, L.; Qi, H.; Xu, D.; Huang, H. Preparation of Fluorescent Cellulose Nanocrystal Polymer Composites with Thermo-Responsiveness through Light- Induced ATRP. *Cellulose* **2020**, *27* (2), 743–753. https://doi.org/10.1007/s10570-019-02845-8.

(127) Le Gars, M.; Bras, J.; Salmi-Mani, H.; Ji, M.; Dragoe, D.; Faraj, H.; Domenek, S.; Belgacem, N.; Roger, P. Polymerization of Glycidyl Methacrylate from the Surface of Cellulose Nanocrystals for the Elaboration of PLA-Based Nanocomposites. *Carbohydr. Polym.* **2020**, *234* (January), 115899. https://doi.org/10.1016/j.carbpol.2020.115899.

(128) Boujemaoui, A.; Cobo Sanchez, C.; Engström, J.; Bruce, C.; Fogelström, L.; Carlmark, A.; Malmström, E. Polycaprolactone Nanocomposites Reinforced with Cellulose Nanocrystals Surface-Modified via Covalent Grafting or Physisorption: A Comparative Study. *ACS Appl. Mater. Interfaces* **2017**, *9* (40), 35305–35318. https://doi.org/10.1021/acsami.7b09009.

(129) Foster, E. J.; Moon, R. J.; Agarwal, U. P.; Bortner, M. J.; Bras, J.; Camarero-Espinosa, S.; Chan, K. J.; Clift, M. J. D.; Cranston, E. D.; Eichhorn, S. J.; Fox, D. M.; Hamad, W. Y.; Heux, L.; Jean, B.; Korey, M.; Nieh, W.; Ong, K. J.; Reid, M. S.; Renneckar, S.; Roberts, R.; Shatkin, J. A.; Simonsen, J.; Stinson-Bagby, K.; Wanasekara, N.; Youngblood, J. Current Characterization Methods for Cellulose Nanomaterials. *Chem. Soc. Rev.* **2018**, *47* (8), 2609–2679. https://doi.org/10.1039/c6cs00895j.

(130) Johansson, L.; Campbell, J. M. Reproducible XPS on Biopolymers: Cellulose Studies. *Surf. Interface Anal.* **2004**, *36*, 1018–1022. https://doi.org/10.1002/sia.1827.

(131) Chanda, M. *Introduction to Polymer Science and Chemistry*, 2nd ed.; Taylor & Francis Group: Boca Raton, 2013. https://doi.org/10.1017/CBO9781107415324.004.

(132) Roberge, S.; Dubé, M. A. The Effect of Particle Size and Composition on the Performance of Styrene/Butyl Acrylate Miniemulsion-Based PSAs. *Polymer (Guildf).* **2006**, *47* (3), 799–807. https://doi.org/10.1016/j.polymer.2005.12.024.

(133) Qie, M. A.; Dubé, L. Manipulation of Chain Transfer Agent and Cross-Linker Concentration to Modify Latex Micro-Structure for Pressure-Sensitive Adhesives. *Eur. Polym. J.* **2010**, *46* (6), 1225–1236. https://doi.org/10.1016/j.eurpolymj.2010.02.014.

(134) Tobing, S. D.; Klein, A. Molecular Parameters and Their Relation to the Adhesive Performance of Emulsion Acrylic Pressure-Sensitive Adhesives. II . Effect of Crosslinking. *J. Appl. Polym. Sci.* **2001**, *79*, 2558–2564.

(135) Ash, B. J.; Rogers, D. F.; Wiegand, C. J.; Schadler, L. S.; Siegel, R. W.; Benicewicz, B.

C.; Apple, T. O. M. Mechanical Properties of AI2O3 Polymethylmethacrylate Nanocomposites. *Polym. Compos.* **2002**, *23* (6), 1014–1025.

(136) Pressure Sensitive Tape Council. *Test Methods for Pressure Sensitive Adhesive Tapes*, 16th ed.; Oakbrook Terrace, IL, 2014.

(137) Cao, X.; Dong, H.; Li, C. M. New Nanocomposite Materials Reinforced with Flax Cellulose Nanocrystals in Waterborne Polyurethane. *Biomacromolecules* **2007**, *8* (3), 899–904. https://doi.org/10.1021/bm0610368.

(138) Kedzior, S. A.; Marway, H. S.; Cranston, E. D. Tailoring Cellulose Nanocrystal and Surfactant Behavior in Miniemulsion Polymerization. *Macromolecules* **2017**, *50*, 2645–2655. https://doi.org/10.1021/acs.macromol.7b00516.

(139) Limousin, E.; Ballard, N.; Asua, J. M. Synthesis of Cellulose Nanocrystal Armored Latex Particles for Mechanically Strong Nanocomposite Films. *Polym. Chem.* **2019**, *10*, 1823–1831. https://doi.org/10.1002/app.47608.

(140) Zhang, Z.; Cheng, M.; Gabriel, M. S.; Teixeira Neto, Â. A.; da Silva Bernardes, J.; Berry, R.; Tam, K. C. Polymeric Hollow Microcapsules (PHM) via Cellulose Nanocrystal Stabilized Pickering Emulsion Polymerization. *J. Colloid Interface Sci.* **2019**, *555*, 489–497. https://doi.org/10.1016/j.jcis.2019.07.107.

(141) Zhang, B.; Zhang, Z.; Kapar, S.; Ataeian, P.; Da Silva Bernardes, J.; Berry, R.; Zhao, W.; Zhou, G.; Tam, K. C. Microencapsulation of Phase Change Materials with Polystyrene/Cellulose Nanocrystal Hybrid Shell via Pickering Emulsion Polymerization. *ACS Sustain. Chem. Eng.* **2019**, *7* (21), 17756–17767. https://doi.org/10.1021/acssuschemeng.9b04134.

(142) Ajelou, Z.; Nikfarjam, N.; Taheri-Qazvini, N. In-Situ Modified Cellulose Nanocrystals as Water Droplet Stabilizer in Polystyrene Beads Targeted for Water Expanded Foam. *Eur. Polym. J.* **2019**, *121*, 109343. https://doi.org/10.1016/j.eurpolymj.2019.109343.

(143) Jiménez-Saelices, C.; Save, M.; Capron, I. Synthesis of Latex Stabilized by Unmodified Cellulose Nanocrystals: The Effect of Monomers on Particle Size. *Polym. Chem.* **2019**, *10*, 727–737. https://doi.org/10.1039/c8py01575a.

(144) Mabrouk, A. Ben; Dufresne, A.; Boufi, S. Cellulose Nanocrystal as Ecofriendly Stabilizer for Emulsion Polymerization and Its Application for Waterborne Adhesive. *Carbohydr. Polym.* **2020**, *229*, 115504. https://doi.org/10.1016/j.carbpol.2019.115504.

(145) Glasing, J.; Jessop, P. G.; Champagne, P.; Hamad, W. Y.; Cunningham, M. F. Microsuspension Polymerization of Styrene Using Cellulose Nanocrystals as Pickering Emulsifiers: On the Evolution of Latex Particles. *Langmuir* **2020**, *36* (3), 796–809. https://doi.org/10.1021/acs.langmuir.9b03583.

(146) Nypelö, T.; Rodriguez-Abreu, C.; Kolena'ko, Y. V.; Rivas, J.; Rojas, O. J. Microbeads and Hollow Microcapsules Obtained by Self-Assembly of Pickering Magneto-Responsive Cellulose Nanocrystals. *ACS Appl. Mater. Interfaces* **2014**, *6* (19), 16851–16858.

https://doi.org/10.1021/am504260u.

(147) Du, W.; Guo, J.; Li, H.; Gao, Y. Heterogeneously Modified Cellulose Nanocrystals-Stabilized Pickering Emulsion: Preparation and Their Template Application for the Creation of PS Microspheres with Amino-Rich Surfaces. *ACS Sustain. Chem. Eng.* **2017**, *5*, 7514–7523. https://doi.org/10.1021/acssuschemeng.7b00375.

(148) Kedzior, S. A.; Dubé, M. A.; Cranston, E. D. Cellulose Nanocrystals and Methyl Cellulose as Costabilizers for Nanocomposite Latexes with Double Morphology. *ACS Sustain. Chem. Eng.* **2017**, *5* (11), 10509–10517. https://doi.org/10.1021/acssuschemeng.7b02510.

(149) Werner, A.; Schmitt, V.; Sèbe, G.; Héroguez, V. Synthesis of Surfactant-Free Micro-and Nanolatexes from Pickering Emulsions Stabilized by Acetylated Cellulose Nanocrystals. *Polym. Chem.* **2017**, *8* (39), 6064–6072. https://doi.org/10.1039/c7py01203a.

(150) Zhang, Y.; Karimkhani, V.; Makowski, B. T.; Samaranayake, G.; Rowan, S. J. Nanoemulsions and Nanolatexes Stabilized by Hydrophobically Functionalized Cellulose Nanocrystals. *Macromolecules* **2017**, *50* (16), 6032–6042. https://doi.org/10.1021/acs.macromol.7b00982.

(151) Errezma, M.; Mabrouk, A. Ben; Magnin, A.; Dufresne, A.; Boufi, S. Surfactant-Free Emulsion Pickering Polymerization Stabilized by Aldehyde-Functionalized Cellulose Nanocrystals. *Carbohydr. Polym.* **2018**, *202*, 621–630. https://doi.org/10.1016/j.carbpol.2018.09.018.

(152) Kalashnikova, I.; Bizot, H.; Cathala, B.; Capron, I. New Pickering Emulsions Stabilized by Bacterial Cellulose Nanocrystals. *Langmuir* **2011**, *27* (12), 7471–7479. https://doi.org/10.1021/la200971f.

(153) Kalashnikova, I.; Bizot, H.; Cathala, B.; Capron, I. Modulation of Cellulose Nanocrystals Amphiphilic Properties to Stabilize Oil/Water Interface. *Biomacromolecules* **2012**, *13* (1), 267–275. https://doi.org/10.1021/bm201599j.

(154) Favier, V.; Chanzy, H.; Cavaille, J. Y. Polymer Nanocomposite Reinforced by Cellulose Whiskers. *Macromolecules* **1995**, *28* (18), 6365–6367.

(155) Elmabrouk, A. B.; Wim, T.; Dufresne, A.; Boufi, S. Preparation of Poly(Styrene-Co-Hexylacrylate)/Cellulose Wiskers Nanocomposites via Miniemulsion Polymerization. *J. Appl. Polym. Sci.* **2009**, *114* (5), 2946–2955. https://doi.org/10.1002/app.

(156) Dastjerdi, Z.; Cranston, E. D.; Dubé, M. A. Synthesis of Poly(n-Butyl Acrylate/Methyl Methacrylate)/CNC Latex Nanocomposites via In Situ Emulsion Polymerization. *Macromol. React. Eng.* **2017**, *11* (6), 1–8. https://doi.org/10.1002/mren.201700013.

(157) Ouzas, A.; Niinivaara, E.; Cranston, E. D.; Dubé, M. A. In Situ Semibatch Emulsion Polymerization of 2-Ethyl Hexyl Acrylate/n-Butyl Acrylate/Methyl Methacrylate/Cellulose Nanocrystal Nanocomposites for Adhesive Applications. *Macromol. React. Eng.* **2018**, *12* (3), 1–10. https://doi.org/10.1002/mren.201700068.

(158) Ouzas, A.; Niinivaara, E.; Cranston, E. D.; Dubé, M. A. Synthesis of Poly(Isobutyl Acrylate/n-Butyl Acrylate/Methyl Methacrylate)/CNC Nanocomposites for Adhesive Applications via in Situ Semi-Batch Emulsion Polymerization. *Polym. Compos.* **2018**, 1–13. https://doi.org/10.1002/pc.24869.

(159) Pakdel, A. S.; Gabriel, V.; Berry, R. M.; Fraschini, C.; Cranston, E. D.; Dubé, M. A. A Sequential Design Approach for in Situ Incorporation of Cellulose Nanocrystals in Emulsion-Based Pressure Sensitive Adhesives. *Cellulose* **2020**, *6*. https://doi.org/10.1007/s10570-020-03060-6.

(160) Gabriel, V. A.; Cranston, E. D.; Dubé, M. A. Pushing the Limits with Cellulose Nanocrystal Loadings in Latex-Based Pressure-Sensitive Adhesive Nanocomposites. *Macromol. React. Eng.* **2020**, *2000027*, 1–9. https://doi.org/10.1002/mren.202000027.

(161) Mabrouk, A. Ben; Kaddami, H.; Magnin, A.; Belgacem, N. M.; Dufresne, A.; Boufi, S. Preparation of Nanocomposite Dispersions Based on Cellulose Whiskers and Acrylic Copolymer by Miniemulsion Polymerization: Effect of the Silane Content. *Polym. Eng. Sci.* **2011**, *51*, 62–70. https://doi.org/10.1002/pen.

(162) Mabrouk, A. Ben; Magnin, A.; Belgacem, M. N.; Boufi, S. Melt Rheology of Nanocomposites Based on Acrylic Copolymer and Cellulose Whiskers. *Compos. Sci. Technol.* **2011**, *71* (6), 818–827. https://doi.org/10.1016/j.compscitech.2011.01.012.

(163) Ben Mabrouk, A.; Rei Vilar, M.; Magnin, A.; Belgacem, M. N.; Boufi, S. Synthesis and Characterization of Cellulose Whiskers/Polymer Nanocomposite Dispersion by Mini-Emulsion Polymerization. *J. Colloid Interface Sci.* **2011**, *363* (1), 129–136. https://doi.org/10.1016/j.jcis.2011.07.050.

(164) Kedzior, S. A.; Kiriakou, M.; Niinivaara, E.; Dubé, M. A.; Fraschini, C.; Berry, R. M.; Cranston, E. D. Incorporating Cellulose Nanocrystals into the Core of Polymer Latex Particles via Polymer Grafting. *ACS Macro Lett.* **2018**, *7* (8), 990–996. https://doi.org/10.1021/acsmacrolett.8b00334.

(165) Karimi Shamsabadi, M.; Moghbeli, M. R. Cellulose Nanocrystals (CNCs) Reinforced Acrylic Pressure- Sensitive Adhesives (PSAs) Prepared via Miniemulsion Polymerization. *Int. J. Adhes. Adhes.* **2017**, *78*, 155–166. https://doi.org/10.1016/j.ijadhadh.2017.06.024.

(166) Yu, Q.; Yang, W.; Wang, Q.; Dong, W.; Du, M.; Ma, P. Functionalization of Cellulose Nanocrystals with γ -MPS and Its Effect on the Adhesive Behavior of Acrylic Pressure Sensitive Adhesives. *Carbohydr. Polym.* **2019**, *217* (November 2018), 168–177. https://doi.org/10.1016/j.carbpol.2019.04.049.

(167) Pakdel, A. S.; Niinivaara, E.; Berry, R. M.; Cranston, E. D.; Dubé, M. A. Cellulose Nanocrystal (CNC) – Latex Nanocomposites: The Effect of CNC Hydrophilicity and Charge on Rheological, Mechanical and Adhesive Properties. *Macromol. Rapid Commun.* **2020**, *2000448*, 1–12. https://doi.org/10.1002/marc.202000448.

(168) Beck, S.; Bouchard, J.; Berry, R. Dispersibility in Water of Dried Nanocrystalline Cellulose. *Biomacromolecules* **2012**, *13* (5), 1486–1494.

https://doi.org/10.1021/bm300191k.

(169) Beck, S.; Bouchard, J. Auto-Catalyzed Acidic Desulfation of Cellulose Nanocrystals. *Nord. Pulp Pap. Res. J.* **2014**, *29* (1), 6–14. https://doi.org/10.3183/npprj-2014-29-01-p006-014.

(170) Hasani, M.; Cranston, E. D.; Westman, G.; Gray, D. G. Cationic Surface Functionalization of Cellulose Nanocrystals. *Soft Matter* **2008**, *4* (11), 2238–2244. https://doi.org/10.1039/b806789a.

(171) Viet, D.; Beck-Candanedo, S.; Gray, D. G. Dispersion of Cellulose Nanocrystals in Polar Organic Solvents. *Cellulose* **2007**, *14* (2), 109–113. https://doi.org/10.1007/s10570-006-9093-9.

(172) Khandal, D.; Riedl, B.; Tavares, J. R.; Carreau, P. J.; Heuzey, M. C. Tailoring Cellulose Nanocrystals Rheological Behavior in Aqueous Suspensions through Surface Functionalization with Polyethyleneimine. *Phys. Fluids* **2019**, *31* (2). https://doi.org/10.1063/1.5046669.

(173) Yoo, Y.; Youngblood, J. P. Green One-Pot Synthesis of Surface Hydrophobized Cellulose Nanocrystals in Aqueous Medium. *ACS Sustain. Chem. Eng.* **2016**, *4* (7), 3927–3938. https://doi.org/10.1021/acssuschemeng.6b00781.

(174) Araki, J.; Wada, M.; Kuga, S. Steric Stabilization of a Cellulose Microcrystal Suspension by Poly(Ethylene Glycol) Grafting. *Langmuir* **2001**, *17* (1), 21–27. https://doi.org/10.1021/la001070m.

(175) Rosilo, H.; McKee, J. R.; Kontturi, E.; Koho, T.; Hytönen, V. P.; Ikkala, O.; Kostiainen, M. A. Cationic Polymer Brush-Modified Cellulose Nanocrystals for High-Affinity Virus Binding. *Nanoscale* **2014**, *6* (20), 11871–11881. https://doi.org/10.1039/c4nr03584d.

(176) Hemraz, U. D.; Campbell, K. A.; Burdick, J. S.; Ckless, K.; Boluk, Y.; Sunasee, R. Cationic Poly(2-Aminoethylmethacrylate) and PolyN-(2-Aminoethylmethacrylamide) Modified Cellulose Nanocrystals: Synthesis, Characterization, and Cytotoxicity. *Biomacromolecules* **2015**, *16* (1), 319–325. https://doi.org/10.1021/bm501516r.

(177) Hu, H.; Hou, X. J.; Wang, X. C.; Nie, J. J.; Cai, Q.; Xu, F. J. Gold Nanoparticle-Conjugated Heterogeneous Polymer Brush-Wrapped Cellulose Nanocrystals Prepared by Combining Different Controllable Polymerization Techniques for Theranostic Applications. *Polym. Chem.* **2016**, *7* (18), 3107–3116. https://doi.org/10.1039/c6py00251j.

(178) Grishkewich, N.; Akhlaghi, S. P.; Zhaoling, Y.; Berry, R.; Tam, K. C. Cellulose Nanocrystal-Poly(Oligo(Ethylene Glycol) Methacrylate) Brushes with Tunable LCSTs. *Carbohydr. Polym.* **2016**, *144*, 215–222. https://doi.org/10.1016/j.carbpol.2016.02.044.

(179) Zoppe, J. O.; Xu, X.; Känel, C.; Orsolini, P.; Siqueira, G.; Tingaut, P.; Zimmermann, T.; Klok, H. A. Effect of Surface Charge on Surface-Initiated Atom Transfer Radical Polymerization from Cellulose Nanocrystals in Aqueous Media. *Biomacromolecules* **2016**, *17* (4), 1404–1413. https://doi.org/10.1021/acs.biomac.6b00011.

(180) Arredondo, J.; Jessop, P. G.; Champagne, P.; Bouchard, J.; Cunningham, M. F. Synthesis of CO2-Responsive Cellulose Nanocrystals by Surface-Initiated Cu(0)-Mediated Polymerisation. *Green Chem.* **2017**, *19* (17), 4141–4152. https://doi.org/10.1039/c7gc01798g.

(181) Wang, H. D.; Roeder, R. D.; Whitney, R. A.; Champagne, P.; Cunningham, M. F. Graft Modification of Crystalline Nanocellulose by Cu(0)-Mediated SET Living Radical Polymerization. *J. Polym. Sci. Part A Polym. Chem.* **2015**, *53* (24), 2800–2808. https://doi.org/10.1002/pola.27754.

(182) Boujemaoui, A.; Mongkhontreerat, S.; Malmström, E.; Carlmark, A. Preparation and Characterization of Functionalized Cellulose Nanocrystals. *Carbohydr. Polym.* **2015**, *115*, 457–464. https://doi.org/10.1016/j.carbpol.2014.08.110.

(183) Hatton, F. L.; Kedzior, S. A.; Cranston, E. D.; Carlmark, A. Grafting-from Cellulose Nanocrystals via Photoinduced Cu-Mediated Reversible-Deactivation Radical Polymerization. *Carbohydr. Polym.* **2017**, *157*, 1033–1040. https://doi.org/10.1016/j.carbpol.2016.10.064.

(184) Lamm, M. E.; Wang, Z.; Zhou, J.; Yuan, L.; Zhang, X.; Tang, C. Sustainable Epoxy Resins Derived from Plant Oils with Thermo- and Chemo-Responsive Shape Memory Behavior. *Polymer (Guildf).* **2018**, *144*, 121–127. https://doi.org/10.1016/j.polymer.2018.04.047.

(185) Abousalman-Rezvani, Z.; Eskandari, P.; Roghani-Mamaqani, H.; Mardani, H.; Salami-Kalajahi, M. Grafting Light-, Temperature, and CO2-Responsive Copolymers from Cellulose Nanocrystals by Atom Transfer Radical Polymerization for Adsorption of Nitrate Ions. *Polymer (Guildf).* **2019**, *182* (August), 121830. https://doi.org/10.1016/j.polymer.2019.121830.

(186) Morits, M.; McKee, J. R.; Majoinen, J.; Malho, J. M.; Houbenov, N.; Seitsonen, J.; Laine, J.; Gröschel, A. H.; Ikkala, O. Polymer Brushes on Cellulose Nanofibers: Modification, SI-ATRP, and Unexpected Degradation Processes. *ACS Sustain. Chem. Eng.* **2017**, *5* (9), 7642–7650. https://doi.org/10.1021/acssuschemeng.7b00972.

(187) Zhang, Z.; Tam, K. C.; Sèbe, G.; Wang, X. Convenient Characterization of Polymers Grafted on Cellulose Nanocrystals via SI-ATRP without Chain Cleavage. *Carbohydr. Polym.* **2018**, *199* (April), 603–609. https://doi.org/10.1016/j.carbpol.2018.07.060.

(188) Wu, W.; Huang, F.; Pan, S.; Mu, W.; Meng, X.; Yang, H.; Xu, Z.; Ragauskas, A. J.; Deng, Y. Thermo-Responsive and Fluorescent Cellulose Nanocrystals Grafted with Polymer Brushes. *J. Mater. Chem. A* **2015**, *3*, 1995–2005. https://doi.org/10.1039/b000000x.

(189) Hansson, S.; Antoni, P.; Bergenudd, H.; Malmström, E. Selective Cleavage of Polymer Grafts from Solid Surfaces: Assessment of Initiator Content and Polymer Characteristics. *Polym. Chem.* **2011**, *2* (3), 556–558. https://doi.org/10.1039/c0py00388c.

(190) Kloser, E.; Gray, D. G. Surface Grafting of Cellulose Nanocrystals with Poly(Ethylene Oxide) in Aqueous Media. *Langmuir* **2010**, *26* (16), 13450–13456.

https://doi.org/10.1021/la101795s.

(191) Braunecker, W. A.; Tsarevsky, N. V; Gennaro, A.; Matyjaszewski, K. Thermodynamic Components of the Atom Transfer Radical Polymerization Equilibrium : Quantifying Solvent Effects. *Macromolecules* **2009**, *42*, 6348–6360. https://doi.org/10.1021/ma901094s.

(192) Dubé, M. A.; Gabriel, V. A.; Pakdel, A. S.; Zhang, Y. Sustainable Polymer Reaction Engineering: Are We There Yet? *Can. J. Chem. Eng.* **2020**, No. April, 1–30. https://doi.org/10.1002/cjce.23865.

(193) Chern, C. S. Emulsion Polymerization Mechanisms and Kinetics. *Prog. Polym. Sci.* **2006**, *31* (5), 443–486. https://doi.org/10.1016/j.progpolymsci.2006.02.001.

(194) Kao, C. S.; Hu, K. H. Acrylic Reactor Runaway and Explosion Accident Analysis. *J. Loss Prev. Process Ind.* **2002**, *15* (3), 213–222. https://doi.org/10.1016/S0950-4230(01)00070-5.

(195) Radchenko, A. V.; Kostjuk, S. V.; Ganachaud, F. Cationic Polymerization of Isobutyl Vinyl Ether in Aqueous Media: Physical Chemistry Tricks to Fight against Thermal Runaway. *Polym. Chem.* **2013**, *4* (6), 1883–1892. https://doi.org/10.1039/c2py20945d.

(196) Roman, M. Toxicity of Cellulose Nanocrystals: A Review. *Ind. Biotechnol.* **2015**, *11* (1), 25–33. https://doi.org/10.1089/ind.2014.0024.

(197) Favier, V.; Canova, G. R.; Cavaillé, J. Y.; Chanzy, H.; Dufresne, A.; Gauthier, C. Nanocomposite Materials Form Latex and Cellulose Whiskers. *Polym. Adv. Technol.* **1995**, *6* (5), 351–355.

(198) Azzam, F.; Siqueira, E.; Fort, S.; Hassaini, R.; Pignon, F.; Travelet, C.; Putaux, J. L.; Jean, B. Tunable Aggregation and Gelation of Thermoresponsive Suspensions of Polymer-Grafted Cellulose Nanocrystals. *Biomacromolecules* **2016**, *17* (6), 2112–2119. https://doi.org/10.1021/acs.biomac.6b00344.

(199) Qiao, C.; Chen, G.; Zhang, J.; Yao, J. Structure and Rheological Properties of Cellulose Nanocrystals Suspension. *Food Hydrocoll.* **2016**, *55*, 19–25. https://doi.org/10.1016/j.foodhyd.2015.11.005.

(200) Liu, D.; Chen, X.; Yue, Y.; Chen, M.; Wu, Q. Structure and Rheology of Nanocrystalline Cellulose. *Carbohydr. Polym.* **2011**, *84* (1), 316–322. https://doi.org/10.1016/j.carbpol.2010.11.039.

(201) Chen, P.; Ogawa, Y.; Nishiyama, Y.; Ismail, E.; Mazeau, K. Linear, Non-Linear and Plastic Bending Deformaton of Cellulose Nanocrystals. *Phys. Chem. Chem. Phys.* **2016**, *18*, 19880–19887. https://doi.org/10.1039/C6CP00624H.

(202) Qie, L.; Dub, M. A. The Influence of Butyl Acrylate/Methyl Methacrylate/2-Hydroxy Ethyl Methacrylate/Acrylic Acid Latex Properties on Pressure Sensitive Adhesive Performance. *Int. J. Adhes. Adhes.* **2010**, *30* (7), 654–664. https://doi.org/10.1016/j.ijadhadh.2010.07.002.

(203) Niinivaara, E.; Ouzas, A.; Fraschini, C.; Berry, R. M.; Dubé, M. A.; Cranston, E. D. How Latex Film Formation and Adhesion at the Nanoscale Correlare to Performance of Pressure Sensitive Adhesives with Cellulose Nanocrystals. *Submitt. to Philos. Trans. A.*

(204) Gicquel, E.; Martin, C.; Heux, L.; Jean, B.; Bras, J. Adsorption versus Grafting of Poly(N-Isopropylacrylamide) in Aqueous Conditions on the Surface of Cellulose Nanocrystals. *Carbohydr. Polym.* **2019**. https://doi.org/10.1016/j.carbpol.2019.01.022.

(205) Hu, Z.; Berry, R. M.; Pelton, R.; Cranston, E. D. One-Pot Water-Based Hydrophobic Surface Modification of Cellulose Nanocrystals Using Plant Polyphenols. *ACS Sustain. Chem. Eng.* **2017**, *5*, 5018–5026. https://doi.org/10.1021/acssuschemeng.7b00415.